THE UNIVERSITY
of EDINBURGH

Highway Bridges in Fire: Characterisation of Fire Loading and Structural Behaviour

THE UNIVERSITY *of* EDINBURGH

Jiayu Hu

School of Engineering
Institute *for* Infrastructure and Environment
The University of Edinburgh
UK

A thesis presented for the degree of
Doctor of Philosophy
2018

Declaration

I declare that this thesis has been composed by myself and that the work has not been submitted for any other degree or professional qualification. Except where states otherwise by reference, acknowledgement or work which has formed part of jointly-authored publications, the work presented is entirely my own.

The work presented in Chapter 3 was previously published in *Journal of Constructional Steel Research* as *'Fire resistance of composite steel & concrete highway bridges'* by **Jiayu Hu**, Asif Usmani (supervisor), Abdel Sanad, Ricky Carvel (supervisor). This study was conceived by all of the authors. I carried out the entire simulation work and conducted data analysis.

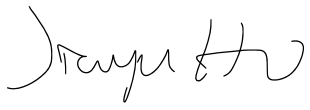

Jiayu Hu

2018

Acknowledgements

I would like to thank Prof. Asif Usmani, who was officially my supervisor in the first year of PhD, and has been my mentor throughout. This work would not have been possible without your advice. Your extensive knowledge has inspired me and deeply changed my way of thinking. This not only make the PhD experience valuable, but will be a lifelong influence on me. A sincere thank you also to my principle supervisor Dr. Ricky Carvel for always providing timely advice.

I would also like to thank the rest of our group: Liming, Xu, Zhujun, Mian, Payam and Ben for being so generous with time to provide truly helpful advice. Thank you Norlizan, Eric and Yu from the Fire Group for their valuable discussions. Thanks to friends in the John Muir building who helped to restart my frozen remote computer a thousand times.

I would like to express my deepest gratitude to my family who have always encouraged and supported me to see the world. Finally, there is one has been more than a friend or companion. A special thanks to Duo for standing by my side when times get hard. You are the best thing that happened to me in this beautiful country.

TO THE 72 LIFE LOSS IN GRENFELL TOWER FIRE ON 14 JUNE 2017.

LAY SUMMARY

When engineers design bridges, the impact of hazards to the structure are required to be considered such as earthquakes, wind and floods. However designing a fire-resistant bridge is not required by current transport standards, despite the fact that nearly three times as many bridges collapsed between 1990 and 2005 due to fires compared to those due to earthquakes. Therefore for bridges on critical highways with heavy traffic, fire resistance design and assessment should be considered.

This thesis consists of three parts. *Part I* analyses computer models of bridges to understand their structural behaviour when exposed to fire and to determine the influence of bridge plan shape on behaviour. Rectangular and skew shape bridges were analysed using a code-based Hydrocarbon fire loading. The above models implemented a commonly used fire curve from the Eurocode, however this fire representation is too intense as it does not consider that the intensity of heat from a vehicle fire should be reduced at locations away from the burning vehicle. Using the Hydrocarbon fire may therefore result in over-design or may provide an overly pessimistic assessment of performance. In *Part II*, the author developed fire representations for four types of vehicles which are more realistic than the code-based curves. The use of these fire models in existing finite element software will require some effort which may not be practical for practicing engineers under the pressure of time, therefore the representations were programmed into the free software OpenSees in *Part III*. This software allows users to use the new design fire representations directly and determine the thermal and structural response of bridges without significant user effort.

ABSTRACT

In bridge design, extreme hazards have been considered as design loads for years, including wind, earthquake, snow, and floods; but fire hazard is not usually considered in the design process. However, severe fire accidents occurring near or under bridges are not as rare as generally perceived compared to the other extreme hazards, especially earthquakes and floods. Therefore fire resistance of bridges along the most critical arteries of transport networks, carrying heavy traffic, should be considered. This should ideally be based upon an estimation of the consequences of a particular level of bridge damage in terms of social and economic costs.

Since there are no codes or standards relating to fire resistance of bridges, assessment must rely upon a performance-based engineering approach. In conducting performance-based studies of bridge fire resistance, most previous researchers have used code-based fire curves, such as the ISO 834 standard or Hydrocarbon fires, which assume uniform heating along the entire bridge span. However, a real vehicle fire will naturally create a non-uniform, localised fire under the bridge span and the hazard intensity will decay with distance away from the burning vehicle. If such a scenario could be implemented in a more realistic fire model, then more realistic thermal and thermo-mechanical response of structures could be predicted, resulting in more reliable estimates of performance.

This thesis consists of three main parts. *Part I* investigates the structural performance of composite steel-framed bridges and the influence of bridge shape on failure time under code-based Hydrocarbon fire loading. *Part II* uses the CFD-based fire dynamics simulation code FDS to generate design fire

curves for four different classes of vehicles. The design fire curves include the expected decay in the intensity of the heat flux due to the fire along the bridge span. These curves were then generalised as mathematical functions that can be easily used by engineers and designers in the assessment of the performance of existing bridges under realistic hazard scenarios, for fire resistance design. Rectangular bridge models were subjected to the most extreme class of design fire (fuel tanker fires) in order to compare with the Hydrocarbon fire. The analysis showed that, for the bridge structure considered, there is no failure for the model in the fuel tanker fire scenario, even with conservative assumptions. However, failure may occur if a higher heat release rate is used, which is possible for large fuel tanker fires. In *Part III* the new design curves (developed as mathematical functions) were implemented into the OpenSees software framework to enable a seamless simulation from fire, to heat transfer and structural response.

PUBLICATIONS

Journal paper:

- **Hu, J.**, Usmani, A., Sanad, A. & Carvel, R. Fire resistance of composite steel & concrete highway bridges. *J. Constr. Steel Res*. 148, 707–719 (2018).

- Wang, Y., & **Hu, J.** Performance of laminated glazing under fire conditions. *Comps Struct*. (2019).

Conference paper:

- **Hu, J.** & Usmani, A. Application of Design Bridge Fires: Fire Performance Assessment of A Highway Bridge. *Interflam - 15th International Conference and Exhibition on Fire Science and Engineering (2019), Royal Holloway College, Egham, UK.*

- **Hu, J.**, Dai, X., Usmani, A. & Carvel, R. Design Fires for Performance-based Engineering of Bridges. *in SiF 2018 – The 10th International Conference on Structures in Fire, London, UK*.

- **Hu, J.**, Usmani, A. & Carvel, R. A framework for the thermo-mechanical analysis of highway bridges for vehicle fire scenarios. *in 2nd International Conference on Structural Safety under Fire & Blast Loading (2017), London, UK.*

- **Hu, J.**, Carvel, R., Sanad, A. & Usmani, A. New Design Fires for Performance Based Engineering of Highway Bridges. *in SiF 2016 – The 9th International Conference on Structures in Fire, Princeton, USA*.

- Jiang, L., Kamath, P., Dai, X., **Hu, J.**, Chen, S., Usmani, A. An integrated tool for performance based engineering of structures in fire. *in Proceedings of the Second International Conference on Performance-based and Life-cycle Structural Engineering* 944–952 (School of Civil Engineering, The University of Queensland, 2015). doi:10.14264/uql.2016.516

- **Hu, J.**, Sanad, A. & Usmani, A. Structure response analysis of a highway bridge when subjected to accidental vehicle fires. *in The First International Conference on Structural Safety under Fire & Blast 465–474 (2015), Glasgow, UK*.

Contents

List of Figures

List of Tables

List of Abbreviations

Abbreviation

BCs Boundary Conditions

CFD Computational Fluid Dynamics

CO Carbon Monoxide

DOFs Degree of Freedoms

DOT Department of Transportation

FAS Fire Affected Span

FDS Fire Dynamics Simulator

FE Finite Element

GUI Graphical User Interface

HA Highways Agency

HGVs Heavy Goods Vehicles

HRR Heat Release Rate

HRRPUA Heat Release Rate Per Unit Area

HT Heat Transfer

KEC Korea Expressway Corporation

LGVs Light Goods Vehicles

MPCs Multiple-Point Constraints

NFAS Non-fire Affected Span

OpenSees Open System for Earthquake Engineering Simulation

PBE Performance-based Engineering

PRI Plume Resolution Index

SCI The Steel Construction Institute

SRN Strategic Road Network

1

Introduction

In bridge design, engineers are required to consider the impact of earthquakes, wind, and floods on the bridge structure. Equivalent consideration of fire hazard is not yet required by codes, however two reports show that fires have caused more bridges to collapse than earthquakes. This is partially because earthquakes have been relatively well-studied and there are code enforcements which reduce the seismic damage to bridge structures. Moreover, the influence of a bridge failure is not restricted to the loss of the structure itself, it may also severely impact commuters and the economy.

The previous research of bridges in fires is mainly focused on the fire resistance of individual structural components. Global behaviour has not been

widely analysed in detail. When considered, the fire loading is commonly specified using code-based fire curves, which are usually applied uniformly along the bridge span. A few studies have used CFD fire models to simulate more realistic fires, which provide a spatially varying thermal boundary conditions that could be used to determine the realistic impact of the fire hazard on the structure. However, such CFD models require fire science knowledge, extensive user effort and long simulation times which are not efficient as part of a preliminary assessment, or routine risk assessments within a large transportation network. Vehicle fires expressed as heat flux correlations could be developed to represent more realistic alternatives to code-based fire curves. In commercial finite element software, applying such non-uniform heat flux correlations to a structure requires creating scripts which are not practical for consultants or practicing bridge engineers. For this reason, a module has been developed in an open-source structural software, OpenSees, containing embedded vehicle fire hazard loadings.

1.1 Aims of the Research

Building fire literature contains various research directions, such as fire development, structural performance, evacuation, fire protection design, and management of occupied buildings, etc. Unlike building fires, research on bridges in fire has tended to concentrate on the structural behaviour of bridges under fire loadings, but generally using simple and unrealistic representations of the fire hazard. This fact is the key driver of the two main components of this thesis: bridge structural performance and bridge fire hazard characterisation. The aims of the research are as follows:

- Understand bridge structural behaviour under a standard Hydrocarbon fire load.

- Characterisation of the most common type of bridge fire hazard, namely localised vehicle fires, with varying heat flux distribution which decays with distance from the fire origin, to generate more realistic hazard scenarios than currently available from code-based prescriptive fire options.

- Generate mathematical functions to generalise the fire hazard characterisation as design bridge fire curves which can be used to represent the heat flux received along the bridge span under a number of vehicle fire scenarios.

- Analyse the structural performance of bridge models under the most severe fuel tanker design fires for comparison with the commonly used prescriptive Hydrocarbon fire.

- Implement the new bridge design fire curves into OpenSees.

1.2 Outline of Chapters

Chapter 2: A literature review of bridges in fire and relevant studies

A review is presented of major incidents involving bridges in fires which happened in the 21^{st} century. This review identifies potential scenarios that could result in structural damage or collapse. Current computational models and experimental studies have also been reviewed. Finally, the author presents some thoughts for future research and suggestions for regulators.

Part I: ABAQUS models+ Hydrocarbon fire

Chapter 3: Fire resistance of composite steel & concrete highway bridges

In order to study the effects of bridge shape and abutment restraint on the fire resistance of a highway bridge, finite element models for heat transfer and thermo-mechanical analysis are performed in ABAQUS. The failure time of the

bridges for the different models are determined based on a number of proposed criteria.

Part II: ABAQUS models + 'Bridge fires'

Chapter 4: Designed localised vehicle fires

This chapter presents a series of idealised CFD vehicle fire models. Four types of vehicles corresponding to different magnitudes of fire intensity have been defined. The heat flux results along the bridge span are obtained for each type of vehicle in order to characterise the fire hazard.

Chapter 5: Fire resistance of highway bridges under fuel tanker fires

Rectangular and skew bridge models are analysed using the fuel tanker design fires in ABAQUS. The bridge models are exposed to two scenarios, with the fire source under the mid-span, and near the abutment, respectively. The results are compared with the assessment using the Hydrocarbon fire from Chapter 3.

Part III: 'Bridge fires' in OpenSees

Chapter 6: Development of 'Bridge Fires' in OpenSees

The bridge design fires are programmed into the open-source software OpenSees. This new module allows the users to apply the design bridge fire curves by simply specifying a tag number.

2

Literature Review

2.1 Introduction

Along with the continuous reports of severe fires in bridge networks as listed in Table 2.1, the following issues motivated this review of bridges in fire and related studies. The facts presented in this section show that the attention and research is inadequate for society needs based on the statistics.

1) **Not so rare:**

   In bridge design, extreme hazards have been considered as design loads for years, such as wind (EN, 2005c), earthquake (EN, 2005b) and snow (EN, 2003b), while fire hazard is not usually considered in the design

process. However, severe fire accidents which have consequences for bridges are not as rare as might be generally perceived, when compared to other extreme hazards, such as earthquake or flood.

Report from 2013 (Lee et al., 2013) listed statistics for bridge failures based on the causes of failure in 10-year intervals (1980-1990, 1990-2000 and 2000-2012). It is shown that when considering only external causes, 3.2% of the bridge failures were caused by fire, while only 1.8% and 2.1% were due to wind and earthquakes, respectively. They opine that this may be caused by code enforcement and the relatively well understood behaviour of structures in earthquakes. This finding is also partially confirmed by another survey conducted in 2008 by the New York Department of Transportation (Garlock et al., 2012), which reports that nearly three times as many bridges collapsed between 1990 and 2005 due to fire compared to those due to earthquakes.

2) **Severe damage to bridge structures is unavoidable**

Another issue regarding fire hazard to bridges is the difficulty for the fire brigade to prevent severe damage, which is especially relevant if the accident occurs under a bridge in a rural area. In the accident involving the CN Rail trestle bridge, a large section of the bridge was already engulfed in flames when the fire department arrived at the bridge Riebe (2017). Early arrival of the fire brigade does not assure a positive outcome, even if the fire brigade arrive at the scene within 20 minutes, partial or total bridge collapses due to fire can still occur, as evidenced by the 9 Mile Road Bridge in 2009 (Kodur et al., 2013) and the MacArthur Maze freeway in 2007 (Bajwa et al., 2012).

The factors leading to rapid damage and failure are:

- If fuel spillages are involved, there will be intense heating from the

liquid fuel fires which reach peak fire size in a short time. This only allows the fire service a relatively short reaction time, compared to building fires which usually take longer to fully develop into a severe fire.

- Commonly used structural materials in bridges, such as unprotected steel, have poor fire performance
- As reported by fire services, winds tend to contribute to the spread of the flames and fire development, and also ”keep the streams of water from reaching deep into the bridge” (New York Post, 2014)
- In some instances, the location of bridges provide ‘limited access to hydrants, requiring water to be hauled in by truck’ (New York Post, 2014)
- Active or passive fire protection measures are very rarely used on bridges

3) **Extreme disruption of the economy and commuters**

Fire accidents not only have devastating first and second order effect on bridges, but also economic losses, heritage loss in case of historic bridges, and bridge-specific functions such as commuter patterns, social service and community commerce.

The economic losses include both direct and indirect costs, where the latter can be considerably greater in terms of financial and political challenges for the bridge authorities than the cost of repair or rebuild. This is mainly caused by the interruption of service and disruption of local commerce, also the repair time, which usually ranges from a few weeks (Gong and Agrawal, 2015) to 6 months (Summers, 2012), in addition to the expense of detours. The direct cost of repair varies largely, not only due to the damage severity, but also due to the commuting demands. This is

reflected by the use of financial incentives which are always expected by the contractor for completing the project sooner. In the US, this cost is provided by the Federal Highway funds for such emergency repair work to restore emergency access and begin the most critical repairs, which can make long-term repair work possible in the weeks ahead (USA TODAY NETWORK 2017). An example is the bridge in Ohio in 2015 where the costs were $1 million (Franko, 2015) and $10 million for the I-85 in Atlanta in 2017, where an estimated 250,000 vehicles drive through daily (Hanna and Boyette, 2017; USA TODAY NETWORK, 2017).

4) **Limited research (simulations & experiments)**

In 2011, the Highways Agency (HA) (Highways Agency, 2011) in England tried to find engineering solutions to enhance the ability of bridges to resist damage due to fire. Risk locations were prioritised based on those *"having potential fire risk from activity beneath or adjacent to strategic road network"*. However, at the time, limited research was available for the HA to consider modifying the existing design practices. Most of the studies conducted in the years since then provide limited experiments, structural analysis and bridge-specific fire models. However, things may now be changing. Recently, the first full span bridge fire experiment was conducted in Valencia, Spain (Alos-Moya et al., 2017).

2.1.1 Objectives

Two reviews regarding bridge fires have been published in recent years. Garlock et al. (2012) presented a review with a particular focus on the post-fire assessment and repair strategy. The author listed 11 cases of major incidents which occurred between 1995 and 2009, and summarised 10 case studies of the structural assessment of fire damaged bridges. With the increasing needs

of performance-based fire design in Canada, Nicoletta et al. (2018) reviewed available research to guide design and assessment as well as direct future study.

This chapter aims to provide a comprehensive review for research institutions, highway authorities and industry, with a useful database to give an insight into the issues concerning bridges and fire. It complements the previous reviews by summarising various recent major accidents (Section 2.2) to identify potential scenarios that could result in a bridge failure or severe damage. For practitioners to select the parameters used in simulations, fire models (Section 2.3) and FE structural models (Section 2.4) have been reviewed and compared in detail. The various failure criteria currently used are also discussed in Section 2.4.3 for post-fire assessment. Experiments involving full scale bridges or structural components of bridges in fire are reviewed in Section 2.5. Risk assessment is usually the ultimate goal for such studies, therefore this process is reviewed in Section 2.6. Finally, in Section 2.7, this chapter identifies the gaps in knowledge that remain, future research needs and suggests ideas for future full-scale fire testing.

2.2 Fire Accidents

Table 2.1 lists major accidents in the 21st century in reverse chronologically order. The two incidents which have been studied in detail and published as case studies are indicated. The details of the incidents have been obtained from journal papers, web news and reports, and the key information including bridge types, fire scenarios, and the structural damage have been presented, where available. For clarity, the structural damage has been listed in three categories:

1) **Total collapse**, which refers the condition in which one or more spans

exhibited large deflections and lose their load-bearing function

2) **Partial collapse**, which implies some of the structural components of one or more spans exhibited large deflections

3) **Critical defect**, which is used when the structure exhibited some deformation or section loss but did not collapsed

In some accidents, even when the damage was merely a critical defect, the bridges or bridge deck were still demolished and replaced (NBC 7 San Diego, 2011), often due to severe damage such as concrete cracking (Apel and Mason, 2014). Another option of defined five damage levels is proposed by Peris-Sayol et al. (2016) which can be used for a more detailed classification.

To predict the CFD and heat transfer results within a reasonable range, the observation from real accidents (mainly by fire department) provide a general idea of outputs for modellers given that very limited validation resources are available. The gas temperature and the temperatures on the structural surfaces are the key results that would be expected from CFD models which can be used as inputs to estimate the heat transfer in structures.

There is very limited information can be found for the structural surface temperatures. The maximum surface temperature of the steel plates was about 500 °C in Wiehltal bridge (Garlock et al., 2012). Temperature of the flames reaches 650 °C∼800 °C estimated by the fire department, based on experience from similar fires in Mathilde Bridge accident (Godart et al., 2015) and 1200 °C in Wiehltal bridge (Garlock et al., 2012). Temperature of the fire below the I-580 overpass was estimated to be 850 °C∼1000 °C based on the samples collected and the results of thermal exposure tests. Near the truck, the maximum exposure temperature is estimated to be at least 720 °C but less than 930 °C (Bajwa et al., 2012).

Table 2.1: Major fire incidents in bridge network since the 21st century

Bridge	Location / Date	Cost (Currency in US Dollar or Pound Sterling)	Structural Damage / Failure Time	Fire Information (Causes / Fire Duration)	References
Cedar Covered Wooden Bridge	Madison County, U.S.A. 15/04/2017	$720,000 to rebuild (This bridge was destroyed by fire once before, in 2012. $1 million on reconstruction cost)	Damage: Critical defect	Causes: Arson Duration: 2 hours (The bridge was fully engulfed when the fire crews and law enforcement got to the scene about 20 min later.)	(Ta 2017)
I-85 Overpass	Atlanta, Georgia, U.S.A. 30/03/2017	Total: $16.6 million ($10 million in emergency relief funds toward clean-up and short-term repair of the highway)	Damage: Partial collapse (a 30 m section collapsed) Failure time: within 30-45 min	Causes: Arson Duration: 90-105 min (The blaze under control after the fire started for around 1.5 hours.)	(Hanna and Boyette 2017; Pirani 2017; USA TODAY NETWORK 2017; Wikipedia 2017)
CN Rail trestle wooden bridge	Mayerthorpe, Alberta, Canada. 26/04/2016	$7.6 million (including the costs of rebuilding the trestle and servicing customers while the bridge was out)	Damage: Total collapse (only some pillars from the truss still standing up) Failure time: It took only hours for the bridge to burn down	Causes: Arson (grass fire) Duration: Within an hour of being spotted, the fire had engulfed the entire bridge	(Riebe 2017)
Wooden Train bridge	Porcupine Plain, Saskatchewan, Canada. 25/03/2016	Not specified (This bridge was a well-known historic landmark)	Damage: Total collapse	Causes: Grass fire (a homeowner started a grass fire which spread to the bridge)	(Weidlimench 2016)
I-70 Highway Bridge	Ohio, U.S.A. 27/06/2015	$1 million	Damage: Critical defect (The flame cracked the concrete, melted metal reinforcement bars and compromised structural steel)	Causes: Vehicle fire (a tanker truck carrying ethanol overturned)	(Franko 2015)

Bridge	Location / Date	Cost (Currency in US Dollar or Pound Sterling)	Structural Damage / Failure Time	Fire Information (Causes / Fire Duration)	References
Peytonsville Road Bridge on I-65	Franklin, U.S.A. 15/08/2014	$10 million +	Damage: Critical defect	Causes: Vehicle fire and explosion (a tanker truck ran into an bridge support column, causing a fire and a large explosion) Duration: 30 min	(Apel and Mason 2014; Franklin Police News n.d.)
Overpass (under construction)	Hesperia, California, U.S.A. 05/05/2014	$6 million	Damage: Total collapse	Causes: Metal-cutting accident accidentally ignited temporary wooden supports of the bridge	(Daily Press 2015; Duchon and Vives 2014)
Al-Sheikh Mansour Bridge	Cairo, Egypt. 11/02/2014	Not specified	Damage: Total collapse	Causes: Gas cylinders and an electric cable exploded caused by a fire broke out in shacks	(Ahram Online 2014)
Ed Koch Queensboro Truss Bridge	Connecting Manhattan to Queens, New York City, U.S.A. 16/08/2013	Not specified	Damage: Critical defect Two exterior stringers of the upper deck supporting an exterior lane were severely deformed and damaged.	Causes: Vehicle fire (tractor-trailer) Duration: 30 min	(Gong and Agrawal 2015)
Harmony Ridge Wooden Trestle Bridge	Lampasas County, Texas, U.S.A. 19/05/2013	$10 million to rebuild	Damage: Total collapse	Duration: Firefighters spent 15 hours attempting to extinguish the blaze, before deciding to let it burn out. The entire trestle was engulfed within 20 min since the fire started	(BagOfNothing.com 2013; BBC NEWS 2013; Train Fanatics n.d.)
Mathilde Bridge	Over Seine River, Rouen, France. 29/10/2012	Not specified	Damage: Critical defect	Causes: Vehicle fire (a tanker truck carrying more than 20,000L of oil and gas caught fire) Duration: 2 hours to control and extinguish the two fires	(Godart, Berthellemy, and Lucas 2015)

Bridge	Location / Date	Cost (Currency in US Dollar or Pound Sterling)	Structural Damage / Failure Time	Fire Information (Causes / Fire Duration)	References
Paramount Boulevard Bridge	Montebello, California, U.S.A. 14/12/2011	$40 million	Damage: Critical defect	Causes: Vehicle fire (a tanker carrying 8,800 gallons of gasoline caught fire)	(NBC 7 San Diego 2011)
Yuqing Bridge	Wuyishan, Fujian Province, China. 28/05/2011	Not specified	Damage: Total collapse Failure time: Collapsed within 40 min	Causes: Children playing with fire	(Jin n.d.)
Deans Brook Viaduct	Mill Hill area, North London, UK. 15/04/2011	£4.5 million	Damage: Critical defect	Causes: Arson	(Highways Magazine 2012; Summers 2012)
Bucheon viaduct	South Korea. 2010	$13 million for the restoration of the bridge Total loss: $200 million	Damage: Critical defect	Causes: A tank-truck under the viaduct	(Park, Cho, and Shim 2018)
9 Mile Road bridge over I-75.	City of Hazel Park, Mich. U.S.A. 15/07/2009	Many millions of US dollars	Damage: Total collapse Failure time: The collapse of one span in about 20 minutes	Causes: Vehicle fire (a speeding driver hit a fuel tanker carrying 13,000 gallons of fuel, causing the tanker to impact into a column supporting the bridge)	(Hedden, Quagliata, and Wandzilak 2010)
MacArthur Maze I-80/880 interchange	Oakland California, U.S.A. 29/04/2007	$6 million a day economic loss during the 26 day closure	Damage: Total collapse Failure time: The collapse of portions of the overpass in less than 20 min.	Causes: Vehicle fire (a double tanker truck carrying 8,600 gallons of gasoline overturned and bursting into flames)	(Astaneh-Asl et al. 2009; Bajwa et al. 2012; Choi, Haj-Ali, and Kim 2012; Garlock et al. 2012)

Bridge	Location / Date	Cost (Currency in US Dollar or Pound Sterling)	Structural Damage / Failure Time	Fire Information (Causes / Fire Duration)	References
Bill Williams River Bridge	U.S.A. 28/07/2006	Not specified	Not specified	Causes: Vehicle fire (fuel truck)	(Davis, Tremel, and Pedrego 2008)
Brooklyn-Queens Expressway	New York, U.S.A. 16/01/2006	Not specified	Damage: Partial collapse (girders and the heavy wooden timbers they supported collapsed)	Causes: Vehicle fire (tanker) Duration: 2.5 hours (For roughly 20 min, flames roasted the large steel girders of a temporary bridge)	(Kilgannon 2006)
Wiehltal bridge	Near Cologne, Germany 26/08/2004	$42 million just for temporary repairs to restore traffic flows and $400 million for the total crash cost	Damage: Critical defect	Causes: A car collided with a tanker truck, causing the truck to fall 100 ft (30.5 m), followed by a fire under the bridge structure. Fuel area: 33 m^3 of fuel	(Garlock et al. 2012; Ray and Carrigan 2014; Wright et al. 2013)
Oaklawn Road Motorway bridge	Surrey, UK. 26/02/2003	Not specified	Damage: Critical defect	Causes: Vehicle fire Duration: 2 hours	(Highways Agency 2003)
Turkey Creek Wooden Bridge	Sharon Springs, Kansas, U.S.A. 12/04/2002	$250,000 to replace the lost coal cars $3.13 million to replace the current timber bridge with concrete structure.	Damage: Total collapse	Causes: A wheel bearing overheated and started to melt causing molten metal to fall onto railroad tracks	(Nexstar Broadcasting n.d.; Snopes n.d.)
I-65 Overpass	Birmingham, Alabama, U.S.A. 05/01/2002	$8.8 million	Damage: Partial collapse (significant deflection of 2.5 m but did not completely collapse)	Causes: Vehicle fire (a gasoline tanker truck collided with the pier of the overpass. 9,900 gallons of diesel fuel was consumed) Duration: 45 min	(J Alos-Moya et al. 2014), (Wright et al. 2013)

2.3 Vehicle Fire Models

In some of the cases presented in Table 2.1, the bridge fire was literally the bridge itself on fire as the primary fuel load. This only really occurs for timber structures. In general, when 'bridge fires' are discussed, the phrase really means fires on or under bridges, which may have an impact on the performance of the bridges. Garlock et al. (2012) defined the term **'bridge fires'** as *"typically petrol fires, also referred to as hydrocarbon fires or liquid pool fires, which are characterized by fast heating rates and can reach very high temperatures within the first few minutes of fire exposure".* In this work, the phrase 'bridge fires' will be used in general terms to denote a vehicle or liquid fuel fire under or on a bridge.

2.3.1 Fire Models

If a fire is considered at all in bridge design, it is typically considered as a source of heating at the surface of the structure. Fire models are used to define these thermal inputs; these are sometimes constant, sometimes varying with time. Having established the thermal input at the surface, heat transfer analysis can be conducted to determine structural temperatures, and the structural response to the fire can be determined.

Currently, the most common way to define the temperature boundary condition is to use prescriptive code-based 'fires curves' such as the Hydrocarbon fire curve (EN, 2002b), the external fire curve (Kodur et al., 2013) or the ISO fire curve (Tonicello and Desanghere, 2012). Occasionally a 't-squared fire' is used where the growth rate is characterised by a parabolic curve. Such analyses require the conversion of the fire into a temperature history which is useable as input for the heat transfer model.

In addition to these pre-defined fire curves, Computational Fluid Dynamics

(CFD) fire simulations are sometimes used to define fire scenarios. The early research on bridge structural response under fire loading focused on predicting the local damage due to a standard fire. However the standard fire models provided only a one-dimensional uniform thermal field. This is a significant simplification of reality, so some studies simulated two and three-dimensional fire spread using CFD models; where the Fire Dynamics Simulator (FDS) is the most commonly used simulation tool.

2.3.2 Fire Intensity

The fire intensity can be defined as a range of HRR for each vehicle category. National Fire Protection Association (2011) suggested the experimental and representative HRR of design fires for "*the bridges spanning moving traffic or a bridge spanning a freeway or interstate highway*", without fixed water-based fire-fighting systems, that corresponds to various vehicle types, as shown in the Table 2.2. Fig. 2.1 summarised the fire growth rate that has been used by other researchers for modelling. The maximum value of HRRPUA is commonly defined to be no more than $2500\,\mathrm{kW/m^2}$.

Table 2.2: HRR for typical vehicles, NFPA 502 (2017)

	Experimental HRR (MW)	Representative HRR (MW)
Passenger car	5 - 10	5
Multiple passenger car	10 - 20	15
Bus	25 - 34	30
Heavy goods truck	20 - 200	150
Flammable / Combustible liquid tanker	200 - 300	300

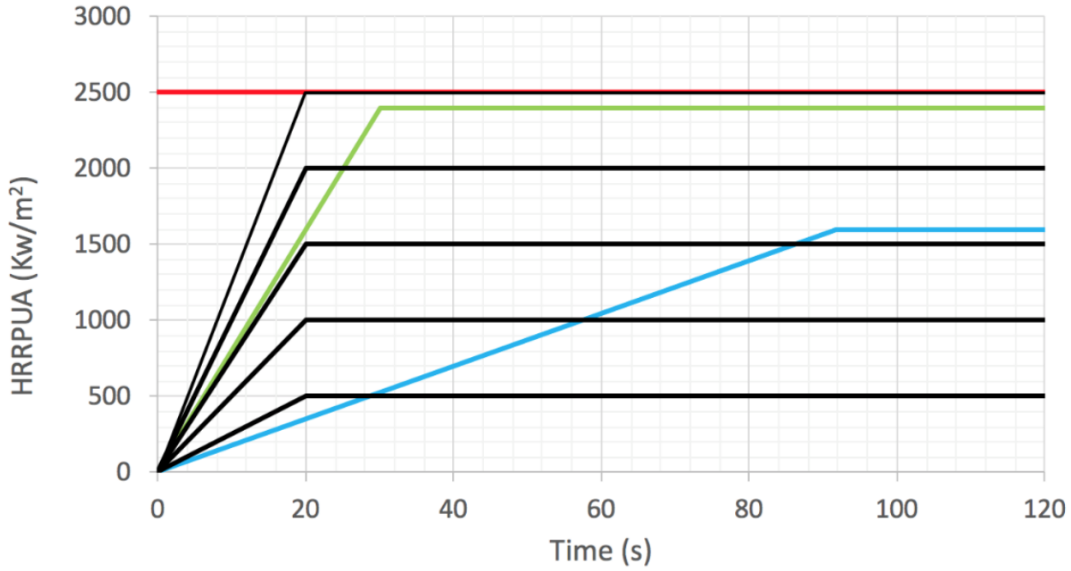

Figure 2.1: Comparison of HRRPUA curves used in CFD models between the recent research (red - Choi et al. (2012); black - Alos-Moya et al. (2014); green - Peris-Sayol et al. (2015b); blue - Gong and Agrawal (2015)). The time beyond 120s is not plotted for better observation of the growth rate. All the curves remain constant until the end of simulations, while the blue line is linearly decaying to zero from 1200s to 1800s.

2.3.3 Fuel Bed Area

In most of the recent research, the fuel bed has been modelled as a rectangular shape and the top surface of the fuel bed was defined as the burning surface. For example, Peris-Sayol et al. (2015a) modelled the size of the fuel bed as $12\,\text{m} \times 2.5\,\text{m}$ at one meter above the road level. A burning area and fuel spilled area have been assumed by Alos-Moya et al. (2014) with the area of $30\,\text{m}^2$ and $155.15\,\text{m}^2$ respectively. Gong and Agrawal (2015) used $1.5\,\text{m} \times 1.8\,\text{m}$ which is approximately equal to the actual size of the cabin. Choi et al. (2012) assumed 90% of the total spilled gasoline (8600 gallons) is on the bridge deck and other 10% of gasoline is on the ground. Wright et al. (2013) used a diameter of $13.1\,\text{m}$ for a fuel bed which is estimated based on visual observation - rectangular in shape with an approximate area of $134\,\text{m}^2$. This model included the ground slope from the piers to abutments.

2.4 Thermo-mechanical FE Models

Bridges in fire have attracted researchers' attention since 2005 when a numerical simulation was performed by Dotreppe et al. (2005) to study the failure mode of a tied-arch bridge exposed to fire. Performance-based models played a significant role in providing a pre/post-fire assessment of bridges under fire loading. By using performance-based methods, bridges can be designed to resist realistic fires and determine the structural weaknesses and strengths in fire. In such analyses, the failure time can be predicted, as well as the load paths in the structure can be identified from the deformation and the change of internal forces (e.g. bending moments and axial forces).

Table 2.3 summarises the published thermo-mechanical models and compares the key inputs for performing FE models. The software ABAQUS is most commonly used and other software packages are popular, such as ANSYS (Aziz et al., 2015; Bajwa et al., 2012), LS-DYNA (Bajwa et al., 2012), SAFIR (Dotreppe et al., 2005) and other self-developed codes (Godart et al., 2015).

2.4.1 Element Types

As shown in Table 2.3, the different mesh types have been used due to various demands. Solid elements have been used to get a close match to the experimental data (Wright et al., 2013). These are also easier for transferring thermal data from FDS to thermo-mechanical analysis in ABAQUS (Wright et al., 2013).

Table 2.3: Parameters used in thermo-mechanical FE models

Authors / Year	Modelled Structures	FE Simulation Tool	Parametric Study	Fire Model	Live Loads	Element Types
(Hu *et al.*, 2018)	Composite highway bridge	ABAQUS	Rectangular vs. skew bridge shape; With and without abutment restraint; Element types	Hydrocarbon fire	None	HT: DC2D4 Structure: B31, S4R, R3D4
(Peris-Sayol *et al.*, 2015a)	Simply supported bridge	ABAQUS	Single girder vs. full bridge (one/three spans); With and without abutment restraint; Vertical clearance: 5, 6, 7, 8, 9 and 10m; Spans numbers in full bridge model	CFD fire model	None	Structure: C3D8 Abutment: R3D4
(Payá-Zaforteza and Garlock, 2012)	Simply supported bridge	ABAQUS	With and without abutment restraint; Type of steel; Load combination	Hydrocarbon fire Stoddard fire	Uniform live load: 10,700 N/m	Structure: C3D8
(Gong and Agrawal, 2015)	A single girder; and Damaged deck	ABAQUS	Vehicular loads	CFD fire model	Vehicular live load has been applied on the upper deck Two load patterns for the lateral distribution, have been assumed to create the most severe loading condition	Steel stringers and cross beams: S4R Concrete slab: C3D8 Vertical and horizontal bracings: two-node linear beams

Authors / Year	Modelled Structures	FE Simulation Tool	Parametric Study	Fire Model	Live Loads	Element Types
(Aziz *et al.*, 2015)	A single girder	ANSYS	Load level; Web slenderness; Spacing of stiffeners;	Temperatures measured in fire tests were applied as a thermal-body-load at the nodal points of the girder	Unknown	Structure: SHELL181 and SOLID185 Contact: CONRA174 and TARGE179
(Alos-Moya *et al.*, 2014)	A single girder	ABAQUS	With and without abutment restraint; Live load	CFD fire model Standard fire Hydrocarbon fire	1.2, 2 and 4 kN/m	Structure: C3D8
(Wright *et al.*, 2013)	The main span was modelled by removing the skew	ABAQUS	Fire intensity (vehicle type); Fire location; Beam material; Vertical clearance; Fire duration (heating + cooling phase)	CFD fire model	None	Deck and girders: quadratic solid elements
(Dotreppe, Majkut and Franssen, 2005)	A tied-arch bridge	SAFIR	Traffic loads	Hydrocarbon fire	Various traffic loading cases	Main structure: 3D beam elements Suspenders: truss elements

2.4.2 Parametric Study

In the past five years, several researchers have investigated the structural behaviour of bridge components under fire loading through FE models or experiments, mainly on a single composite girder (Aziz and Kodur, 2013; Aziz et al., 2015; Naser and Kodur, 2018). Parameters affecting failure time/mode, such as web slenderness and spacing of stiffeners, have been studied. The estimated failure time and failure mode of a single component is questionable to represent the failure behaviour of a whole bridge frame. Therefore, other researchers (Alos-Moya et al., 2014; Choi et al., 2012; Peris-Sayol et al., 2015b) have simulated full-scale bridges and Alos-Moya et al. (2017) conducted a 6-metre span bridge test in Valencia which will be discussed in Section 2.5. In these studies, certain key factors which may affect bridge fire resistance have been discussed, including vertical clearance (Peris-Sayol et al., 2015b; Wright et al., 2013), fire intensity (Wright et al., 2013), fire position (Wright et al., 2013), the exposure scenario, the number of spans (Peris-Sayol et al., 2015b), bridge shape (Hu et al., 2018), material types (Payá-Zaforteza and Garlock, 2012; Wright et al., 2013) and load combination (Alos-Moya et al., 2014; Dotreppe et al., 2005; Gong and Agrawal, 2015; Payá-Zaforteza and Garlock, 2012).

The simulation of abutments has been considered in FE models (Alos-Moya et al., 2014; Payá-Zaforteza and Garlock, 2012; Peris-Sayol et al., 2015b) since Payá-Zaforteza and Garlock (2012) first studied their influence on structural response. Then, Hu et al. (2018) conducted simulations including the abutment for a skew shape bridge and concluded that modelling the abutment is of little benefit for both rectangular and skew shape bridges.

The main challenge for simulating the structural response of bridges is validation, due to a lack of experimental data. Some studies have used other fire test results and validated by comparing the deformation (Gong and Agrawal, 2015; Wright et al., 2013), in which experimental results for building compo-

nents were used (Gong and Agrawal, 2015). These case studies used estimated or observed accident information such as deflection (Alos-Moya et al., 2014) or the decrease of temperature along the span (Dotreppe et al., 2005) to compare with simulated results.

2.4.3 Failure Criteria

Failure criteria are necessary for interpreting results of the structural analysis of the effect of fire on bridges. This section discusses the global and local failure criteria specifically for bridges in fire. Global failure is determined to happen when:

- Runaway behaviour of deflection in the slab or beams (drastic increase in the rate of vertical deflection)
- Reversal of horizontal displacement at the free end-supports. This would suggest that the bridge span has softened to a point where the loads overcome the effect of thermal expansion (Lamont et al., 2003; Usmani et al., 2001) and the ends of the structure are pulled back towards the centre
- If the inward horizontal displacement at the free end exceeds the distance between bearing centreline and abutment edge, this will indicate that the superstructure has lost vertical support
- British Standards criteria (BS476-20:1987): a beam shall be regarded as failed if there is no capacity to support the test load which is determined if either of the following empirical criteria are exceeded:
  - A deflection of $L/20$

- The rate of deflection (in mm/min), calculated over 1 min intervals, on each minute from the commencement of the heating period, exceeds the limit set by the following equation:

  Rate of deflection = $L^2/9000d$

  Where L is the clear span (mm) of specimen, d is the distance (mm) from the top of the structural section to the bottom of the design tension zone. *Note this rate of deflection limit shall not apply before a deflection of* $L/30$ *is exceeded*.

  Note that the code-based failure criteria are based on standard furnace tests which do not account for the complex behaviour in a 3D bridge. Therefore, the BS476 criterion is merely a reference and should not be considered as true indicator of failure. For example, the above criteria for global failure have been used in Hu et al. (2018) showing no global failure in a bridge model. However the maximum deflection is more than 0.5 m which shall be replaced in reality.

Local failure is determined to happen when:

- Exceeds bending moment capacity
- Exceeds shear capacity
- Fracture occurs, which is assumed to happen when the ultimate strain of the material is attained. This mode of failure is checked by comparing the maximum principal strain of the structure with ultimate strain based on true values.
- A sudden change in the out-of-plane displacement, which implies the failure due to the initiation of web buckling.

2.5 Experiments

Due to expensive cost and complicated performance, the available tests were mainly performed on structural components of bridges, such as composite girders (Aziz et al., 2015). The first whole bridge test, reviewed in this section, overcame the limitations of furnace test.

Valencia Bridge Fire Tests (2017)

The first experiment of a whole bridge structure was conducted in Valencia, Spain, in 2017 (Alos-Moya et al., 2017) and experimental data has been used to validate CFD models performed by FDS (Alos-moya et al., 2019). The bridge was a one span (6 m) steel grillage consisting of two girders, compositely supporting a reinforced concrete slab. The fire was represented by a square fuel pan and was placed under the bridge. In total, eight tests in four scenarios were performed with considerations of different fuel bed sizes, fire magnitude and locations (varied at both longitudinal and vertical direction). Two types of square pan dimensions have been used with side lengths of 0.5 m and 0.75 m, corresponding to fire magnitudes of HRR 415 kW and 1131 kW, respectively. In the tests, the deflection of the bridge deck was monitored while the results showed a small deflection. The results provide validation for numerical studies and proves the temperature decay along bridge span is significant and cannot be neglected.

2.6 Risk Assessment

Risk assessment is useful for ranking the priorities of structures that need fire protection or other strategies. Some authorities have been working on risk assessment for bridges in recent years. Following the scrapyard fire which oc-

curred beneath the M1 near Mill Hill, North London in 2011, the Secretary of State for Transport requested that a survey be carried out by both the Highway Agency (HA) and Network Rail (NR) to identify the locations of bridge structures at potential risk. HA assessed the potential fire risk locations around the motorways and trunk roads in England. Their report (Highways Agency, 2011) provides recommendations for improving resilience in fire risk situations and suggests 50 priority locations which warrant further investigation. In the assessment, the vulnerability of the structure to fire damage was considered and 50 bridges and viaducts (out of a total of 3205 across the Strategic Road Network (SRN)) were identified as vulnerable.

A few studies have contributed to the future risk assessment policy for bridges. Naser and Kodur (2015) proposed an approach to assess the vulnerability of bridges to fires. This paper suggests fire resistance requirements for various fire risk categories. Quiel et al. (2015) proposed a framework for analysing bridge structural response. This framework synthesizes calculation techniques to provide an efficient tool for industry, although not using a detailed analysis. Liu et al. (2017) proposed a method to evaluate and classify fire risk of liquid chemical transport vehicles passing highway bridges. An application was demonstrated for the Taizhou Bridge.

2.7 Review and Knowledge Gaps

2.7.1 Fire Models

The observations from past accidents and collected information can be used to identify potential fire scenarios that could result in bridge failure. According to the review, the fire hazard in bridges is typically associated with gasoline spillage from vehicle fire incidents.

Most severe damage is caused by accidents under the bridge. While fire incidents have occurred on top of the bridge deck, this usually has very limited influence on the bridge structure, such as the cab fire on Blackfriars bridge (Vulliamy, 2017) and the car fire on Aberdeen bridge (Aitken, 2017). This was also proved by Peris-Sayol et al. (2016), showing the damage level is significantly higher when the tanker is under the bridge by analysing 154 cases of bridge fires. There has been only one accident on a bridge which resulted in severe damage, this was however due to the fuel spillage which spread downwards (Peris-Sayol et al., 2016).

Fully developed fires have the greatest impact on structures which can be used for conservative analyses. Uniform fire is widely used such as the Hydrocarbon fire. However the detailed analyses of bridge performance under uniform or prescriptive fires is potentially unrealistic and can be over conservative. A heterogeneous fire model is therefore needed. This can be achieved using fire inputs from CFD models or other fire curves, with spatial decay considered.

The fire duration can vary with the bridge material. The author suggests a 20-min fire duration for a vehicle fire under concrete/steel bridge, however up to 15 hours fire duration has occurred in wooden bridges (BBC NEWS, 2013). Usually a growth rate of 5 MW/min corresponds to a tunnel fire under low ventilation conditions (Carvel, 2008) which is broadly similar to the situation under a bridge, since peak intensity would be reached very rapidly in an open environment. The value of HRRPUA used in FDS models is suggested not larger than $2500\,\mathrm{kW/m^2}$.

2.7.2 Structural Models

FE simulations are able to offer low-cost assessment to avoid the necessity of conducting complicated and expensive full-scale tests. Also, we can learn how

the structural design affects the performance under fire. However, this requires the knowledge of finite element or fluid dynamics and may lead to extensive user effort and simulation times.

According to the HA report (Highways Agency, 2011), there are over 17,600 structures within the Strategic Road Network (SRN), including 3205 bridges and viaducts. 1558 of these structures have clear spans in excess of 5 m. Therefore such bridges with spans larger than 5 m should be the top priority for studying.

Not all the studies considered live loads on such bridges in fire, which is a reasonable assumption as the massive black smoke would be a clear stop signal for the drivers. There appear to be no simulations studying wooden bridges in fire, which often have historic and cultural value. Peris-Sayol et al. (2016) found that there are no statistically significant differences in the fire response of composite, concrete or steel bridges, although composite bridges seem to sustain higher average damage than the other two types.

Different types of finite elements can be used for different purposes. Shell and solid elements can be used to capture local phenomena such as web buckling that might determine the global response and the failure mode of the bridge. For most bending dominated problems beam and shell elements are much more efficient and accurate than solid elements (Simulia, 2012). 3D beam elements deal with large displacements, material non-linearity and progressive spread of plasticity within the cross-section as well as along the length of elements. Structural beam-column elements can be used for a low-cost analysis if local buckling behaviour is not important. This may be of interest to practising engineers.

The key result that researchers are most interested in is displacement, but this is sensitive to the applied boundary conditions (BCs). However, it may sometimes be difficult to model the BCs that can provide the accurate predic-

tion of displacement. Other outputs such as section force, reaction force and bending moment can be reliable indicators to understand the load distribution.

Given the stiffeners are commonly designed, local buckling which may not result in the collapse of the bridge can be neglected for ordinary bridges to avoid over-conservative design. The accepted criteria should vary with different bridge types.

2.7.3 Risk Assessment

Performance based structural fire engineering is beginning to have an impact on bridge design, because of limited information from codes and standards and increased understanding of structural fire response from building fires and case studies of bridge fires.

The main reasons for bridge failure induced by fire are usually a combination of structural damage including compromised structural steel, or buckled girders or supports. Therefore the vulnerability of those structural components can be ranked. Similar to building fire design, reduction factors can be used to establish a level of safety.

Implementing design codes which require engineers to follow prescribed maximum credible vehicle fires, similar to other actions such as earthquake, wind and floods is desirable. However, there is no need to consider the fire load at all locations. A priority list can be presented to rank the locations which are critical for a vehicle fire to occur. Simulation packages can be used to perform fault-tree analyses to determine the factors and potential failure modes leading to a failure.

2.7.4 Experiments

To the author's knowledge, there have been very few tests to understand bridge fires, and most of these tests were performed using small fuel pools. In order to truly understand the response of bridges subjected to fires, CFD fire models have been applied by researchers to allow the possibility of a decay of heat fluxes along the span away from the fire, which is not provided by prescriptive curves.

2.7.5 Suggested Policy for Government

As presented at the beginning of this chapter, severe fire accidents which have consequences for bridges are not as rare as might be generally perceived. Therefore code implementation should be considered. Similar to building codes, prescriptive design is needed especially for common bridge types, which would not be affected too much by the limitations of codes. The design fire loads could be considered in a similar way to design loads of wind or earthquakes.

Highways Agency (2011) reported that there are more than one third of bridges and viaducts have clear spans in excess of 5 m. Therefore, the government could focus on setting up regulations for only the bridges with span larger than 5 m. Defining an allowed fire resistance time can be a start for code implementation, and remaining operational after damage may be a key requirement.

Legal storage beneath bridges and flammable goods in adjacent areas are another reason of fire accidents. In the I-85 Overpass accident in the USA in 2017, the material had been stored in the area for as long as 6 years (Hanna and Rodgers, 2017). Following this accident, CNN (Hanna and Rodgers, 2017) contacted departments of transportation about the storage policies in all 50

states and got responses from 44 of them. "*Some said that material under bridges are not allowed, but practices vary from state to state, and even the definition of 'hazardous' may be part of the reckoning. Until now, Maryland might have allowed contractors or its own workers to store high-density polyethylene on state-owned space under bridges during a construction project.*" The positive news is that *"some DOTs have decided to draft or revamp written policies"* according to CNN.

The same issue also exists in the UK, for example the M1 Motorway's Deans Brook viaduct accident which happened in 2011 (Highways Magazine, 2012; Summers, 2012), where the fire started in a scrapyard. After this fire, the Highways Agency (HA) and Network Rail undertook a high level scoping study to understand "*the scale of potential risk from activities beneath and adjacent to the elevated sections.*" According to the report (Highways Agency, 2011), "*To reduce the need for compensation payments, avoid severance and prevent sterilization of land, it has been government policy since the 1960's to generally acquire only land required to accommodate the footprint of any bridge piers or abutments needed to support structures.*" This policy therefore results in the difficulty of managing material storage on land not under HA ownership. It was found that some high-risk locations have restrictive covenants on land immediately beneath bridges on the network. This report developed a risk assessment criterion and scored the structure vulnerability for prioritization ranking, which shows that structures with a reinforced concrete deck have a lower risk than those structures with vulnerable features (e.g. pre-tensioned, post-tensioned and steel beams etc.).

The industrial estates underneath the motorway flyovers are common in the UK. A simple ban of sites or car parking under the bridges are not recommended as social influence outweigh the potential fires. However, for critical bridges or motorways, management should intervene to mitigate the fire risk.

Immediate attack of a small fire may have the greatest effect in avoiding a major incident. First aid firefighting such as hand-held extinguishers can be the most cost-efficient way to prevent the fire damage to the bridges.

Various types of storage or parking also happen in Asian countries, such as South Korea (Joo et al., 2017). Joo et al. (2017) carried out a field survey to investigate the exact risk due to fire on bridges. It was found that construction materials and other flammable material such as tyres, furniture and straws stored under the bridge cause a potential hazard which may lead to a fire. Other risks include the fuel tankers parked under a bridge. Since 1990, the Korean government and public institutions "*had used spaces underneath bridges as parking lots and facilities for distribution, convenience and sport* (Park et al., 2018)". After the Bucheon viaduct accident in 2010, Korea Expressway Corporation (KEC) modified the practices by performing surveys, classifying representative materials under bridges, combustion tests, fire resistance tests and CFD simulations of the items (Park et al., 2018). Then, KEC assessed "*fire safety for all existing bridges in the metropolitan area*" based on the new modified manual.

2.8 Summary

The commuting function of bridges characterise the importance of this topic in comparison to other types of fire. Unlike the complexity of building fires, the worst case fire loading of bridges is easier to determine. This review analysed the existing research and suggests the knowledge gaps for future simulation and experiments.

Part I

ABAQUS Models + Hydrocarbon Fire

3

Fire Resistance of Composite Steel & Concrete Highway Bridges

3.1 Introduction

This chapter presents a thorough computational analysis of a composite steel framed bridge superstructure subjected to a large fire to investigate the effect of bridge shape, considering that skew bridge shapes are quite commonly used.

The insights presented here should help engineers to propose improved bridge structural systems and enable innovative design of structural elements to improve the inherent fire resistance of a composite steel and concrete bridge

superstructure.

The above purposes are achieved by simulating the thermo-mechanical response of bridges for both rectangular and skew shaped bridge superstructures with and without modelling the abutment. The investigation has been carried out in the following steps:

1) Heat transfer analysis under a specified Hydrocarbon fire;

2) Simulation of the thermo-mechanical response of the bridge superstructure over the entire duration of the fire using beam or shell elements to represent the structural components;

3) Detailed processing and interpretation of the simulation results to understand and illustrate the global and local response of the structure by comparing the models.

4) A collapse mechanism and failure phases specifically for bridges are clearly defined based on a well-defined criterion without recourse to ad-hoc considerations of deflections or deflection rates.

In assessing the eventual failure of the bridge, detailed descriptions of the thermo-mechanical response are presented as the authour has not found this kind of insight in existing literature. Composite behaviour has also been included, considering composite structural components experience thermal elongation and thermal bowing because of the heating from the fire. Thermal bowing induced rotation may cause the bridge superstructure to impinge upon the abutment due to its significant depth, therefore this effect has also been considered in the modelling.

3.2 The Stirlingshire Link Motorway Bridge

The models presented in this chapter are based on the Stirlingshire Link Motorway Bridge (see Fig. 3.1), which is located near Falkirk, UK. This bridge was constructed in 1980 (Irons and Turner, 2011), in order to connect the M9 and M876 motorways.

(a) **(b)**

Figure 3.1: The Stirlingshire link motorway bridge (Irons and Turner, 2011): (a) looking downlink on M9; (b) detail view of steelwork typical

The structural framing is a skew two-span steel grillage consisting of 1.1 m deep welded plated girder with internal diaphragms, supporting a 300 mm deep top slab which forms the carriage way. The spread footings on rock foundation provide three supports for the bridge. Two end supports are full height cantilever abutments, and the intermediate support is a solid wall pier. Transverse diaphragms are placed between the webs of the steel girders, which play an important role in the lateral stability of bridge girders and in evening out the distribution of the dead and imposed loads.

The original design of the bridge was provided by Transport Scotland, showing that the bridge consists of six primary beams with lengths 57.975 m, 56.870 m, 55.767 m, 54.666 m, 53.572 m and 52.480 m respectively. The primary beams are not exactly parallel to each other and the distance between concrete diaphragms also varies. The models used in this study are based on this bridge, however with simplified dimensions actually used as described in detail in Sec-

tion 3.4.1.

3.3 Thermal Analysis

To determine the impact of the fire on the bridge superstructure, a heat transfer analysis is first required in order to define the equivalent thermal regime to be applied to the structural models. A nominal fire curve, namely the Hydrocarbon fire (EN, 2002a), is used to perform a 2D uncoupled transient heat transfer analysis using Abaqus 6.12. The bridge is assumed to suffer a vehicle fire for 20 min, which could potentially result from a fuel tanker accident under the central girder of Span 2 (fire affected span, FAS, see Fig. 3.5). The 20 min fire duration is assumed based on a review of real bridge fire accidents (Kodur et al., 2013), which suggests that failure/collapse occurred at that level of exposure.

According to the drawings, the fire and hot smoke should be able to spread to Span 1 through the gap between top pier and steel sections. However, in this chapter, Span 1 (non-fire affected span, NFAS, see Fig. 3.5) is assumed to be insulated from the fire due to heat shielding effect of the central solid pier.

3.3.1 Model Description

The element DC2D4 was employed to construct the heat transfer models, which is a 4-node linear diffusive heat transfer quadrilateral element. The adopted size of mesh and discretization can be seen in Fig. 3.2, in which 1680 and 3900 elements are used to model the primary composite beam and the concrete transverse diaphragm respectively. A non-uniform mesh has been used in concrete slab, where more elements are used above the steel section to better capture the heat transfer between the concrete and steel. A mesh sensitivity study was performed by comparing the heat transfer results between

the primary beam model using only 420 elements and 1680 elements. It produces identical results which prove that even the coarser mesh is adequate for this study (Fig. 3.3).

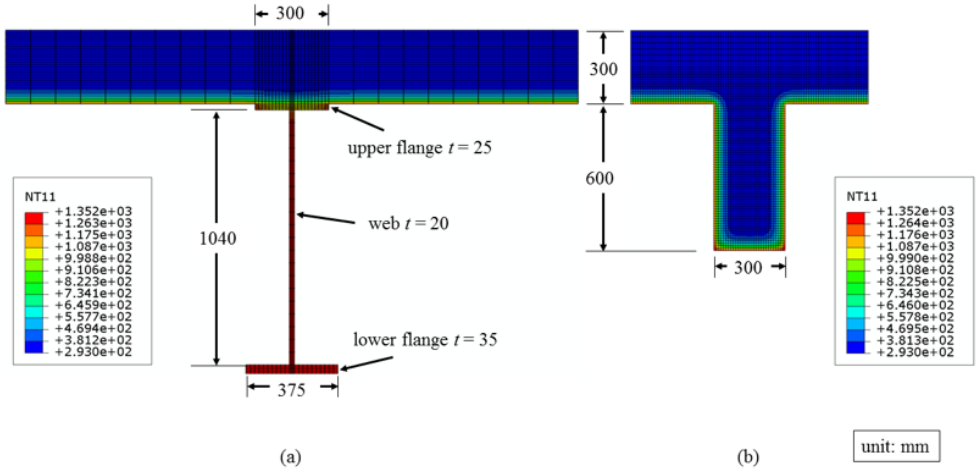

Figure 3.2: Heat transfer model at 20 min: (a) primary beam, (b) transverse diaphragm. All temperatures are given in K

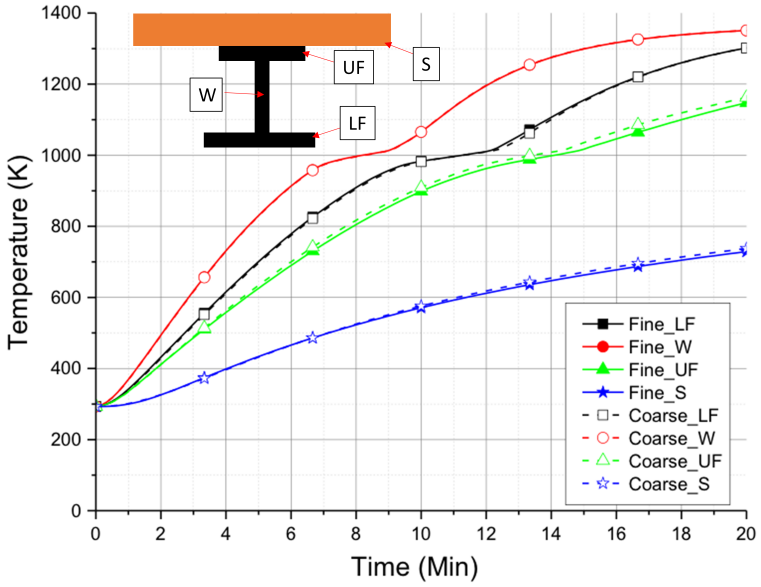

Figure 3.3: Primary beam model heat transfer results using fine mesh (1680 elements) and coarse mesh (420 elements)

In the heat transfer models, the exposed surfaces of both sections received the incident heat flux through the mechanisms of convection and radiation,

while the slab is assumed to be heated from the bottom only. The upper unexposed surface of the slab is allowed to lose heat by convection and radiation to ambient air. Thermal boundary conditions are specified as prescribed temperature, surface convection (Eq. 3.1) and radiation (Eq. 3.2)).

$$\dot{q}^{"} = h(\theta - \theta_0) \tag{3.1}$$

$$\dot{q}^{"} = \varepsilon\sigma(\theta^4 - \theta_0^4) \tag{3.2}$$

Where $\dot{q}^{"}$ is the heat flux, *h* is the film coefficient, θ is the prescribed temperature, θ_0 is the sink temperature, ε is the emissivity, σ is the Stefan-Boltzmann constant.

Radiation and convection boundary conditions were specified for both the fire-exposed and unexposed surfaces of the structure. The convection coefficient (Franssen et al., 2009) was set to $50\,\mathrm{W/(m^2K)}$ for fire-exposed surfaces under Hydrocarbon fire and $4\,\mathrm{W/(m^2K)}$ for the unexposed surfaces. Some of the literature studies (Aziz et al., 2015) use $25\,\mathrm{W/(m^2K)}$ for the unexposed surfaces which should also be reasonable as this chapter performed a sensitivity study and proves that no differences are caused by the value of convective coefficient used for the slab top. This is due to the thick depth ($300\,\mathrm{mm}$) of a bridge deck. An effective emissivity factor of 0.7 was used for both concrete and steel at all surfaces (EN, 2004, 2003a).

Heat conduction is assumed governed by the Fourier law: $\dot{q}^{"} = -k\frac{\partial\theta}{\partial x}$, where k is the thermal conductivity and x is the position. Isotropic thermal conductivity and specific heat are used for both steel and concrete and assumed to vary with temperature in accordance with Eurocode (EN, 2004, 2003a). The upper limit of thermal conductivity of normal weight concrete composed of siliceous aggregate was adopted in the study for a more conservative result

as calcareous aggregate concrete has better performance in terms of residual strength at elevated temperatures.

3.3.2 Heat Transfer Analysis

The temperature variation along the composite section is determined as a function of fire exposure time from the heat transfer analysis as shown in Fig. 3.4. As expected, the temperature in concrete is significantly lower than that in the steel section due to its lower thermal conductivity. Also, the steel web heats up at a much higher rate compared to the flanges due to its smaller thickness. The upper flange has a lower temperature because of the heat loss to the adjacent concrete slab. However, because of the high thermal conductivity of steel, the temperatures at different positions in the steel section would tend to approach the same value after about 30-min exposure (not shown in Fig. 3.4 as this is beyond the time of interest in this analysis).

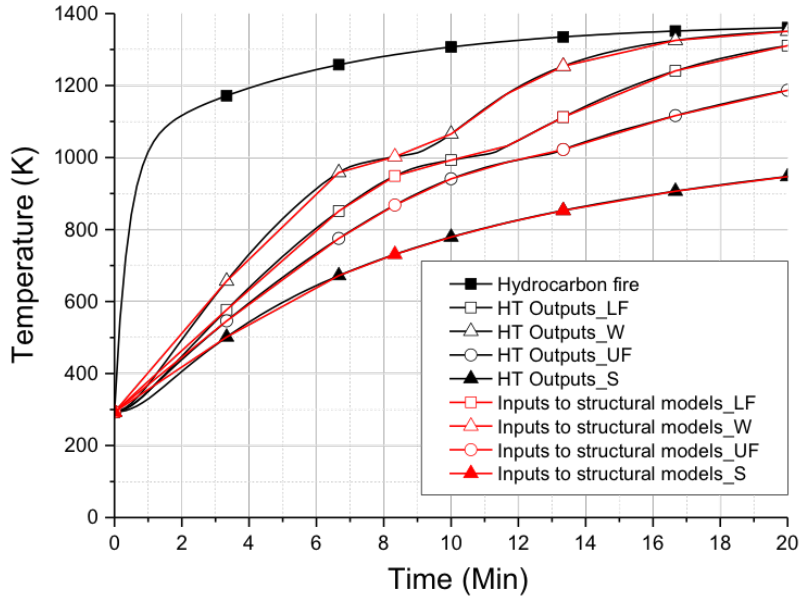

Figure 3.4: Temperature evolution with time within the composite section, comparison of heat transfer analysis and structural model inputs

The output temperature variations from the heat transfer analysis were applied to the structural model using smaller time steps, in order to apply the thermal loading regime with small increments. As shown in Fig. 3.4, the temperature profile applied to the structural model is sufficiently close to that obtained from the heat transfer analysis and should produce an acceptable simulation of the structural response.

3.4 Structural Models (Shell Element for Slab Only)

This section investigated the effect of bridge shape on the structural response of a highway bridge under Hydrocarbon fire. To analyse the global behaviour of the bridge models with a relatively low cost analysis, the FE models are built using beam elements for primary steel girders and shell elements for the slab only. The local buckling effects that may occur in the web or flanges of the composite steel girders will be analysed in Section 3.5, by using shell elements instead of beam elements to model the primary steel girders.

3.4.1 Geometry

In order to investigate the influence of bridge shape and abutment restraint, discretised models have been built to conduct thermo-mechanical analysis, using rectangular or skew models with and without the modelling of abutment restraint.

The dimensions of the skew bridge based on the drawings were regularised (see Fig. 3.5a) to obtain more generic results. Five primary beams were used to capture the behaviour of the central region of the structure accurately. All the beams have identical lengths of $57.6\,\mathrm{m}$ (from North to South, namely BEAM

No.1 to BEAM No.5) and the distance between primary beams and transverse diaphragms are kept constant at 3 m and 4.8 m respectively.

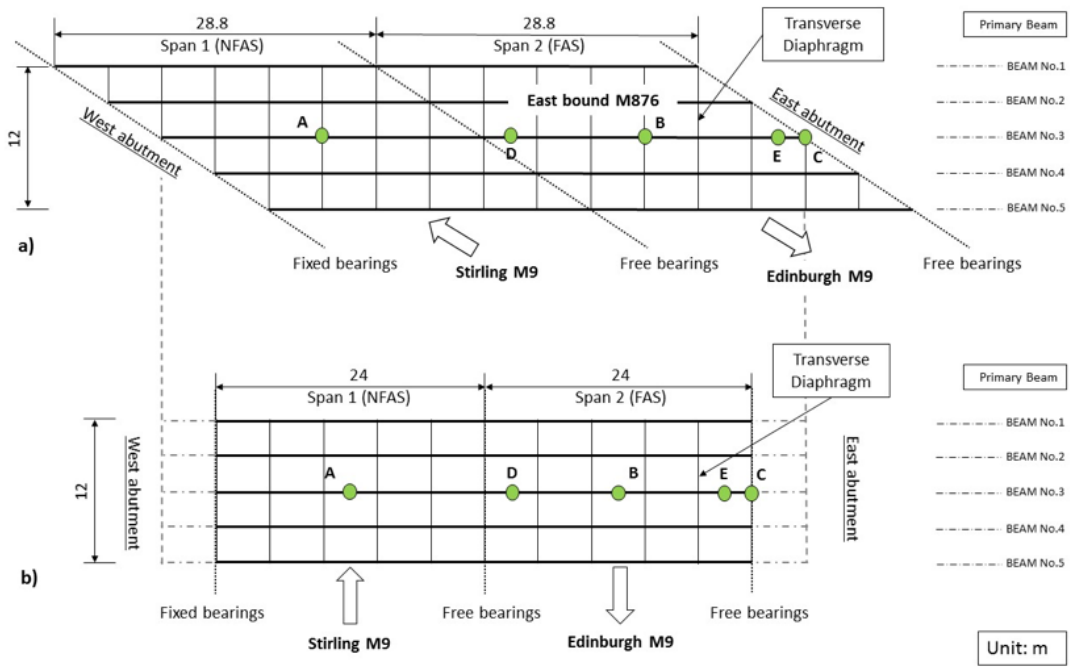

Figure 3.5: Schematic representations of the skew (a) and rectangular grillage (b)

The rectangular models were studied in order to establish the baseline structural behaviour of a similar span non-skew bridge. However, it is not possible to perform a like-for-like comparison of a rectangular bridge with a skew shape bridge as there is no clear equivalence between these two very different structural systems with significantly different structural behaviour. Estimation of an equivalent span length in a rectangular bridge is difficult as the effective span length in a skew shape bridge is not well defined. However, it is important to establish the reference behaviour of a somewhat similar rectangular bridge to understand the skew bridge behaviour better.

The rectangular bridge plan was defined to be consistent with skew bridge with a grillage framework composed of primary universal beams and trans-

verse diaphragms arranged in a 48 m x 12 m grid (Fig. 3.5b). Like the skew shape, the distance between primary beams and transverse diaphragms was defined as 3 m and 4.8 m respectively. A total length of 48 m (based on 4 diaphragms spaced 4.8 m apart in each span) was assumed for the rectangular bridge models compared to 57.6 m (6 diaphragm spacings per span) for the skew bridge models. This is relatively arbitrary but a conservative estimation for comparison purposes. Using the same beam length in both shapes (as the extended dash dot lines show in Fig. 3.5b would obviously make the rectangular bridge too weak compared to the skew bridge because the rectangular bridge can only carry loads in one-way bending. The skew shape provides additional capacity because of the contribution from two-way bending and the intrinsically stiffer behaviour from the reserves due to torsional serviceability requirements. Therefore, a shorter span has been used for the rectangular bridge to allow for some equivalence, but as mentioned earlier, this is not a like-for-like comparison but simply a device to provide a contrast or reference to understand the skew bridge behaviour better.

3.4.2 Material Properties

The properties of carbon steel and concrete at ambient and elevated temperatures are defined according to the Eurocode values. The stress-strain curves are proposed as a function of temperature, in which the maximum yield stress of the steel at ambient was taken as 275 MPa and the concrete has a maximum compressive strength of 30 MPa.

The concrete constitutive behaviour is assumed to be consistent with the damaged plasticity and smeared crack model for slab and transverse diaphragms respectively in Abaqus. The tensile strength of the concrete was defined as 10% of the compressive strength with a minimum value of 0.1 MPa. This may be deemed to be unrealistic as far as it allows the concrete slab to absorb more

energy in tension than it would in a reality due to limited ductility. This issue should not overly affect the global response of the model as thermal strains act in a compensating manner to the tensile strains and enhance the available ductility.

3.4.3 Applied Loads

The applied loads include mechanical and thermal loads. In the mechanical part, transient loads such as the vehicular gravity load are not included based on the assumption that no vehicles would pass over the bridge when smoke and flames are visible below. The self-weight of beams, slab, parapet and pavement are considered as follows:

1) The self-weight of beams and slab are applied automatically through the defined dimensions with density of steel and concrete equal to $7850\,\mathrm{kg/m^3}$ and $2400\,\mathrm{kg/m^3}$.

2) Parapet: P1 type parapet which is a three-rail, cast-in post, steel parapet has a very small self-weight and therefore is neglected for the purposes of this chapter.

3) Pavement: 100 mm surfacing with hot rolled asphalt of $23\,\mathrm{kN/m^3}$ density (EN, 2003b), is applied as surface load in the Abaqus models.

As per the applied load above, in the rectangular models, the total load applied is $764.8\,\mathrm{kN}$ for primary beams, $406.4\,\mathrm{kN}$ for transverse diaphragms, $5080\,\mathrm{kN}$ for slab and $1656\,\mathrm{kN}$ for the pavement. In the skew models, the resulting total load is $918\,\mathrm{kN}$ for primary beams, $610\,\mathrm{kN}$ for transverse diaphragms, $6096\,\mathrm{kN}$ for slab and $1987\,\mathrm{kN}$ for the pavement.

Once the self-weight is applied, the thermo-mechanical analysis step commences. Since the central pier is a solid wall, the fire is considered to be

intense within FAS when caused by a tanker accident. Therefore, this chapter assumes the fire to be uniformly spread across FAS.

3.4.4 Finite Element Models

The models were developed as a superstructure made out of a grillage of steel beams and concrete diaphragm acting compositely, with the concrete shell representing the carriageway. Each finite element in the model represents a discrete segment of the beams and slab. The B31 element was used for the primary beams and transverse diaphragms, which is a first-order, 2-node linear Timoshenko beam allowing for transverse shear deformation. For a more realistic and rigorous structural representation of concrete slab, the shell element S4R was adopted which is a 4-node, quadrilateral, stress/displacement shell element with reduced integration and a large-displacement formulation.

Only structural elements (beam and shell element) are used in the models because: 1) to demonstrate the utility of a relatively low cost analysis that would be of interest to practicing engineers considering this problem; 2) for most bending dominated problems beam and shell elements are much more efficient and accurate than solid elements (Simulia, 2012); 3) Based on SCI steel and composite bridge structures report (Iles, 2012), the girders in the models will fail by yielding (275 MPa) rather than flange or web buckling (theoretical critical stress is 2136.51 MPa and 1597.71 MPa, see calculations below).

$$\sigma_{cr} = \frac{k\pi^2 D}{td^2} = \frac{k\pi^2 E}{12(1-\nu^2)(\frac{d}{t})^2} \tag{3.3}$$

1) Buckling of web:

   Web slenderness d/t = 52, k= 23.9. σ_{cr}= 1597.71 MPa.

2) Buckling of compression flange:

   Flange slenderness d/t = 6, k= 0.4255. σ_{cr}= 2136.51 MPa.

The undeformed view of the rectangular and skew models (with and without the abutment) with rendered section profiles are shown in Fig. 3.6. Non-linear geometry is toggled on in the FE models. Reinforcement has been included in the slabs as a smeared layer of steel with the sectional area running through the slab. According to the drawings, the diaphragm steel is threaded through predrilled holes in the steel web of the beams. The steel in the diaphragm is included in the models.

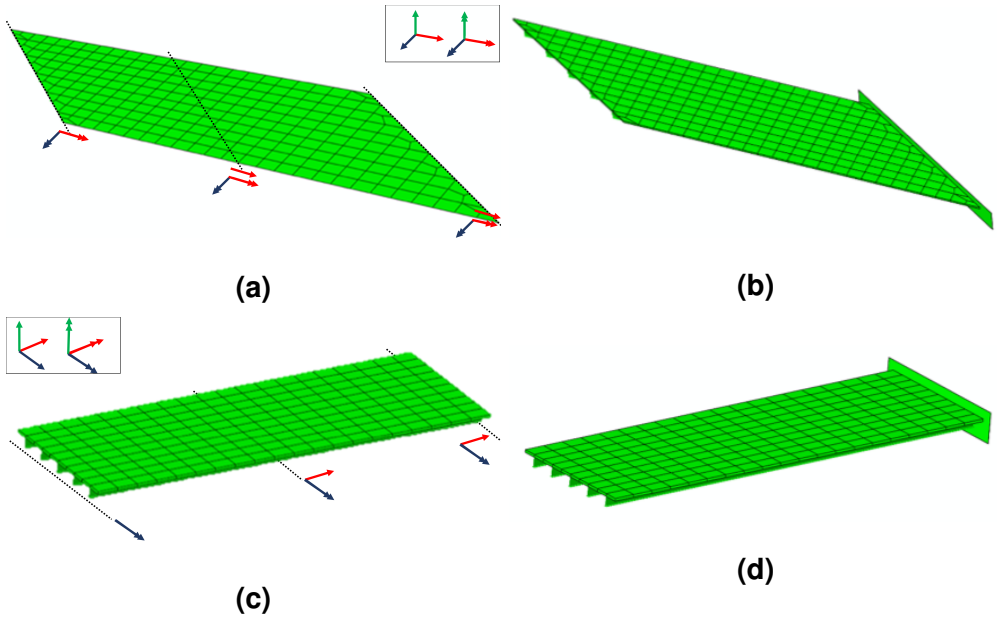

Figure 3.6: Skew models without (a) and with (b) abutment; and rectangular models without (c) and with (d) abutment

The influence of the expansion joint width has been partially studied in Payá-Zaforteza and Garlock (2012); Peris-Sayol et al. (2015b) for non-composite bridges with a small span (12.2 m) and Alos-Moya et al. (2014) for composite bridges in the event of Alabama bridge fire. In this chapter, this effect is fully considered as the horizontal movement of the right support is expected to exceed the width of the expansion joint. Therefore a rigid surface is modelled using R3D4 elements to simulate the abutments, and is placed at a distance of 125 mm from the right end of primary beams to model the free expansion joint

gap. This type of element is used to provide a reaction to the superstructure when it impinges upon the abutment.

3.4.4.1 Boundary Conditions

Simple rigid boundary conditions are used in the static analysis, and the support or foundation stiffness is not considered. According to the bridge drawings, the bearings at the west abutment are fixed, while the bearings at the central pier and the east abutment are free. Therefore, for the rectangular models (shown in Fig. 3.6c), the primary beams were fully fixed in 5 degree of freedoms (DOFs) at the left support other than the rotation about the horizontal axis perpendicular to the longitudinal beam axis. At the middle and right support, the horizontal displacement and the same rotation are free while all other DOFs are restrained. The two ends of the concrete deck are also vertically constrained using roller supports, while there is no support defined at the middle support for the concrete slab because of its composite connection with the primary beams. For the skew models (shown in Fig. 3.6a), boundary conditions are the same except that rotation is free about the longitudinal beam axis at all supports.

Composite action between the primary beams and concrete slab is achieved via multiple point constraints (MPCs). All nodes along the length of the beam and the corresponding slab nodes are so constrained. MPCs were also defined between the diaphragms and the slab to ensure that they acted as a single section in the transverse direction.

3.4.5 Thermo-mechanical Analysis

This section describes the global response of the bridge models to a Hydrocarbon fire with special consideration for the effect of abutment restraint. The

analysis results are presented in various forms in order to gain useful insight into the fire resistance mechanisms of composite steel bridge superstructure. The following outputs are reported for both rectangular and skew bridge models to illustrate the response:

1) Deflection at the mid NFAS and FAS (Points A and B in Fig. 3.5);
2) Horizontal displacement at right end pinned support (Point C in Fig. 3.5);
3) Variation of deflection with time along NFAS;
4) Horizontal steel section force near middle and right support (Points D and E in Fig. 3.5);
5) P-delta moment generated when the bridge impacts the abutment;
6) Vertical reaction force at all three supports;
7) Composite bending moment along both NFAS and FAS.

3.4.5.1 Defined Phases of Bridge Structural Response

Progressive bridge damage is a dynamic process where the structure transits between alternative equilibrium paths. The structural response of the bridge during fire can be divided into the following three phases based on the change in flexural stiffness of the bridge structure and the effect of thermal bowing upon it. Table 3.1 describes the key structural features in each phase.

1) *Phase I*: High flexural stiffness with low thermal bowing.
2) *Phase II*: Reduced flexural stiffness with increased thermal bowing.
3) *Phase III*: Impending global failure.

Table 3.1: Key structural behaviours during fire

	Curvature in FAS	Curvature in NFAS	Load Redistribution	U1 Reversal
PHASE I	Sagging curvature	From sagging curvature to the maximum hogging curvature (or negative curvature)	FAS attracts more load	N/A
PHASE II	Sagging curvature with an increasing rate of deflection	Reduction in hogging curvature	FAS begins to shed the overload	N/A
PHASE III	Runaway deflection	Sagging curvature at a relatively steady state	Load redistributes from FAS to NFAS	Yes

Phase I is the period where the temperature increases in FAS while the bridge stiffness remains largely unchanged. In this phase, the two spans are initially in sagging curvature because of the applied self-weight. Then, FAS deflects further downwards due to the increasing thermal gradient in the bridge structure which introduces a curvature resulting in thermal bowing (Lamont et al., 2003; Usmani et al., 2001). Meanwhile, NFAS deflects upwards to a maximum hogging (or negative) curvature enforced by the compatibility of deformation due to the continuity of the composite structure over the middle support. Horizontally, the free end in FAS displaces outwards due to thermal expansion.

Phase II is the period where thermal bowing increases together with strong reduction of stiffness. During this phase, FAS continues to deflect downwards at an increasing rate because of the reduced stiffness and NFAS begins to deflect downwards after reaching a maximum hogging curvature also due to reduction of rotational stiffness over the middle support. The free end of FAS continues to displace horizontally outwards.

Phase III is the period where global collapse occurs. This phase starts when the outward horizontal displacement of the right ends of the beams begins to reverse. This can be considered to be the onset of global structural instability of the bridge. During this phase, the rate of deflection in FAS accelerates and runaway behaviour can be observed. NFAS continues to deflect in

sagging curvature at a relatively steady rate.

3.4.5.2 Rectangular Models

The deflected shape of the model with and without abutment at 20 min of fire are shown in Fig. 3.7. This demonstrates that all composite primary beams have nearly identical behaviour resulting in a 'striped' pattern contour plot with maximum downward displacement near the middle of FAS. BEAM No.3 is therefore analysed and plotted in graphs as a representative beam.

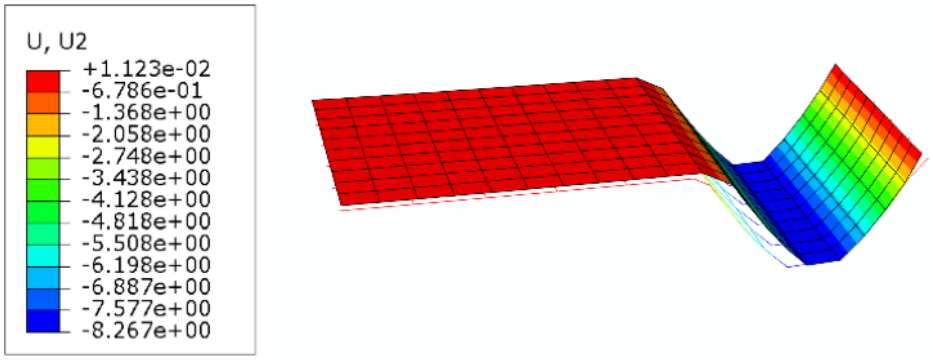

(a)

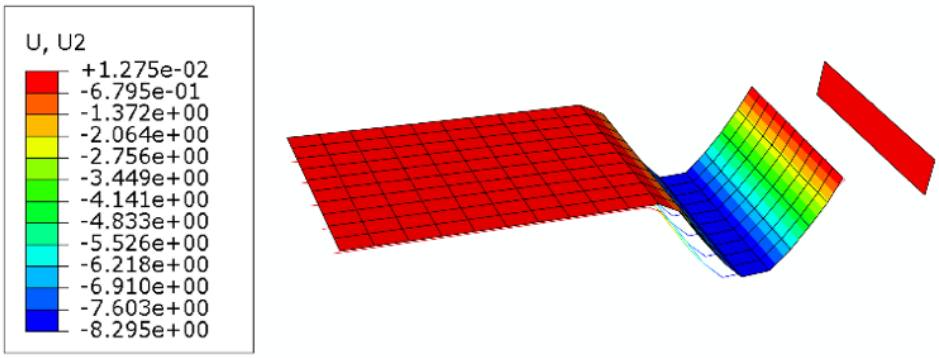

(b)

Figure 3.7: Deformed rectangular model without (a) and with (b) abutment after 20 min of fire. All deflections are given in m

Fig. 3.8 compares the deflection history at mid FAS and mid NFAS with deflections beyond 2 m not plotted for better observation of physical phenomena.

The deflection behaviour is identical for both models in Phase I and Phase III showing that abutment has little effect on deflection during these phases. During Phase II, in the model with the abutment, NFAS has an additional upward deflection. This is because of the abutment restraint, inducing an increasing compressive force along the section. While FAS seems to deflect slower after impacting the abutment up to 10.3 min (Period A, shown in Fig. 3.8). At the end of Period A, the model shows a sudden increase in deflection and then stabilises until the beginning of runaway collapse in Phase III (identified as Period B in Fig. 3.8).

The phenomena seen in Period A and Period B can be explained by the P-delta effect (see Fig. 3.9), which is derived from the eccentric horizontal reaction force at the abutment, located at the bottom of the steel section. During Period A, the girder longitudinal axis is above this resisting force, when the deflection in FAS is relatively small compared to the span length $24\,\mathrm{m}$ (4%). This causes a hogging (negative) moment which acts against the increasing thermal bowing curvature. During Period B, the girder longitudinal axis moves below the abutment reaction force resulting in a sudden increase in deflection in FAS.

Fig. 3.10 presents the horizontal displacement of free end during fire, it shows that displacement starts to change direction (inward) after 10.3 min when there is no abutment indicating the onset of collapse and after 11.7 min when the abutment exists. The deflected shapes along NFAS are also plotted in Fig. 3.11 during the fire at key time points.

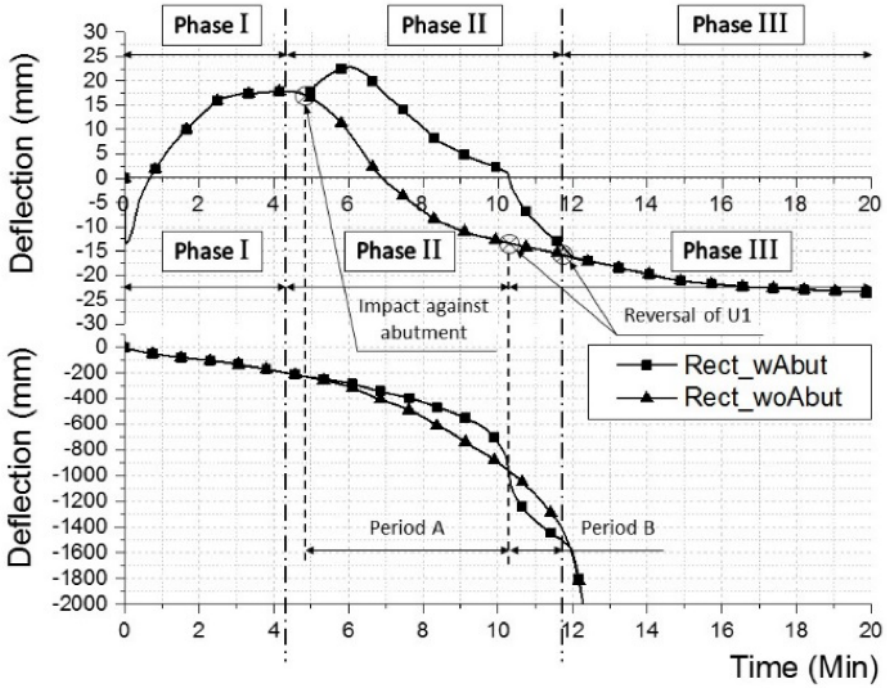

Figure 3.8: Comparison of the mid NFAS (top) and mid FAS (bottom) deflection variation with time

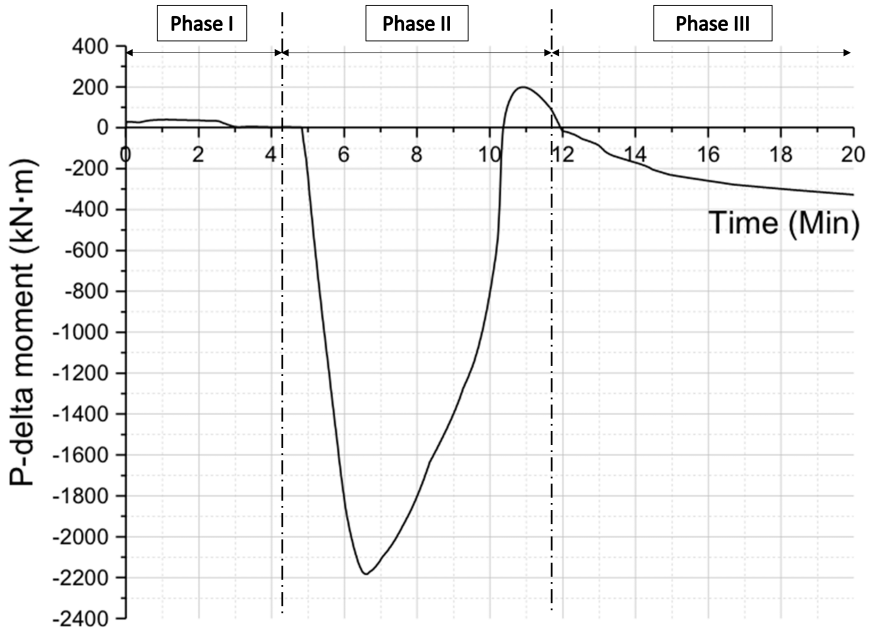

Figure 3.9: Change in P-delta moment with time in BEAM No.3 (rectangular model with abutment)

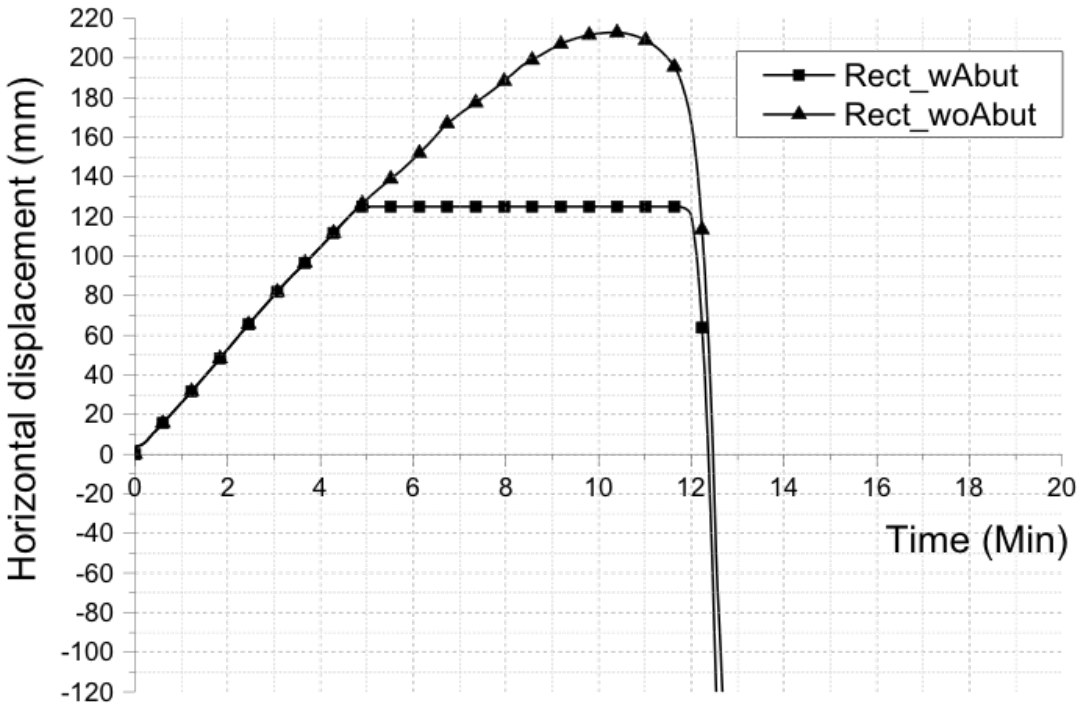

Figure 3.10: Comparison of the horizontal displacement at the right support

Fig. 3.12 illustrates the comparison of horizontal steel section force between the rectangular models. In Phase I, the composite connections, of hot steel section to the relatively cooler concrete slab, restrain the thermal elongation of steel beam creating compressive force along the beam and tensile force in the concrete slab. The compressive force in the steel section near middle support increases due to the additional hogging moment caused by the rotational restraint at the middle support and thermal bowing in FAS. During Phase II, the steel section of the model without abutment attracts no further compression due to material degradation. While the model with abutment has an increasing compressive force derived from the thermal-expansion-induced abutment restraint force. At the end of Period A, the right support compressive axial force suddenly decreases because of the reversal of the P-delta moment (as shown in Fig. 3.9).

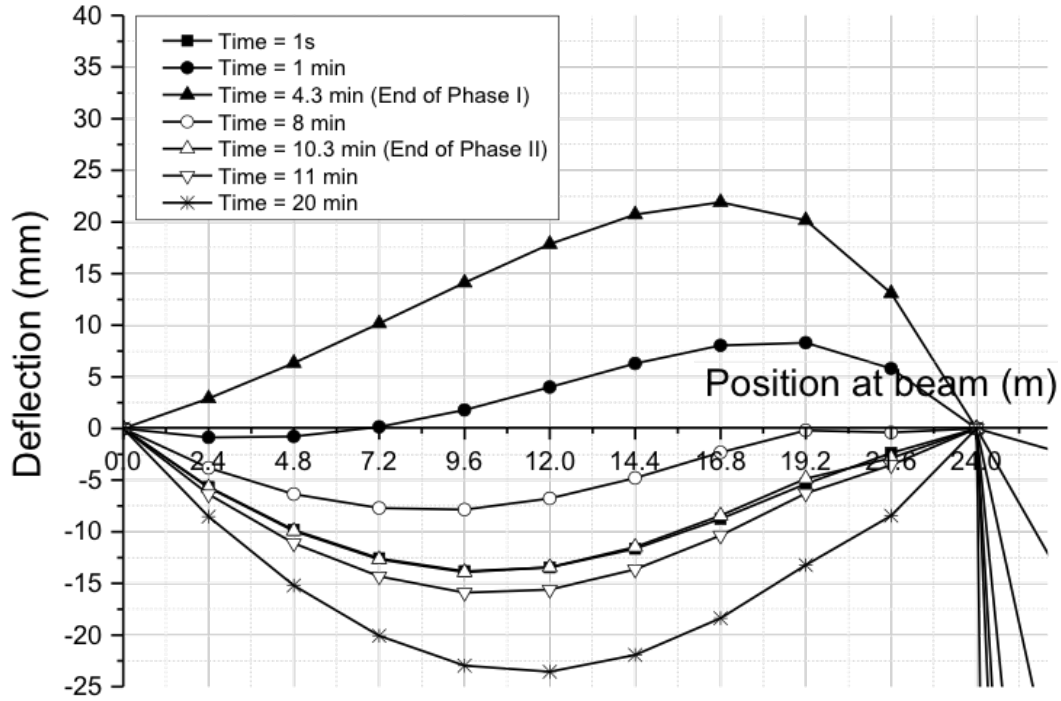

(a)

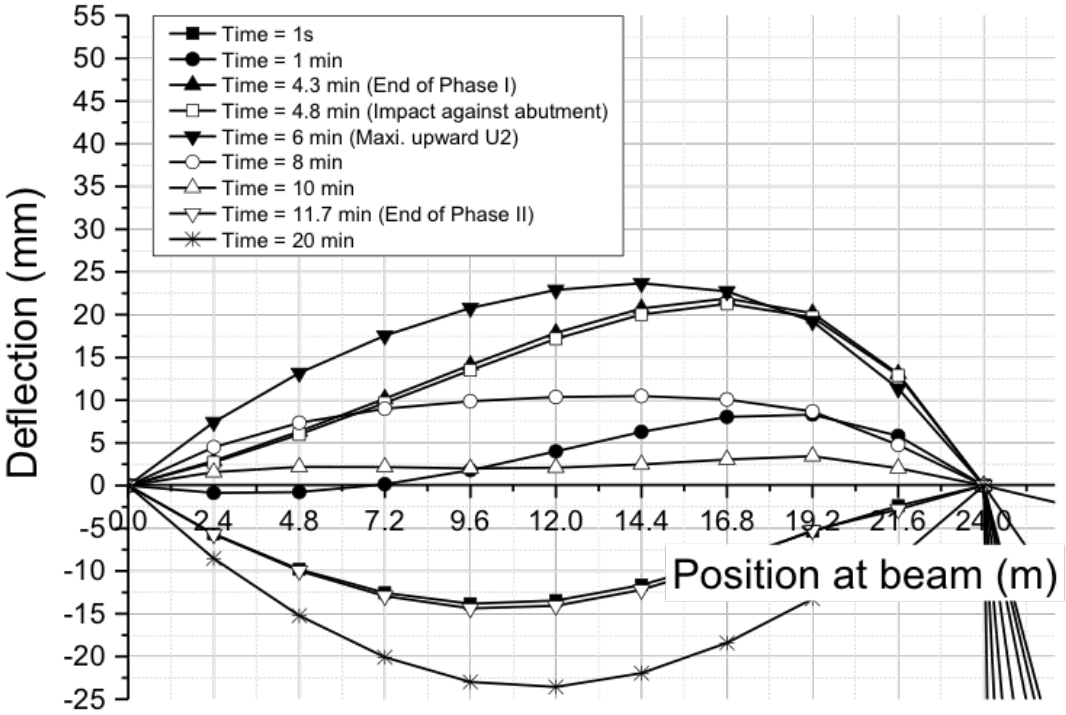

(b)

Figure 3.11: Deflection along NFAS for the rectangular model without (a) and with (b) abutment

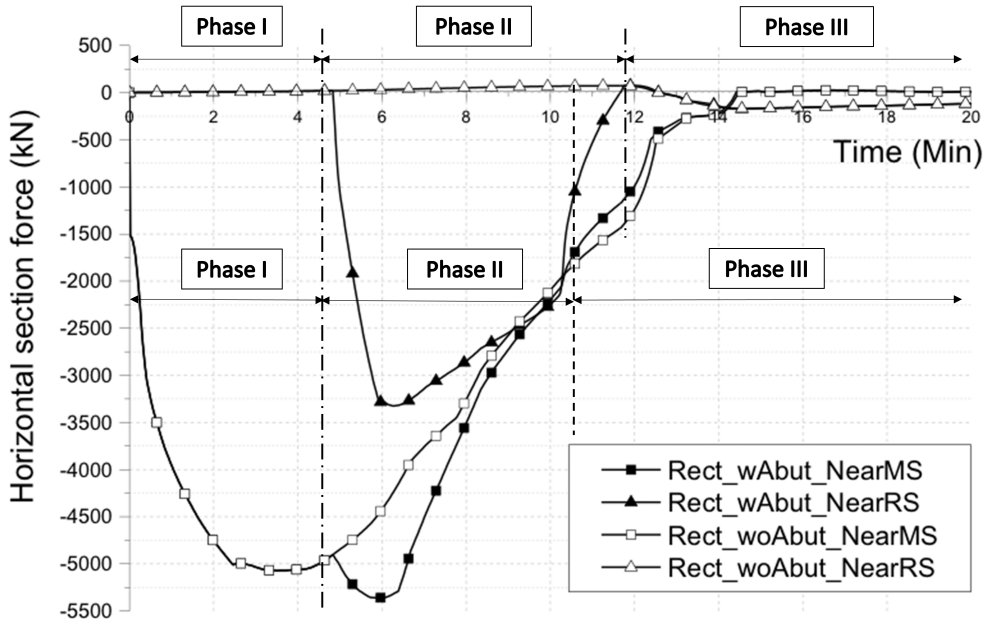

Figure 3.12: Comparison of horizontal steel section force near middle and right support

Fig. 3.13 plots the vertical reaction force at all three supports in BEAM No.3, where load redistribution can be observed. As observed earlier from the deflected shapes, all five beams are expected to show identical behaviour, therefore results are shown only for the middle beam. Under the mechanical loading, the middle support takes greater load than the two end supports as expected. During Phase I, the vertical reaction force at the middle support increases because of the rotational restraint and increasing hogging moment. Meanwhile, the reaction force at the right support also increases because of the thermal bowing induced sagging curvature in FAS and the compatibility induced counter (hogging) curvature in NFAS, causing a pulling up force at the left support. Therefore, there is an overall redistribution of load from NFAS to FAS.

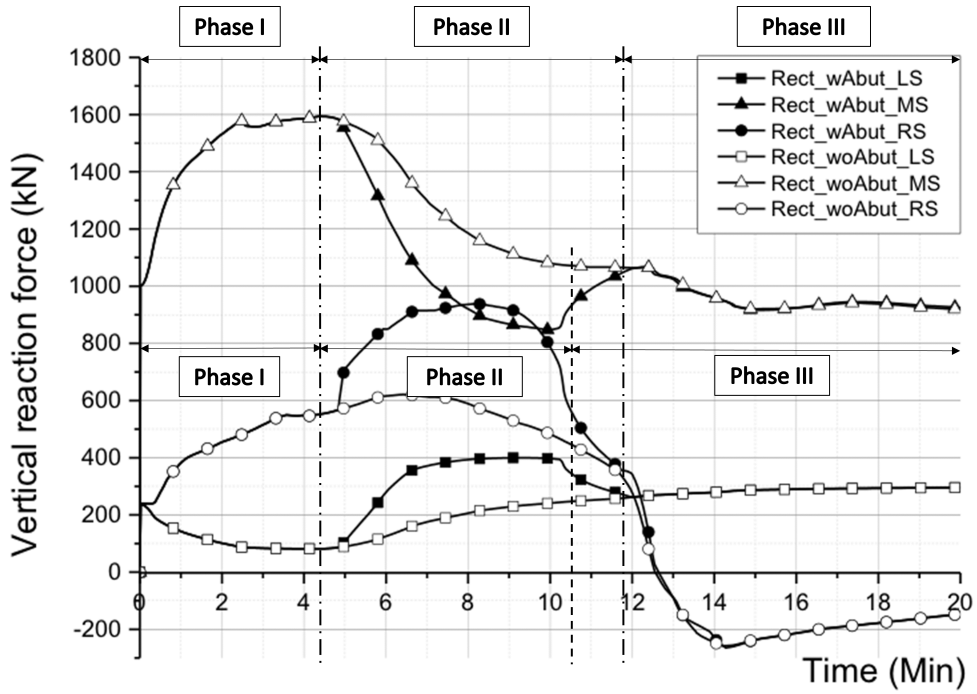

Figure 3.13: Comparison of change in vertical reaction force at supports with time

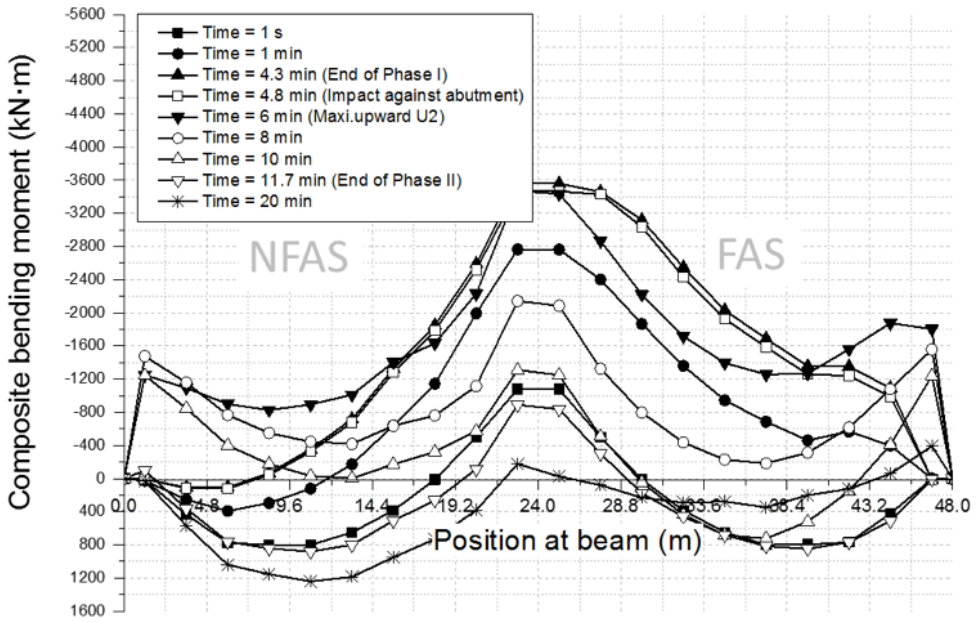

Figure 3.14: Composite bending moment variation with time along FAS and NFAS (rectangular model with abutment)

As discussed earlier, Phase II is dominated by the effect of reducing flexural stiffness of the bridge structure in FAS, which results in the reversal of the load redistribution from FAS to NFAS and as a result the reaction forces in the middle and right supports reduce while increasing at the left support. The model with abutment shows that lateral restraint induced at the right support prolongs the increase in vertical reaction at the right support and causes a load redistribution between the middle and right support, however the models coincide at the beginning of Phase III.

Fig. 3.14 illustrates the composite bending moment along NFAS and FAS for the rectangular model with abutment. Assuming that the girder longitudinal axis lies at the interface of the steel beam and the reinforced concrete deck, the section forces in the beam and membrane forces in the slab can be used to estimate the composite bending moment.

As shown in Fig. 3.14, the maximum bending moment along FAS and above middle support is achieved at the end of Phase I (4.3 min). It then begins to reduce due to reducing stiffness in FAS in Phase II. The bending moment at middle support eventually reduces below the value resulting from the gravity loading only, marking the end of Phase II and beginning of Phase III at 11.7 min. Load redistribution from FAS to NFAS can be seen clearly from this figure as well during both Phases II and III.

3.4.5.3 Skew Models

Fig. 3.15 shows that the beams in the skew models behave considerably differently from the rectangular models, resulting in a 'gourd' pattern contour plot and a clear two-way spanning behaviour which is captured by the model. The maximum downward deflection experienced is $0.54\,\mathrm{m}$ and $0.57\,\mathrm{m}$ for the model with and without abutment respectively, which are both located near the midpoint in BEAM No.5 (in the foreground). The two-way spanning action is ap-

parently because of the difference in stiffness along the two diagonals in FAS, with the short diagonal showing stiffer behaviour resulting in a band of lower deflection along it.

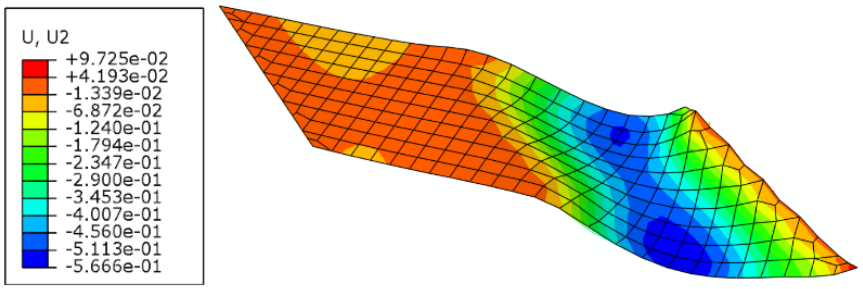

(a)

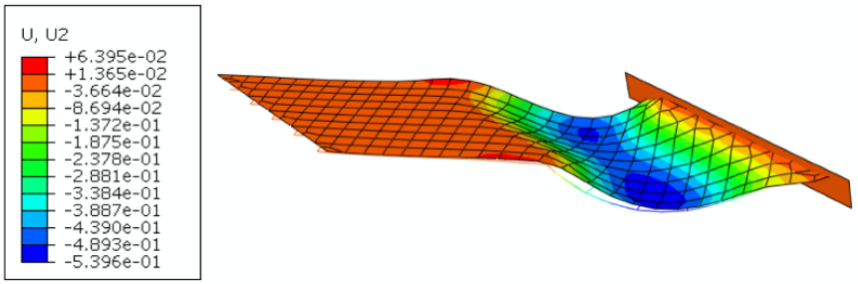

(b)

Figure 3.15: Deformed skew models without (a) and with (b) abutment at 20 min (deformation scale factor 10). All deflections are given in m

Fig. 3.16 compares the deflection history between the two skew models at midpoint of NFAS and FAS for the most deflected beam (BEAM No.5). The figure also presents the deflection in NFAS for the other four beams in the model with abutment. It can be noticed that the durations of Phases I and II are almost identical in all beams. There is no sign of Phase III in the skew models, showing no horizontal displacement reversal or runaway failure.

The deflection history in NFAS shows that the initial stiffening of FAS, as seen in Phase I of the rectangular models, is also present in the skew models and lasts for about 4 min (as seen by the peak upward deflection in the NFAS

of approximately 30 mm and 25 mm for the models with and without abutment). Also, as seen in the rectangular models the effect of reducing stiffness because of the elevated temperatures in FAS begins to govern the behaviour marking the beginning of Phase II.

Furthermore, as described in the context of Period A of the rectangular model, the skew model with abutment also shows lower deflections in FAS because of the negative P-delta moments induced by the abutment restraint. However, unlike the rectangular model there is no Period B in the skew model as the FAS deflections are not large enough to cause the reversal of the P-Delta moment.

Fig. 3.17 shows the horizontal displacement history in all five beams of the skew models. The bottom flange of Beam No.5 impinges against the abutment first because of its greater deflection at around 4 min. The other beams follow and also impinge against the abutment restraint from BEAM No.4 at 4.9 min to BEAM No.2 at 7.83 min.

Fig. 3.18 shows the variation of horizontal section force in FAS near right and middle support for the two skew models. For the skew model without abutment, only BEAM No.3 is plotted in Fig. 3.18a as the representative of other three beams because of their nearly identical behaviour. Both skew models show identical behaviour in beam axial force at middle and right supports until approximately 4 min when BEAM No.5 impinges against the abutment. Fig. 3.18a shows clearly the sequence of the impingent of each beam against the abutment, which corresponds to the sequence seen in Fig. 3.17. As each beam impinges against the abutment, the section forces near the right support increase dramatically as shown by the deviation of the section force plots of the skew model without abutment.

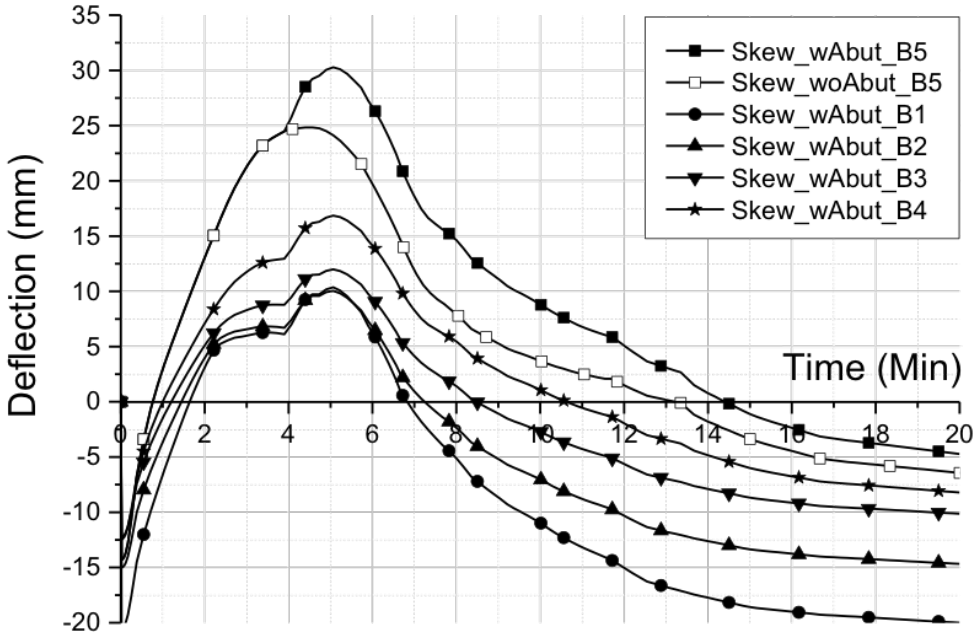

(a)

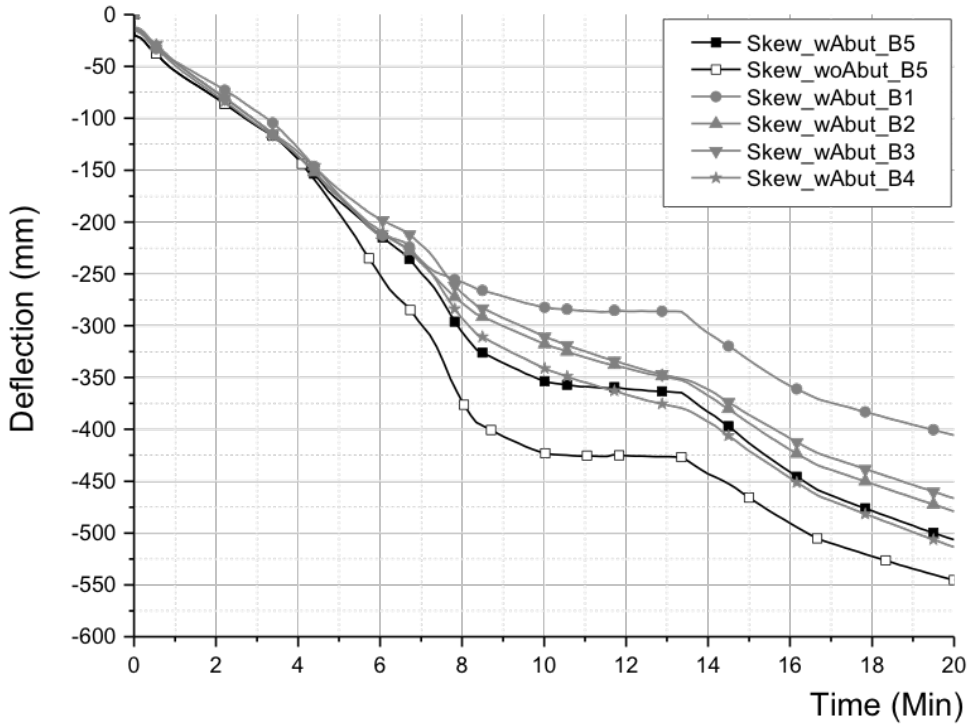

(b)

Figure 3.16: Comparison of the mid NFAS (a) and mid FAS (b) deflection variation with time

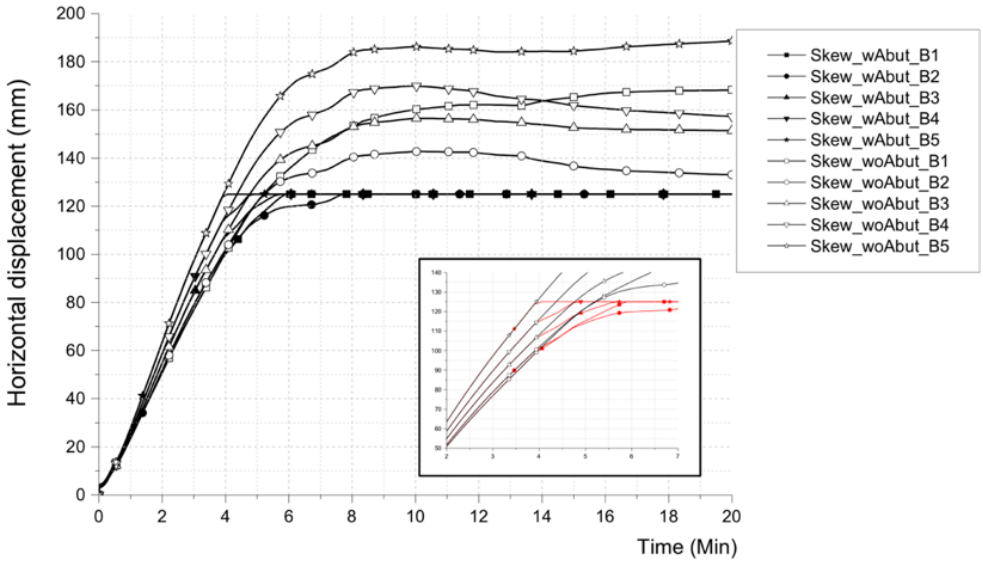

Figure 3.17: Comparison of the horizontal displacement at right support in all 5 beams between skew models (insert shows the details of first few min for clarity)

In BEAM No.5, the section force is close to zero near the right support before impingement because the beam is not composite to the slab at the support points (as this results in the model being over-constrained). The increasing section force in the other beams in FAS before impingement is due to their connection to the diaphragm beams, unlike BEAM No.5.

The section forces in beams near the middle support (Fig. 3.18b) show a highly non-uniform distribution of forces within the structure in FAS, with the highest force in BEAM No.1 reducing sequentially to BEAM No.5 which has the lowest. This is likely to be the result of a complex interplay of factors, such as non-uniform deflections and two-way behaviour interacting with thermal bowing and the rotational restraint caused by structural continuity at the middle support. In the model with abutment the axial force generated in BEAM No.5 after impingement (Fig. 3.18a) is distributed into the structure generating axial forces in all other beams, as shown in Fig. 3.18b by the deviation from the plots of section forces. The magnitude of these deviations reduces with distance from BEAM No.5 with BEAM No.1 showing the least increase in section

force at the middle support.

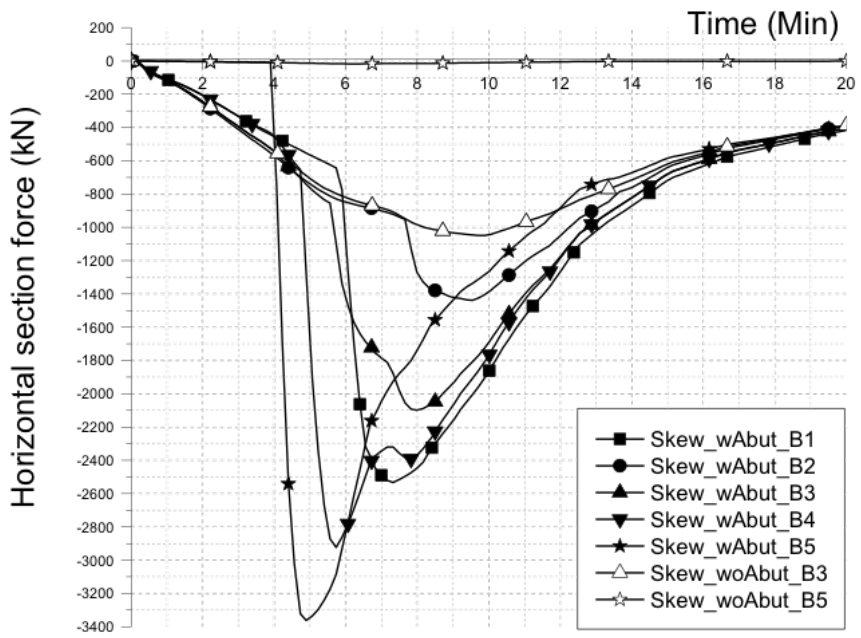

(a)

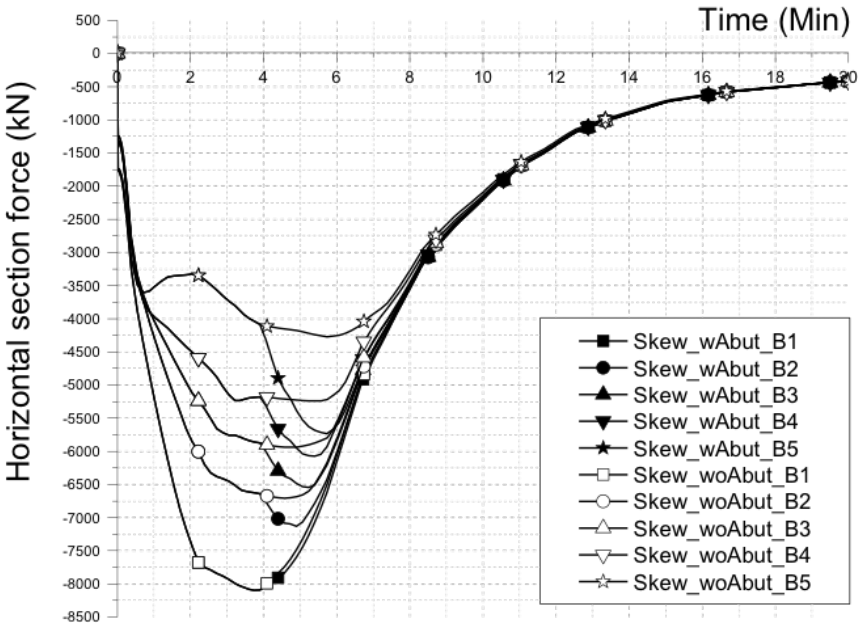

(b)

Figure 3.18: Comparison of the horizontal section force near right (a) and middle (b) support

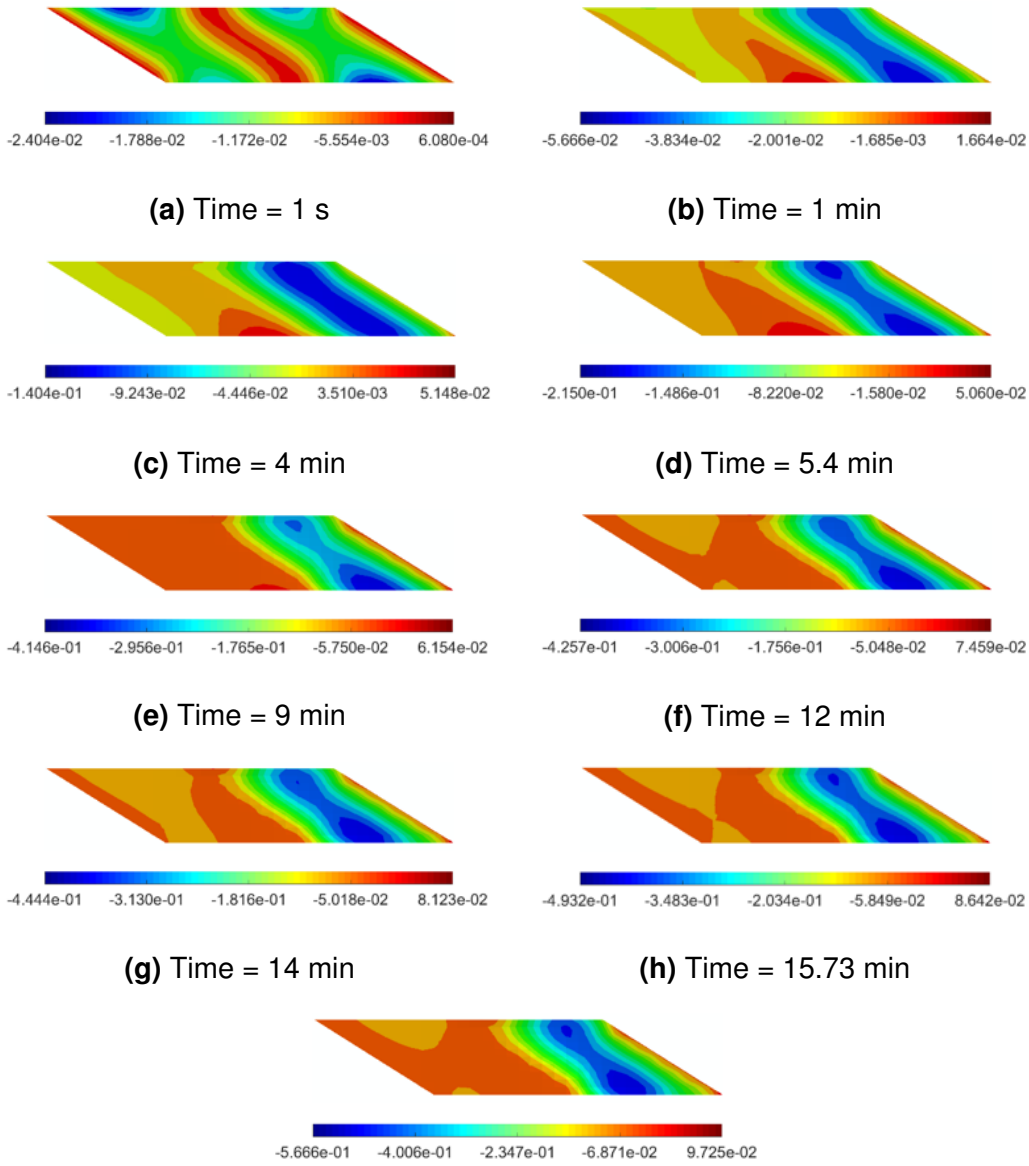

(a) Time = 1 s

(b) Time = 1 min

(c) Time = 4 min

(d) Time = 5.4 min

(e) Time = 9 min

(f) Time = 12 min

(g) Time = 14 min

(h) Time = 15.73 min

(i) Time = 20 min

Figure 3.19: The deflection (m) contours of the skew model without abutment

As discussed earlier, the skew models have a two-way behaviour, therefore instead of plotting the deflections in NFAS for each beam, the deformation contour plots of the whole deck slab are shown in Fig. 3.19 and the vertical reactions at all supports in both skew models are presented in Fig. 3.20.

When only gravity load is applied (Fig. 3.19a), the end beams exhibit the most deflection: BEAM No.1 in NFAS and BEAM No.5 in FAS. This is consistent with the vertical reaction force shown in Fig. 3.20, where BEAM No.1 at the left support and BEAM No.5 at the right support take the least load, 68.56 kN and 59.25 kN respectively. The shorter diagonals of the bridge spans attract greater load because of their greater stiffness with BEAM No.5 at the left support and BEAM No.1 at the right support carrying an order of magnitude larger load with reactions of 586.91 kN and 489.35 kN respectively. The structure of the bridge model is anti-symmetric and this is reflected in the magnitudes of the initial vertical reaction forces at left and right supports. However, these reaction forces are not identical at corresponding points of anti-symmetry because of the nonlinear geometry used in the modelling. At the middle support, the vertical reactions at the locations of BEAM No.1 and BEAM No.5, due to the gravity load, are larger than at the locations of the middle three beams. This also reflects the higher stiffness of the short diagonal as in the case of the end supports.

During Phase I response to fire loading the stiffest part of the structure is the short diagonal in FAS (because of the added stiffness due to thermal deformation) and therefore it attracts a very large magnitude of the load, most of which goes to the right support at the location of BEAM No.1 (Fig. 3.20a). The thermally induced curvature in FAS causes curling up along the long diagonal, resulting in negative reaction force in the right support at the location of BEAM No.5 and a reduced reaction at the middle support at BEAM No.1. The counter curvature in NFAS also produces a negative reaction at the left support at the

location of BEAM No. 5 (Fig. 3.20e).

In Phase II the short diagonal in FAS continues to attract greater load as the stiffness of the adjacent regions declines (Fig. 3.20a). Load is also redistributed from FAS to NFAS as in the rectangular models but not as distinctly.

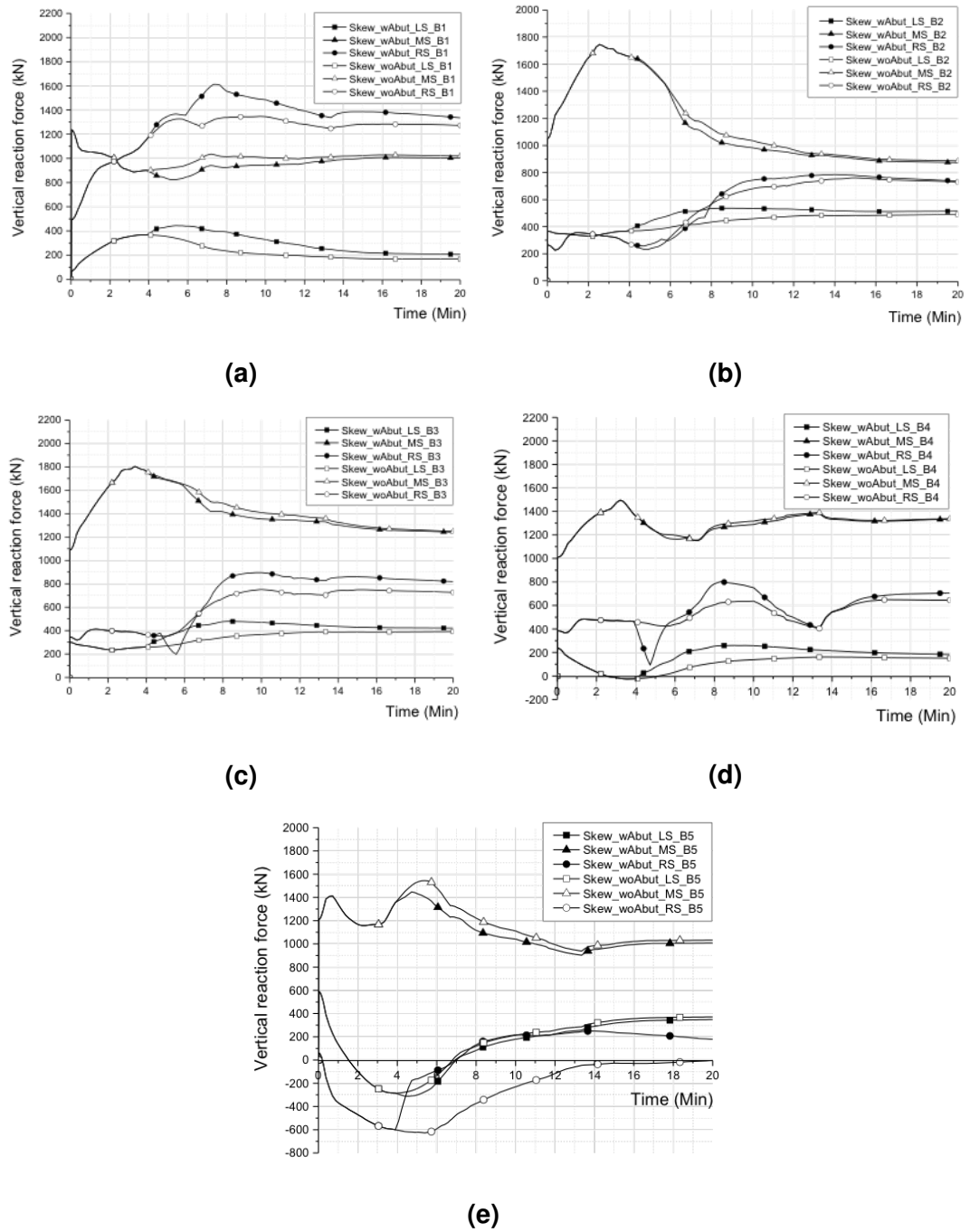

Figure 3.20: Comparison of vertical reaction force between skew models (a. BEAM No.1, b. BEAM No.2, c. BEAM No.3, d. BEAM No.4, e. BEAM No.5)

3.5 Structural Models (Shell Element for All)

The above models in Section 3.4 are simulated based on global behaviour without considering local buckling effects that may occur in the web or flanges of the composite steel girders due to the action of fire. To further consolidate the study, this section investigates the potential for local buckling and how this may impact upon the global behaviour by using shell elements instead of beam elements for primary steel girders.

As analysed in Section 3.4, failure times have no significant difference for the models with and without abutment. Therefore the rectangular and skew bridge models without abutment are used for the analyses in this section.

3.5.1 Finite Element Models

To investigate the local behaviour, solid or shell elements may be considered. Given that shell elements perform better for bending dominated problems and are less computationally expensive compared to solid elements, the 4-node quadrilateral shell element S4R is used.

The main difference between the models in this section and Section 3.4 is the element type for the primary beams, therefore the detailed information of the following definitions will not be repeated:

- Structural geometry
- Layout and dimensions of primary and transverse beams
- Material properties
- Applied mechanical loads

The output temperature profiles from the heat transfer analysis in Section 3.3.2 are applied to the structural models. The function of transverse

diaphragms is simulated by defining a pinned rigid link to prevent the lateral movement of the primary beams. This is achieved via MPC type constraints at the location of transverse diaphragms.

3.5.2 Thermo-mechanical Analysis

In this section, the rectangular and skew model are presented separately, then the key indicators of failure (deflection history and horizontal displacement) are compared in Section 3.5.2.3.

3.5.2.1 Rectangular Models

The deflected shape of the rectangular model after 11 minutes of Hydrocarbon fire exposure is shown in Fig. 3.21. The beams in rectangular model have very similar behaviour, therefore BEAM No.3 (middle beam) will be analysed in Section 3.5.2.3 to compare with the skew model. The model stops at 655 s as a result of convergence failure, however structural failure is observed before 655 s. Fig. 3.22 shows the out-of-plane displacement at 11 minutes. The steel web near the middle support laterally displaced by 3.8 cm at the end of the simulation.

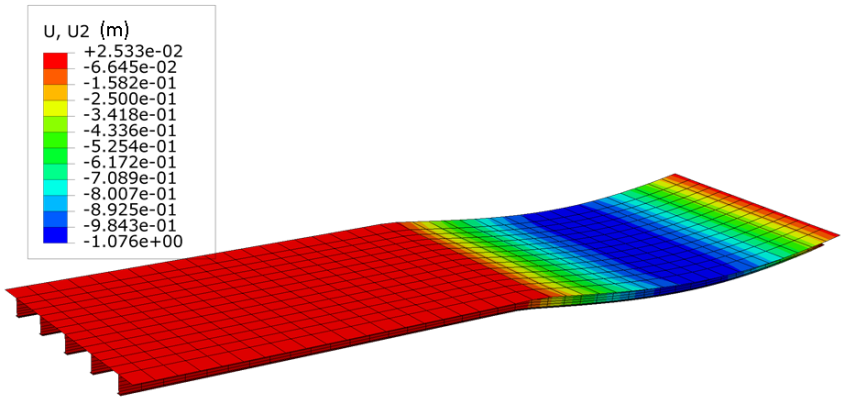

Figure 3.21: Deformed rectangular model after 11 min of fire

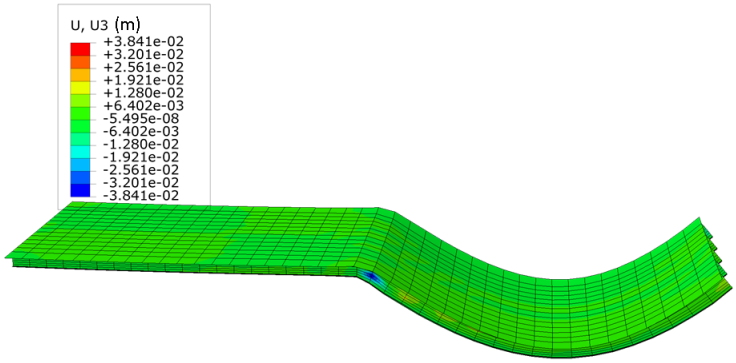

Figure 3.22: Web buckling location near the middle support (scale factor 5) at 11 min

3.5.2.2 Skew Models

The deflected shape of the skew model after 20 minutes of Hydrocarbon fire exposure is shown in Fig. 3.23. Same as the observation from the skew model with beam elements, the maximum downward deflection is located at the midpoint of BEAM No.5 (in the foreground), however with a larger deflection of nearly 3.7 m at 20 minutes (0.54 m in beam-element model). The large difference between the two models is because of the fact that the shell model shows failure while the beam models do not. The large deflections occur after the observation of structural failure.

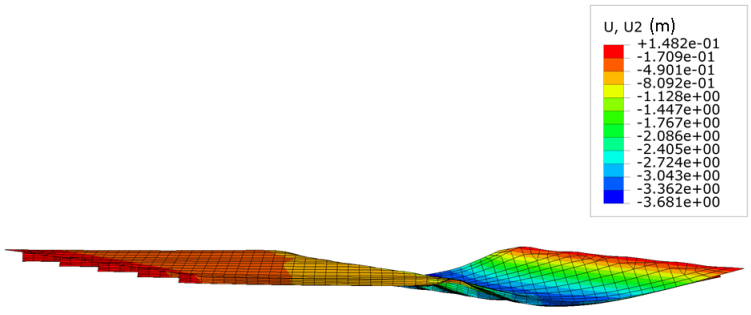

Figure 3.23: Deformed skew model without abutment at 20 min

The deflection history at midpoint of FAS is compared between the five primary beams, given in Fig. 3.24a. The horizontal displacement at the right supports is compared in Fig. 3.24b. A sharp transition can be seen in both of the vertical deflection and horizontal displacement history at around 15 min.

This near free-fall deflection is deemed to be caused by the web buckling as observed in Fig. 3.25a. The right side supports were pushed out due to thermal expansion until 11.3 minutes.

The out-of-plane displacement at the web centre of the two adjacent nodes at the buckling location is plotted as a function of fire exposure time (see Fig. 3.25b). The sudden change of lateral displacement of the web occurred at around 15 min, representing the initiation of web buckling.

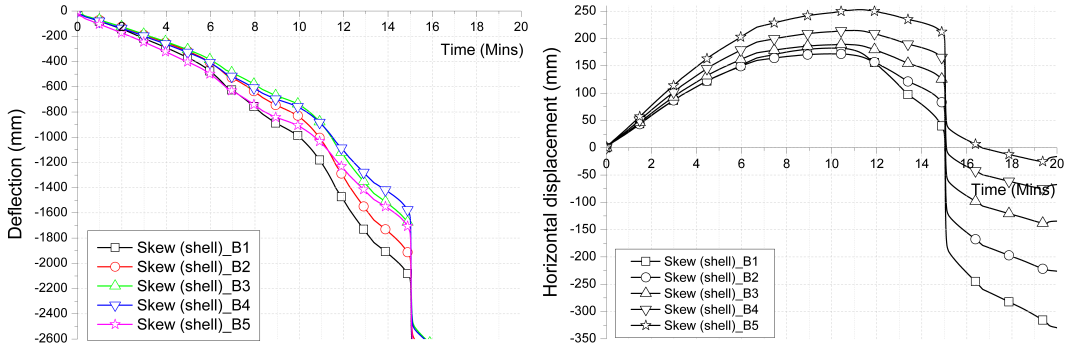

(a) **(b)**

Figure 3.24: Comparison of the (a) mid FAS deflection variation and (b) horizontal displacement at right support with time between five primary beams

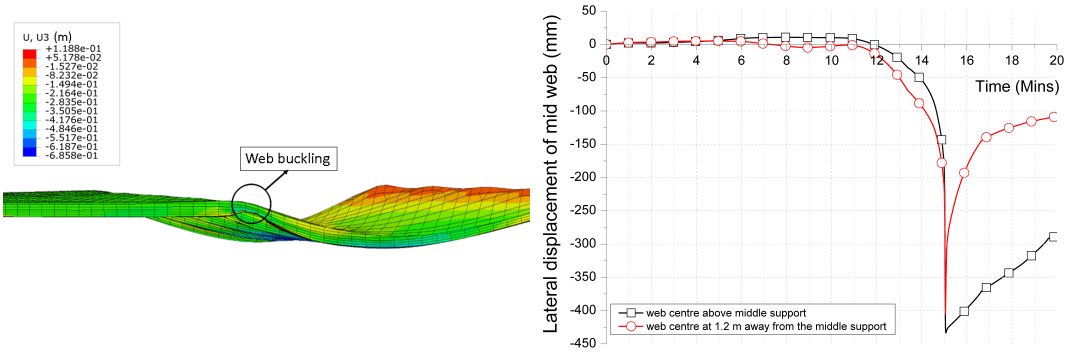

(a) **(b)**

Figure 3.25: Web buckling location (a) at BEAM No.5 near the middle support (at around 15 min), and the corresponding (b) out-of-plane displacement at the web centre

3.5.2.3 Comparison

Fig. 3.26 compares the deflection history at mid NFAS (top) and mid FAS (bottom) between the models using beam elements for the primary girders (details described in Section 3.4) and the models using shell elements for the primary girders (details described in Section 3.5).

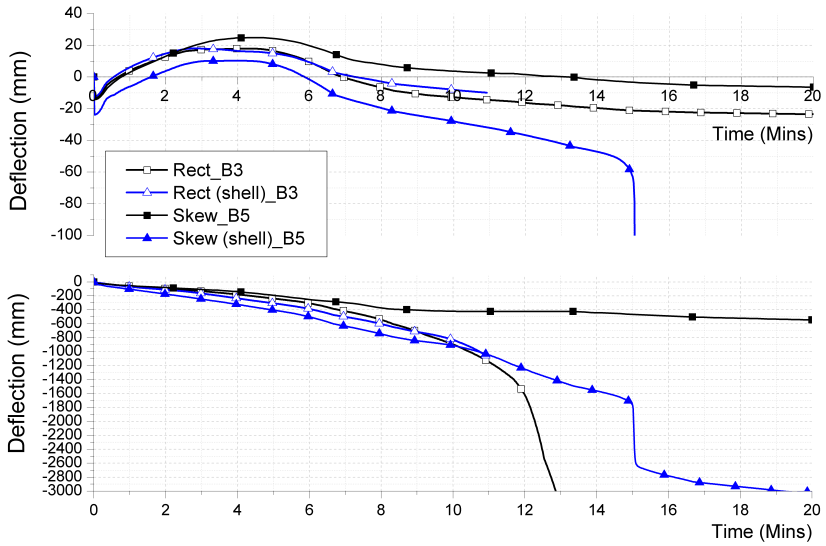

Figure 3.26: Comparison of the mid NFAS (top) and mid FAS (bottom) deflection variation with time. 'Shell" in brackets represents the model using shell elements (instead of beam elements) for the primary girders. B3 = Beam No.3. B5 = Beam No.5

A sharp increase in deflection at 15 minutes is observed in the skew model with shell elements for the primary girders. This may not be deemed to be runaway failure as the beams revert back to steady behaviour right after the sharp deflection, however it is unlikely that in a physical bridge such sharp deformation will be arrested because of dynamic forces and therefore it can be concluded that the skew bridge will fail at this point. This behaviour is caused by web buckling which can be confirmed by the observation in Fig. 3.25 which initiated at 15 minutes.

The horizontal displacement at right supports are compared in Fig. 3.27. Both of the rectangular models show the reversal of horizontal displacement

at 10.3 min indicating onset of structural failure. In the skew model with shell elements for the primary beams, Beam No. 5 shows a reversal of horizontal displacement at 11.3 min. This is a behaviour not observed when the primary beams are modelled as beam element.

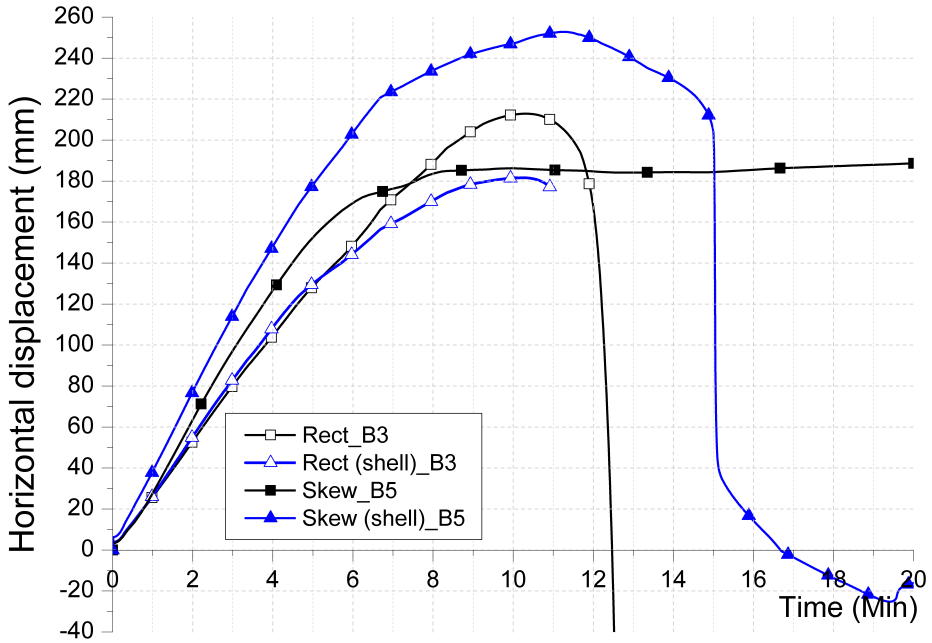

Figure 3.27: Comparison of the horizontal displacement at the right support

3.6 Failure Assessment

In this chapter, the bridge is deemed to have failed if replacement of a girder or the deck would be required. The occurrence of failure is assumed as long as any one of the following conditions are fulfilled:

1) Runaway behaviour of deflection in the slab or beams.

2) Reversal of horizontal displacement at the free end-supports. This would suggest that the bridge span has softened to a point where the loads overcome the effect of thermal expansion (Lamont et al., 2003; Usmani et al., 2001) and the ends of the structure are pulled back towards the centre.

3) If the inward horizontal displacement at the free end exceeds the distance between bearing centreline and abutment edge (350 mm in this case study), which will indicate that the superstructure has lost vertical support.

4) British Standards criteria (EN, 1987): a beam shall be regarded as failed if there is no capacity to support the test load which is determined if either of the following empirical criteria are exceeded:

   - A deflection of *L*/20;
   - The rate of deflection (in mm/min), calculated over 1 min intervals, on each min from the commencement of the heating period, exceeds the limit set by the following equation:

     Rate of deflection = L^2 / 9000d

     Where L is the clear span (mm) of specimen, d is the distance (mm) from the top of the structural section to the bottom of the design tension zone. *NOTE. This rate of deflection limit shall not apply before a deflection of L/30 is exceeded.*

In this study, BS476 criterion suggests a deflection of $1.2\,\mathrm{m}$ or the rate of deflection 45.71 mm/min (when the deflection is more than $0.8\,\mathrm{m}$) for rectangular models to fail. For skew models, failure could be considered to have occurred if the deflection reaches $1.44\,\mathrm{m}$ or the deflection rate reaching 65.83 mm/min.

5) To consider the effect of local behaviour, the following criterion is also used: a sudden change in the out-of-plane displacement, which may imply failure due to the initiation of web buckling.

Note that the code based failure criteria are based on standard furnace tests which do not account for the complex behaviour in a 3D bridge as illustrated in this chapter. Therefore, the BS476 criterion is merely a reference and should not be considered as true indicator of failure.

Table 3.2: Comparison of the different failure criteria

Model	Reversal of horizontal displacement	Fall off from right abutment	Initiation of web buckling	British standard: L/20	British Standard: vertical deflection rate
Shell for slab only + with abutment					
Rectangular shape	11.7 min	14.9 min	N/A	10.6 min	11.1 min
Skew shape	No failure	No failure	N/A	No failure	No failure
Shell for slab only + without abutment					
Rectangular shape	10.3 min	13 min	N/A	11.2 min	10.4 min
Skew shape	No failure	No failure	N/A	No failure	No failure
Shell for all + without abutment					
Rectangular shape **Simulation stops at 11 min*	10.3 min	Unknown (due to convergence)	No failure before 11 min	No failure before 11 min	No failure before 11 min
Skew shape	11.3 min	No failure	15 min	13.1 min	13 min

Table 3.2 shows the failure time in each model based on various failure criteria. It shows that the rectangular models have identical failure time (10.3 min) when modelled either using shell or beam elements based on the criteria of horizontal displacement reversal. The web deformation is very small and does not affect the analysis significantly. If a conservative estimate is used, the rectangular models suggest that failure may occur around 10.6 min and 10.3 min in the model with and without abutment respectively.

For the models with shell element for slab only (beam elements used for primary girders), the skew shape seems to have a much more stable behaviour in fire with no failure. There is no indication of runaway or reversal of horizontal displacement and BS476 failure criteria is not reached either. However, a failure time of 11.3 min is suggested by the skew model using the shell elements for the primary beams.

3.7 Conclusions

This chapter provides new insights in understanding of global and local structural behaviour of bridges under vehicle fire loadings. The local behaviour has been studied by modelling the primary girders using shell elements. The effect of bridge shape (skewness) and the influence of abutment restraints on the overall fire performance of the bridge has been examined. The following conclusions were drawn:

- The structural system of the bridge chosen for analysis is based on a representative bridge type commonly found on the UK highway network and therefore the findings of the work should have significant practical relevance.
- The findings from this chapter can help practising engineers to improve the inherent fire resistance of the bridges.
- Three phases have been defined for the structural response of the bridges under fire. The defined phases describe the key structural features during different stages, which will help engineers to understand the progressive bridge damage under fire.
- Various outputs of the thermo-mechanical analysis haven been presented, including horizontal displacements, vertical deflections, horizontal sec-

tion force, P-delta effect, reaction forces and composite bending moment. This is the first detailed analysis of bridges in this field which will provide useful materials for the future study.

- Different failure criteria have been discussed. Based on the investigation presented in this chapter, the author believes that the reversal of horizontal displacement at the free end is a more reliable indicator of runaway failure for bridges.

- The BS476 deflection or rate of deflection criteria is not reliable for the failure assessments of structures in fire. For example, in this study, the deflection criterion gives an unrealistic suggestion of $1.2\,\mathrm{m}$ and $1.44\,\mathrm{m}$ deflection for the rectangular and skew bridge respectively to fail. A bridge could be considered as failed before the deflection reaching the suggested values due to the replacement of a girder or deck would be required after such severe deformation. Therefore the BS476 failure criterion based on the furnace test should not be used as an failure indicator.

- The behaviour of the rectangular bridge models are almost identical when the bridge girders are modelled with either beam or shell elements.

- In the skew bridge models modelled entirely using shell elements, failure occurs due to web buckling concentrated near the middle support which does not manifest in the beam element model.

- For the purpose of implementing a methodology for performance-based fire resistance of a bridge network, it is suggested that, for rectangular bridges, beam element models for bridge girders are used for a preliminary analysis of vulnerable bridges because of the significantly lower user effort involved particularly in the context of hundreds of bridges in the network. Based on the results from the preliminary analysis, indi-

vidual bridges should be identified for more detailed analysis using shell models where considered necessary. The simulation show that for the skew shapes, beam elements are not able to capture the local buckling behaviour of the bridge girders and therefore it is not advisable to use such models for skew shaped bridges. Even in case of rectangular shape bridges, a great deal of care must be taken before reliance on beam element only models to make critical decisions. Future research may however show that using web stiffeners in strategic locations in the girders may reduce or eliminate the risk of local buckling and then it would be possible to use beam element models of bridge girders even beyond preliminary assessment.

Given the limitations of modelling approaches used in this chapter, the following future work is suggested:

- For a more equivalent comparison between using beam elements and shell elements for modelling bridge girders, stiffeners should be used (and modelled) to prevent local buckling which is not an uncommon strategy in bridge design.

- The Hydrocarbon fire has limitations for application to bridges as it makes the bridge undergo rapid heating to $1000\,^{\circ}\mathrm{C}$ within a few minutes, which is perhaps too onerous a demand for bridges. There would be a time lag for the steel to reach equivalent temperatures with less conservative and more realistic fire loading scenarios. A more bespoke fire would perhaps be more suitable based on a risk assessment including traffic flow information etc. Besides, the reduction of temperatures away from the burning vehicle is significant which was demonstrated by the first fire experiment of a bridge structure, conducted in 2017 (Alos-Moya et al., 2017). In order to better understand the response of bridges subjected

to fires, more realistic fire models should be used to take account of the decay fire intensity along the bridge span, none of which are captured by prescriptive curves.

- The model constructed is unable to model the lifting up of the bridge deck above the bearings. This however is considered to be a minor limitation as the lifting up of the slab occurs after the global structural failure in case of the rectangular bridge models, while in case of the skew model it occurs in an edge beam for a short duration in the very early stages of the analysis.

- A risk assessment methodology would be proposed to evaluate the vulnerability of bridge network to vehicle fires.

Part II

ABAQUS Models + ‘Bridge Fires’

4

Designed Localised Vehicle Fires

4.1 Introduction

The most serious bridge fire incidents usually involve fuel tanker fires as listed in Chapter 2, which has led researchers to use the Hydrocarbon fire to characterise fire hazard for bridges. This may be a reasonably conservative assumption in the context of an extreme load, but it is not consistent with reality or the principles of performance based engineering (PBE). Another assumption commonly used is that prescriptive fire curves are uniformly applied along the entire bridge span (Garlock et al., 2012; Kodur et al., 2013). However, for

highway bridges in open environment, localised fires are expected to depict the scenarios more accurately.

In reality, it is expected that a bridge can be subjected to a variety of fires depending upon the locations and sizes of the vehicles involved in an incident. Further uncertainties arise from the unknown magnitude of liquid fuels and/or other combustibles present in the burning vehicle and the resulting heat release rate (HRR), which determines the fire size and enables the quantification of the likely fire behaviour and its interaction with adjacent structures. The fuel bed height (corresponding to the distance between the fuel bed and the bridge deck) is another factor that may influence the impact of the fire on the bridge superstructure.

4.1.1 Objectives

In order to define the different magnitudes of hazard intensity which correspond to different levels of performance (see Table 4.1), this chapter introduces the concept of idealised vehicle fire scenarios. A series of fire scenarios have been developed and quantified using computational fluid dynamics (CFD) models with the public domain software Fire Dynamics Simulator (FDS) 6.5.3 developed by NIST (USA).

Envelopes of suitably designed vehicle fires will be presented for engineers to ensure that a bridge structure has adequate level of performance for all possible fire scenarios. Acceptable threshold performance measures such as deflections, rotations and horizontal displacements can be specified for all fire scenarios (including collapse for the most severe fires). The uniformly spread Hydrocarbon fire may result in an overly conservative thermo-mechanical response. By using localised fire models, a realistic decay of hazard intensity along the span away from the vehicle is simulated and should result in more realistic thermo-mechanical responses.

Table 4.1: Correlation of hazard intensity and damage level in the context of expected performance levels

Damage level/ Hazard Intensity (HRR in MW)	None or Superficial Damage	Minor Damage	Major Damage	Collapse
Low to Moderate (<5)	Expected performance	Bad	Poor	Catastrophic
Moderate to High (5-20)	Conservative design	Expected performance	Bad	Poor
High to Very High (20-50)	Overdesigned	Conservative design	Expected performance	Bad
Exceptional (>50)	Massively overdesigned	Overdesigned	Conservative design	Expected performance

The above mentioned purposes are specifically achieved by:

1) Four ranges of HRR referring to four standard vehicle types are investigated in FDS associated with three accident locations, consisting of 12 scenarios in total.

2) The vehicle fire CFD results will be simplified to exponential functions (Appendix B) and implemented into OpenSees (Chapter 6) corresponding to the uncertainties mentioned above.

3) The fitted exponential functions represent a spatially varying heat flux that is used to provide the thermal boundary conditions for the bridge superstructure (Chapter 5).

4.2 Parameters

The new design fires for bridges in natural environment predominantly varies with geometry (boundary condition, ceiling height) and fire (fire intensity, dimensions and location). Therefore, the design fires are categorised into four types of vehicles (Section 4.2.1) corresponding to different magnitude of hazards: *low to moderate* (cars), *moderate to high* (light goods vehicles, LGVs),

high to very high (heavy goods vehicles, HGVs) and *exceptional* (fuel tanker trucks). For each category, a different range of HRR magnitude is assumed to represent different levels of fire intensity (Section 4.2.4). The influence of parameters on the predicted heat fluxes have been considered in three directions (Section 4.2.2 & Section 4.2.3): along the bridge span length (x-axis) and bridge width (z-axis) at distances away from the fire centreline; and at four positions along the height (y-axis) of the bridge superstructure. The x direction matters because the impinged flame will project horizontally forming a jet that will affect heat transfer (HT) into the ceiling medium (Drysdale, 2011). The y direction matters because fire is treated as a plume, which may impinge on the bottom of the bridge considering the beam depth is thick. The influence of smoke has been considered in CFD models as described in Section 4.2.5. The finally generalised values for each parameter in all categories are presented in Section 4.2.6.

4.2.1 Vehicle Types and Sizes

Standard trucks are commonly used for gravity load characterization on bridges, which makes this way of representing the fire hazard a logical extension of a familiar notion used in structural engineering. The inferred probability of the crash of a specific vehicle type is assumed proportional to the frequency of that type on the road. Using one most common single vehicle size for each category is thereby acceptable as the data in appendixes show little correlation between the vehicle size and HRR.

The representative vehicles are selected from the database in the UK (GOV.UK). According to the vehicle licensing statistics report for 2011-2016 Q2 provided by Department for Transport (Department for Transport, 2012; Grove, 2012, 2013, 2014, 2015a, 2016), in the car category, the top make was Ford over 5 years, which accounted for 14% of all cars on the road in 2015. The most com-

mon car model was Ford Focus since 2011, and Ford Fiesta was marginally ahead of the Focus for the first time in 2015. However, Vehicle Licensing Statistics (Department for Transport statistics, 2016) show that Ford Fiesta was the most registered (numbering 62,585,766 from 1994 to quarter 2 of 2016) in Great Britain, with the model Ford Fiesta Zetec accounting for the greatest share (13.26%) of the Fiesta models. Ford Fiesta Zetec was therefore chosen as the prototype car in this research, the dimensions of which are shown in Table 4.2.

Table 4.2: Dimensions of representative models in each vehicle type

		Length (m)	Width (m)	Height (m)	Reference
Cars	Ford Fiesta Zetec	4.0	1.7	1.5	Ingram (2014)
LGVs	Ford Transit 190 Lwb	5.6	2.0	2.5	Smart Contract Services Ltd
HGVs	Mercedes Actros	12.2	2.5	3.5	Mercedes-Benz UK Ltd. (2011)
Buses & Coaches	Volvo B11R coach	13.8	2.6	3.8	Volvo
Fuel tanker trucks	User defined				

As explained in the report of Vehicle Licensing Statistics (Grove, 2015b), the term LGVs is defined for the goods vehicles with a gross vehicle weight up to 3.5 tonnes, and those with a gross vehicle weight over 3.5 tonnes are referred to as HGVs. In the LGVs category, the Ford Escort 50D is the most popular model since 1994 numbering 1,912,406. While the make Ford Transit has the greatest registered number of 28,814,525, in which the model Ford Transit 190 Lwb is the most common type with 1,862,101.

In the HGVs category, the make Mercedes accounts for the greatest numbers, in which a model type is the most common numbering 2,928,386. In

the Buses & Coaches category, a type of Volvo has the greatest numbers: 835,181. The model Mercedes Actros and Volvo B11R coach are chosen as the prototype of HGV and coaches category respectively. Since the dimensions of buses and coaches are similar to HGVs, the category of buses and coaches will be merged with HGVs. HGVs are likely to have a higher averaged HRR compared to the buses and coaches due to the transporting goods which may be flammable. However, such details are not considered in this work, HRR of buses and coaches is therefore assumed identical to the HGVs.

The size of fuel tanker trucks can vary significantly depending upon the manufacture, volume capacity, attached trailers and country regulations. Therefore the author has assumed the nominal dimensions for this category as listed in Table 4.3.

4.2.2 Fuel Bed Locations

With respect to the highway fire scenarios, only the vehicle fires which occurred *under* bridges are considered in this research. As shown in Fig. 4.1, three locations under the span have been investigated: 1) under the mid-span; 2) quarter points of the span; 3) near the abutment. Fire location has been situated at the mid-span to quantify the heat flux due to the fire exposure resulting from an accident below the centre of span as this is the most critical location in terms of potential damage level. The fire location adjacent to the abutment is expected to generate the largest heat flux because of the abutment boundary effect (as a result of heat feedback from the abutment) and this will also test the reduced shear capacity of the bridge superstructure. The quarter point under span is investigated as an intermediate case.

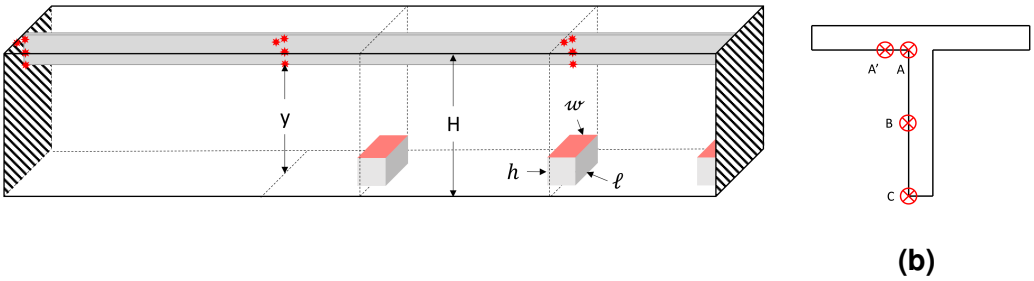

(a) (b)

Figure 4.1: Positions of received heat flux (a) in domain scale; (b) across the composite section

4.2.3 Measured Positions of Received Heat Flux

The heat flux is used for formulating the new design fires, which is suggested by Torero et al. (2017) for the problem of heat transfer from the fire to a structural element. In the CFD models, the lines of devices (red points in Fig. 4.1a) are needed to record the time history of the incident heat flux at chosen points. Three directions have been considered to capture the received heat flux: across beam depth (Fig. 4.1b), along the length (Fig. 4.1a) and width (Fig. 4.2) of the bridge span.

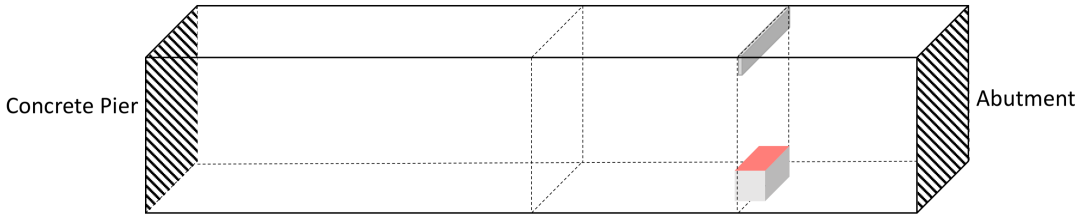

Figure 4.2: Beam along the bridge width when the fuel bed under the mid-span

As shown in Fig. 4.1a, in the direction of bridge span length, a beam is positioned above the centreline of the domain width to provide the solid surfaces for obtaining heat flux output. The beam was modelled as the web only with 0.2 m width excluding the lower and upper flanges. The beam width of 0.2 m

is defined so because obstruction dimension is not allowed to be smaller than the cell size in FDS. In order to capture adequate outputs along the span, devices were placed at every 0.2 m to capture the flux distribution with adequate resolution of the decay into the nearfield above the fuel bed.

The author has considered to determine the flux distribution in two directions for setting up devices in one model, however in this configuration the beams will create barriers that are not representative of the real bridge superstructure and may result in inaccurate fire/flow behaviour. Another way to observe the flux variation along bridge width is modelling a few parallel beams along bridge length at the specified spacings. This method allows a realistic set of flow barriers as commonly seen in highway bridge structures, and can be varied based on the spacings and depth of the bridge beams. In order to create generic fire curves, the compartment effect will be neglected. The variation along bridge width is captured by separately modelling a beam for devices along the z-axis (Fig. 4.2).

4.2.4 Fire Intensity

Idealisation concept for different fire intensity categories is defined in Section 4.2.4.1. The flame behaviour is expected to reflect the severity of fires associated with vehicle types as shown in Fig. 4.3. The fire intensity is defined as a range of HRR for each vehicle category. Four categories have been defined corresponding to vehicle types including low to moderate car fires (2 MW-5 MW), moderate to high LGV fires (5 MW-20 MW), high to very high HGV fires (20 MW-50 MW) and exceptional fuel tanker fires (50 MW-100 MW).

Section 4.2.4.2 presents the estimated HRR of burning vehicles in a fuel-controlled regime based on the available literature on vehicles, goods trailers and liquid pool/spill fires experiments (Appendix A.1 - A.5).

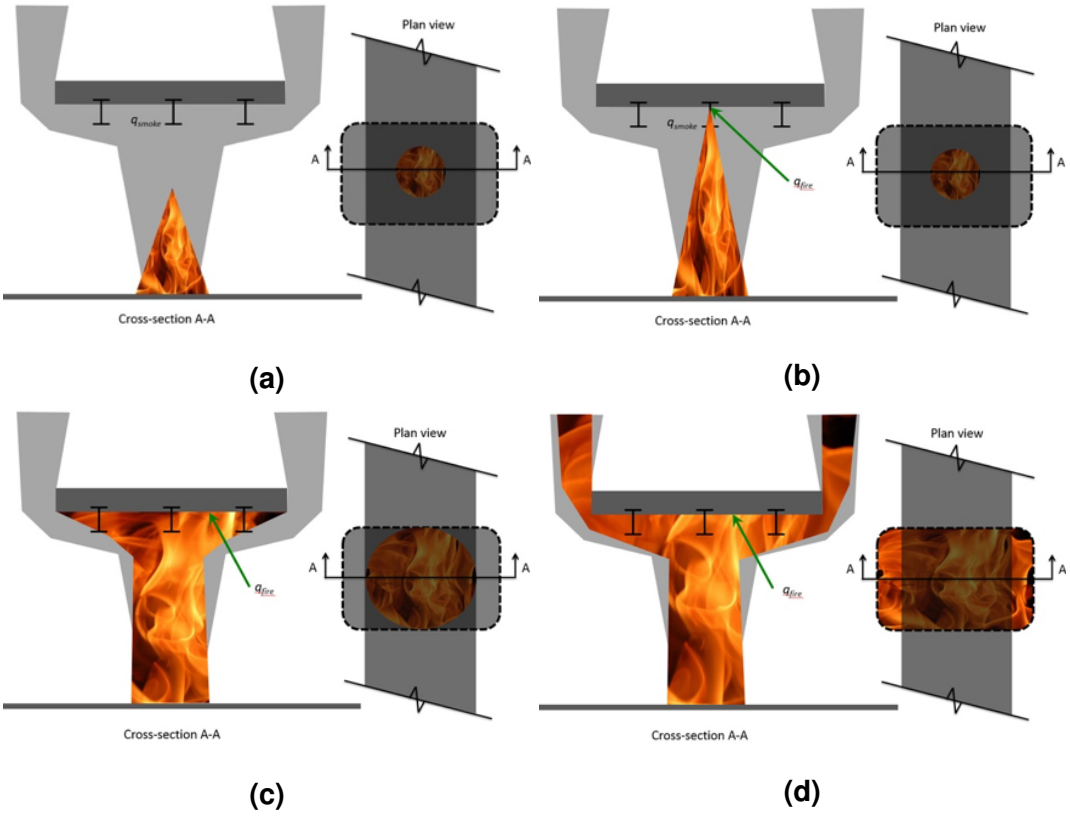

Figure 4.3: Four types of fire intensity in vehicle fires (not to scale). (a) Low to moderate: 2-5 MW in car fire; (b) Moderate to high: 5-20 MW in LGVs fire; (c) High to very High: 20-50 MW in HGVs fire; (d) Exceptional: 50-100 MW in fuel tanker fire

4.2.4.1 Idealisation Concept of Fire Intensity Categories

In the low to moderate intensity fire, the bridge structure is expected to be exposed only to heat flux from the smoke with an assumption that the bridge is only engulfed by the smoke because of the short height of the flame, which happens in reality, especially for car fires, e.g., a Lamborghini fire under Blackfriars Bridge in 2016 (Barnes, 2016). The moderate to high intensity fire is considered as an intermediate fire likely to occur in an LGV accident, in which the flame directly impinges upon the soffit of the bridge deck. Such a scenario may also exist in a larger car fire or an accident involving multiple cars. The high to very high intensity fire is considered to be caused by HGV fires and is defined by assuming the flames affect all the bridge deck but with limited

spread to air. The exceptional fire is defined for depicting fuel tanker fires with an extremely high value of HRR which is usually obtained in tunnel fires.

4.2.4.2 Estimated HRR for Each Category

HRR for each category was estimated based on a few assumptions:

1) For the existing liquid pool fires, the fire size in experiments are smaller than the magnitude expected in real vehicle fires.

2) Vehicles burned in experiments usually had all fuel and battery removed out for safety and environmental reasons, which results in the fire load being significantly less than for a roadworthy vehicle.

3) Usually the experimental values from semi-closed facilities such as a tunnel would be much higher than other open environments due to more radiation feedback to the vehicle from the tunnel walls.

4) In this research, the experimental results of pool fires and tunnel fires will be used as the lower and upper bound of estimation respectively.

Appendix A.1 illustrates a series of experiments for liquid pool and spill fires. It shows that spill fires have a thin depth of up to 4 mm. The pool fires would have a relatively deeper depth, resulting in a larger value of HRR per unit area (HRRPUA) caused by lower heat loss in comparison to spill fires (Wright et al., 2013). Most of the listed experiments result in a small magnitude of HRR compared to vehicle fires. Only pool fire experiments performed in a tunnel have an HRR around 5 MW. Most of the experiments obtained HRR of less than 1 MW.

The pool fire experiments are expected to provide a lower bound of estimated magnitude for vehicle fires. Consider the fire intensity of such low magnitude of HRR from pool fire experiments with small dimensions would not be

of interest for bridges in fires, only magnitudes of the order of *MegaWatts* will be considered for the defined vehicle fires in this study.

Appendix A.2 summarises the experimental data of HRR for cars carried out in a wide range of test facilities. The measured peak HRR ranging from 0.484 MW to 9.854 MW and the HRR for cars seem not sensitive to the test facility. Therefore, the average value of HRR (3.81 MW) from all the experiments can be used to stand for the low-intensity car fire. Note that the listed experiments mostly consist of cars manufactured before 2000, which may produce relatively lower peak HRR due to more plastics and synthetic material being used in new cars. Therefore a range of HRR 2 MW-5 MW was assumed for the low-moderate intensity car fires.

Appendix A.3 lists HRR measured from experiments for LGVs. There are only a few tests available. A range of HRR 5 MW-20 MW was used for the moderate to high intensity LGV fires, which can provide an intermediate fire intensity. Currently there are no experiments specifically for HGVs therefore experiments on trailers with goods are considered, as shown in Appendix A.4. Tractor trailers with goods were measured to have significantly higher HRR in comparison to cars and LGVs, ranging from 13 MW to 202 MW and several experiments provide very high peak HRR, such as 201.9 MW in Runehamar Road tunnel test and 128 MW in Repparfjord Tunnel test. The accumulated smoke in an enclosed environment test would provide too high a predicted HRR for a bridge fire.

As stated by Lönnermark and Ingason (2005), the HRR of HGVs is between 20 MW and 30 MW in the PIARC document (PIARC Committee on Road Tunnels, 1999) and the NFPA 502 standard (National Fire Protection Association, 2011). Note that the vehicle HGVs were not included in the experiments and wind is involved in some of the tests. Combined with the assumption that the fire load in experiments is significantly less than a roadworthy vehicle due to

the battery and fuel removal in tests. Finally a range of HRR 20 MW-50 MW was assumed for the High-very High intensity HGV fires.

There are no experiments involving fuel tanker truck fire, but it is assumed that HRR in the exceptional category is 50-100 MW. Considering that HRR would be much greater in the case of HGVs transporting fuel, a tanker fire is used with slightly greater length and height than that of HGVs and an exceptionally high value of HRR.

4.2.5 The Effect of Smoke

In reality, the primary and secondary beams can provide spaces for smoke to accumulate which is likely to provide a smooth decay of fire load along the span. This scenario is not considered in any prescriptive code-based fire curves. In order to create more realistic fire curves, the effect of smoke accumulation has been at first included in the CFD models by modelling two beams of depth 1.4 m along the two sides of slab. The simulated geometry is designed to trap the smoke. However, it was found that the simulation of beams has a very limited effect on the magnitude of the received heat flux along the bridge. The steel beam is assumed to be fully engulfed in the plume. This might be caused by the significant amount of smoke generated from large vehicle fires which reduces the radiative loss from the fire (SFPE, 2016). In the finalised CFD models, the side beams were not simulated. It was found that the influence of modelling beams to capture the trapped smoke behaviour can be neglected.

4.2.6 The Finalised Parameters

Table 4.3 lists the finalised HRR used with the corresponding vehicle types and dimensions. The area of the localised fire source is taken to be the footprint of

the four standard vehicles. For all the categories, the fuel bed is assumed to be a fixed rectangular region which is positioned above the ground based on the fact that most of the burning material would be at some height above ground level. In order to arrive at general fuel bed dimensions, length and width for each vehicle category was based on the available data in Table 4.2.

Table 4.3: Parameters used in CFD models for each category

	HRR (MW)	Length (m)	Width (m)	Height (m)	Fire Locations (under span)	Received heat fluxes locations (on bridge surfaces)
Low – Moderate (Cars)	2-5	3.2	1.6	1 1.6	Mid-point; Quarter point; Near abutment.	Slab bottom; Section corner; Beam centre; Beam bottom.
Moderate – High (LGVs)	5-20	5.2	2	1.6 2.6		
High - v. High (HGVs)	20-50	12	2.4	2 3 4		
Exceptional (Fuel tanker)	50-100	14.8	2.4	2 4.6		

Another researcher Alos-Moya et al. (2014) used an estimated fuel burning area of 30 m^2 and a spilled fuel area of 155.13 m^2 to analyse the structural response of a real tanker accident under a bridge. The fuel bed areas were used based on the pictures of the fire event and the structural damage, which supports the feasible estimation of fuel bed dimensions shown in Table 4.3.

4.3 CFD Models

This section presents the results from the CFD simulations conducted using FDS for the design bridge fires. The fire characterisations are presented in Section 4.3.1. The sensitivity study for grid resolution and control volume are described in Section 4.3.2. The HRR in the FDS models will use the two ends of defined HRR range (Table 4.3) for each category. This is enough for capturing the trend for each fire intensity and it is not necessary to perform simula-

tions for mid-range values of HRR.

4.3.1 Defined Fire Development

A rectangular fuel bed with different HRR and dimensions located below the flat slab span is used to represent vehicle fires. Usually high magnitude vehicle fires especially HGV and fuel tanker fires are described as the hydrocarbon fire, so a pool fire is a reasonable representation. In this study, the fuel is defined as heptane with heat of combustion of $44.6\,\mathrm{kJ/g}$ (SFPE, 2016). The carbon monoxide (CO) and soot yields are the mass of CO or soot produced per mass of fuel reacted, with specified value of 0.01 and 0.037 respectively (SFPE, 2016). An emissivity factor of 0.7 was used for the steel section (EN, 2005a).

The fire intensity is presented by a time-dependent heat release rate per unit area (HRRPUA) curve, as shown in Fig. 4.4, which is a critical parameter reflecting the heat flux from the fire. Considering that the FDS results are inherently transient, a sufficient run time is necessary to eliminate the influence of the initial conditions and averaging out the time-dependent outputs. In this research, fires were modelled for 30 minutes allowing 60 seconds of growth and flow stabilisation (curves beyond 5 minutes not plotted in Fig. 4.4 for better observation).

The HRRPUA curves in reality include three stages of fire development: growth, steady burning and decay. Fig. 4.4 shows the HRRPUA curves for each category where curve was defined to linearly increase from zero to a capped value, $HRRPUA_{max}$, which varied for each category. The HRRPUA curves remain constant for the rest of the run time where the averaged values of $HRRPUA_{max}$ can be obtained at steady state and no decay period considered. This assumption gives a conservative result since a variable HRR would normally occur in reality.

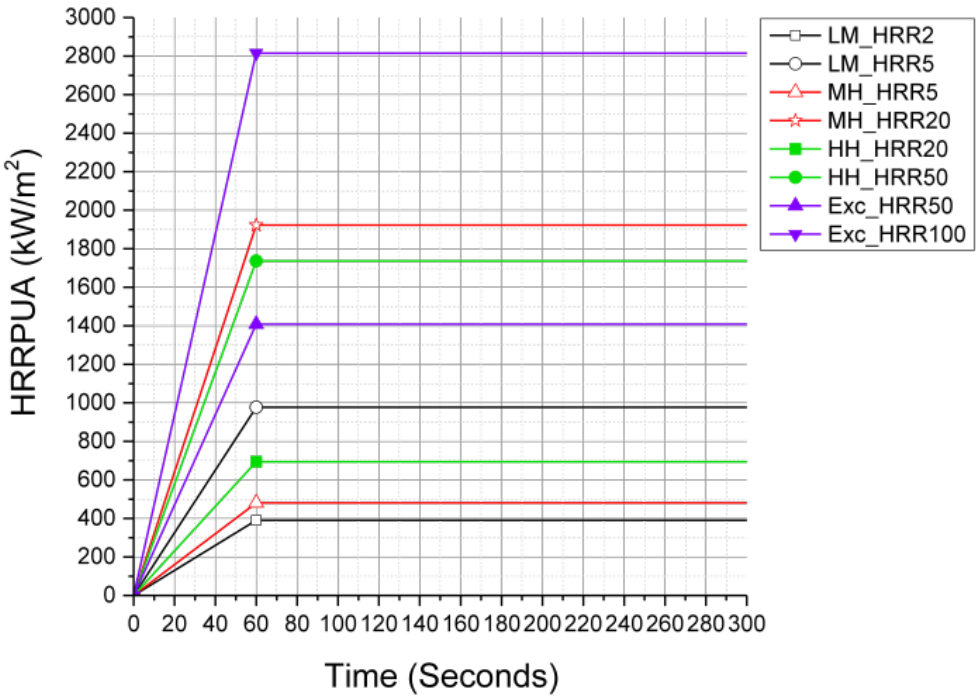

Figure 4.4: HRRPUA curves for four categories of fire intensity (shown as 5 min run)

4.3.2 Sensitivity Study

To make sure the models are able to capture the peak heat fluxes, a sensitivity study was performed to check the impact of changing grid resolution and control volume on results.

Radiation plays an important role in large fires with high gas temperatures and high soot content, especially when the heat flux near the fire source is the main concern. In the CFD models, each additional radiation angle increases the simulation time. A sensitivity study on number of radiative angles are usually required to find a balance between the accuracy of the radiation and the computational cost. However in this research, the received heat flux along beam is far away from the fire source, especially for the far-field area. According to SFPE (SFPE, 2016), the radiative fraction is associated with the pool diameter. The radiative fraction is 0.15-0.5 for a pool fire with diameters of 2-5 m. Convection dominates the heat transfer at low temperature in the far-

field area, therefore minor variations in radiation, due to varying the number of discrete angles modelled, will have negligible influence on the predicted fluxes.

4.3.2.1 Grid Resolution

According to a few of rules of thumb, an estimation of grid cell can be made based on Eq. 4.1 where D^* is characteristic fire diameter incorporating HRR of the fire. According to Hostikka et al. (2015), Plume Resolution Index (PRI) is defined as $D^*/\delta x$, which is the number of grid cells of length δx that span the characteristic diameter of the fire. Where the standard ambient properties were used ρ_∞ = 1.204 kg/m^3, C_p = 1.005 kJ/(kgK), T_∞ = 293 K, g = 9.81 m/s^2.

$$D^* = (\frac{\dot{Q}}{\rho_\infty C_p T_\infty \sqrt{g}})^{2/5} \tag{4.1}$$

The low-moderate HRR (cars) fire model with HRR 2 MW was used to perform the sensitivity study, resulting in a value of D^* 1.27 m. This is because the grid resolution or control volume should be accurate enough for the other models if they are sufficient to capture the results for a model with low magnitude.
when $D^*/\delta x$ = 4 (coarse mesh), δx = 0.32 m
when $D^*/\delta x$ = 10 (moderate mesh), δx = 0.13 m
when $D^*/\delta x$ = 16 (fine mesh), δx = 0.08 m
Therefore, a 24 m $\times$ 24 m $\times$ 12 m space was modelled with the size of cubic cells 0.1 m and 0.2 m (0.3 m was not used for an easier setting up). While there is some variation of output (Fig. 4.5) with cell size for the smallest fire scenario, this variation is expected to be negligible for larger fires, so using the 0.2 m cell size is justified. The gird size of 0.2 m is also consistent with both rules of thumb: number of cells in D^*, number of cells across the burner, number of cells spanning the fire.

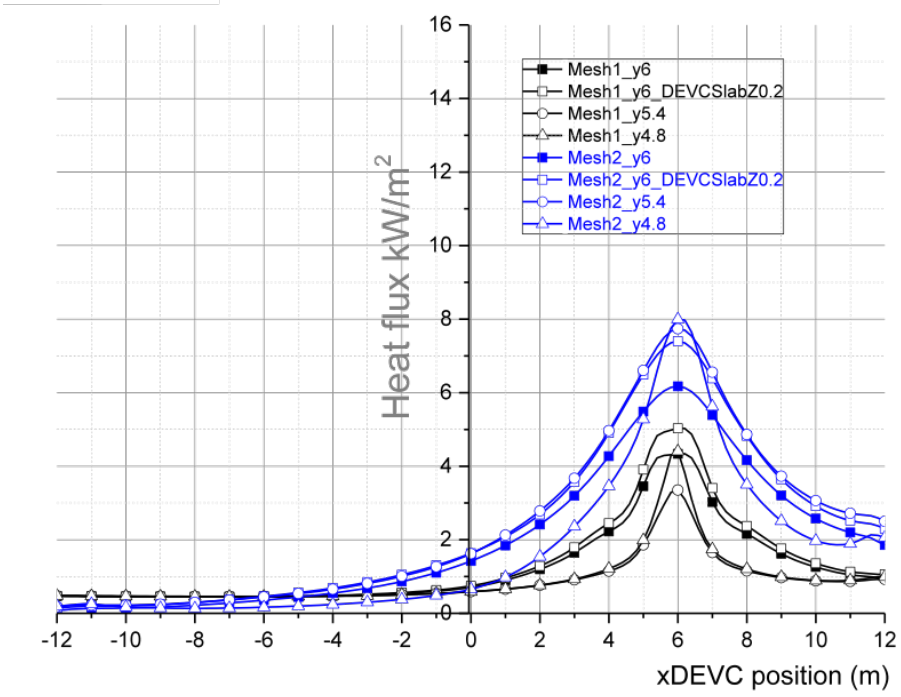

Figure 4.5: Heat flux variation with the distance from the mid-span (Low-Moderate models with HRR 2 MW) using Mesh 1 (0.2 m) and Mesh 2 (0.1 m)

4.3.2.2 Control Volume

The top, foreground and background side boundaries of the domain were left open to ambient conditions while the left and right surfaces of domain were defined as adiabatic surfaces to represent the concrete pier and abutment respectively. The bottom surface was modelled as concrete to represent the roadway. The material properties for concrete were taken from the Eurocode (EN, 2004).

Space between the domain edge and fuel bed would have significant effects on the fire performance. In order to control the domain size without compromising the accuracy, a sensitivity study for the domain size has been performed. A sharp decrease along the width of span and a lower heat flux output are very likely caused by the insufficient domain space where fuel is not completely burning with air. The models were finally conducted in a 24 m-length,

24 m-width, 12 m-high computational domain to generate sufficient space beyond the physical boundaries to provide adequate environment for the fire and smoke spread and the interactions of inflow and outflow.

In order to save the computational expense, the author once considered to model only half or quarter of the whole span. However, the difference between the spaces on the two sides of the fuel bed cannot be captured in this way. Therefore, the original dimensions was used to better capture all the behaviours of interest.

4.4 Results and Analysis

The heat flux imposed on the bridge structure is dependent on the fire characterisation, bridge geometry and thermal properties of the boundaries. This section compares the temperature results and flame behaviour in Section 4.4.1. The heat fluxes resulting from all scenarios are analysed in Section 4.4.2.

4.4.1 Fire Behaviour and Temperatures

Fig. 4.6a shows the flame shape when the fuel bed is located below the mid-span, where an unconfined axisymmetric plume is produced. However for the case where the vehicle is near the abutment (Fig. 4.6b), the flame was adhesive the abutment (known as Coandă effect). This phenomenon was also observed by an experiment where the presence of a column affects the flame shape (Alos-Moya et al., 2017; Tondini and Franssen, 2017).

When comparing with the commonly used Hydrocarbon fire for bridges, it was found that the highest temperature in most of the scenarios of design vehicle fires are much lower. The exceptional fire of fuel bed above 2 m with HRR 50 MW has the highest temperature of around 1020 ℃. The growth rate is not able to be compared as only the steady-state is considered for the design

fires. Fig. 4.7 shows the example of the temperature distribution for the low to moderate model. It shows that the temperature is uniform within an area of diameter around 1.6 m - 3.2 m, illustrating that the uniform fire can be used for a short span as proved by Alos-Moya et al. (2014).

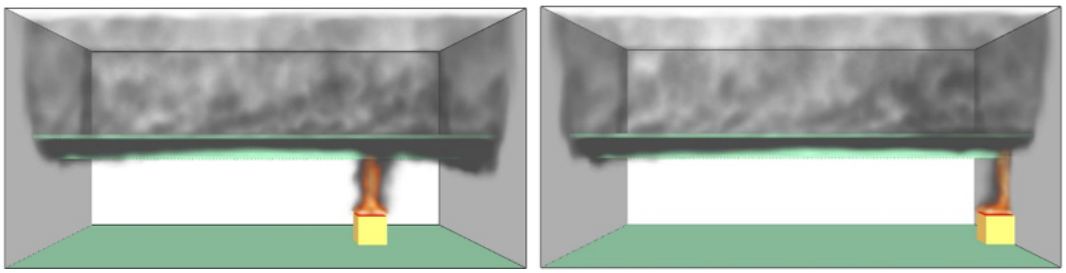

(a) (b)

Figure 4.6: Fluid dynamic vehicle fire model (Low to Moderate, 5 MW, 3.2 m $\times$ 1.6 m $\times$ 1.6 m) under (a) mid-span and (b) near the abutment

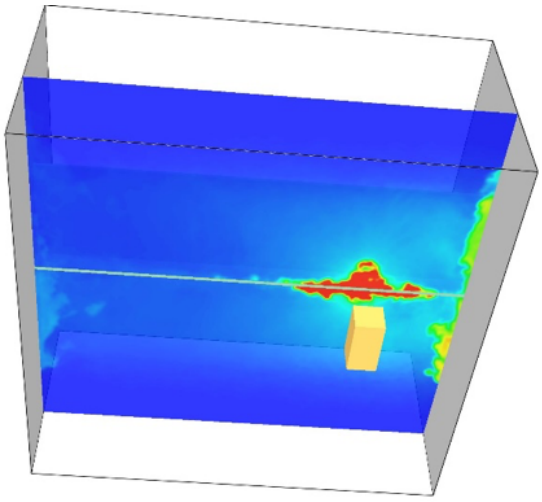

Figure 4.7: Temperature distribution on the surface at the bottom of the beam for the model Low to Moderate, 2 MW, 3.2 m $\times$ 1.6 m $\times$ 1.6 m

4.4.2 Beams to Set Up the Measure Devices

The simulation of the beam along the span width seems unable to capture the trend of heat flux variation, where the maximum value does not match with the maximum values obtained in the models with a beam along the span length. This is probably caused by the flow barrier effect created when the beam is

defined along the bridge width. As seen in Fig. 4.8, for high-v.high models with HRR 50 MW, the received heat flux tends to be uniform above the fuel bed length with some variations caused by the non-uniform flame shape. However the range of uniform heat flux varies with the height of fuel bed. The heat flux sharply decays beyond the vicinity of the fuel bed (Fig. 4.8a), however the lowest values are not always at the edges of the slab (red curves in Fig. 4.8b).

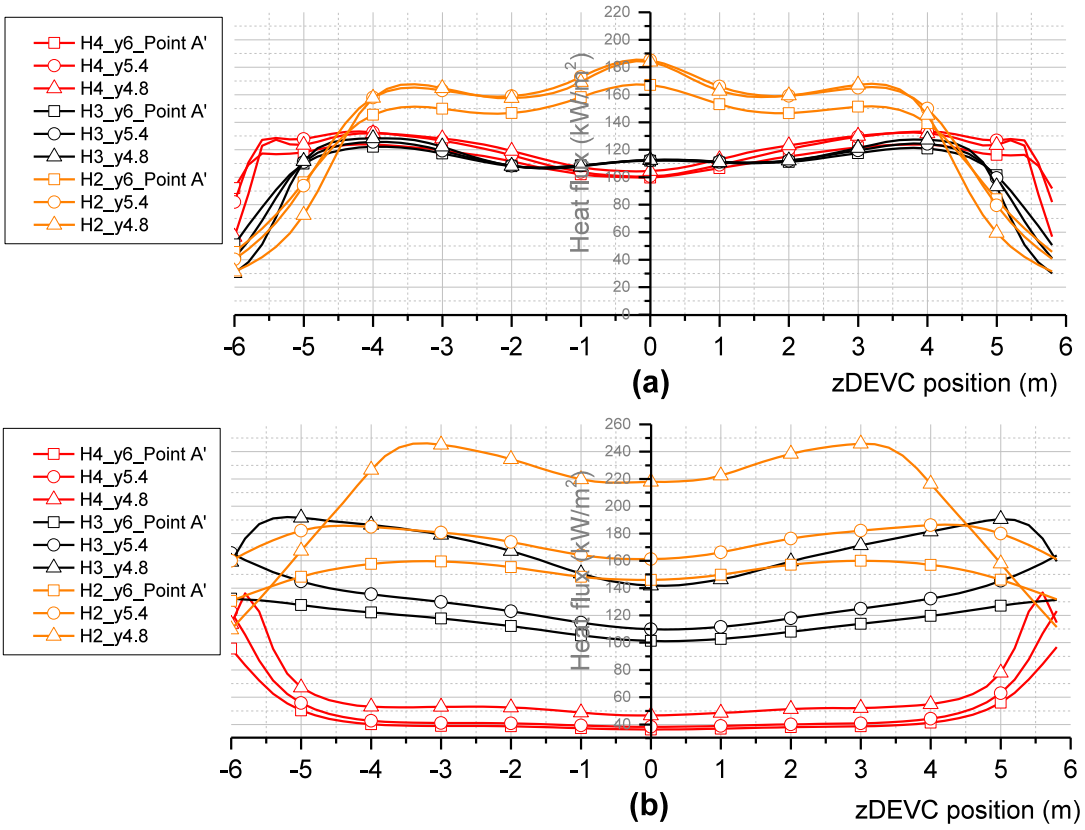

Figure 4.8: Heat flux variation with the distance from the centreline of the span width for the High - v.High model when HRR is 50 MW and the fuel bed (a) under quarter span and (b) near abutment

4.4.3 Heat Fluxes Results

Fig. 4.9 - 4.12 shows the magnitude of heat flux received over the fire-affected span of the bridge for different scenarios. For clarity, only the curves received at Point A' (illustrated in Fig. 4.1) are plotted for better observation. The maximum

heat fluxes were obtained to be as high as $250\,\mathrm{kW/m^2}$ when the HRR was $100\,\mathrm{MW}$ (as shown in Fig. 4.14). As fires became larger in HRR magnitude, the maximum value of heat flux to the structural surfaces increases due to the radiation feedback between the fire and the structure.

As shown in the exponential shape of received heat flux curves, the value is maximum above the fire source and decays with increasing distance from the fire origin. The positions of peak values represent the three fire locations. The received heat flux at locations near the abutment is usually higher than the other two locations, especially for low to moderate fires (Fig. 4.9), which is considered reasonable due to the feedback effect. This phenomena was also explained by Drysdale (2011), if the fire is by a wall, or in a corner, the temperatures will be greater, due to not only the lower rate of entrainment into the vertical plume, but also due to the "*restriction under the ceiling where the flow is no longer radial and symmetric*".

However, in some cases, the maximum heat flux received when the fuel bed is near the abutment is lower than the other two locations. This is probably caused by the fact that when the height of fuel bed is higher than 2 m (under a bridge deck of 6 m height), the released fuel vapours have to travel away from the vehicle before sufficient air is found to allow burning, so the flames (and hence the higher temperatures) happen away from the vehicle location. This phenomenon suggests that the open environment may not always be fuel controlled when the fire is large. The environment may change from 'open air' to 'partially enclosed' when a large lorry is burning only a short distance below the bridge deck.

As the fuel bed dimensions (length, width and height) are different in each category, it would be difficult to show the correlation between HRR and heat fluxes as the variables are not identical. Figure 4.13 is just for visualisation purposes only.

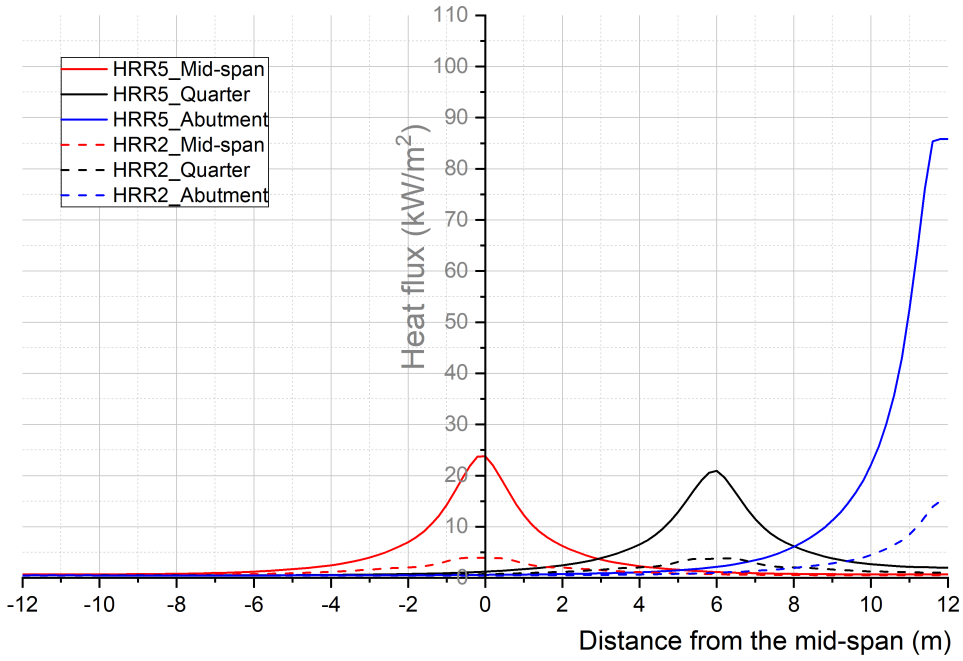

(a)

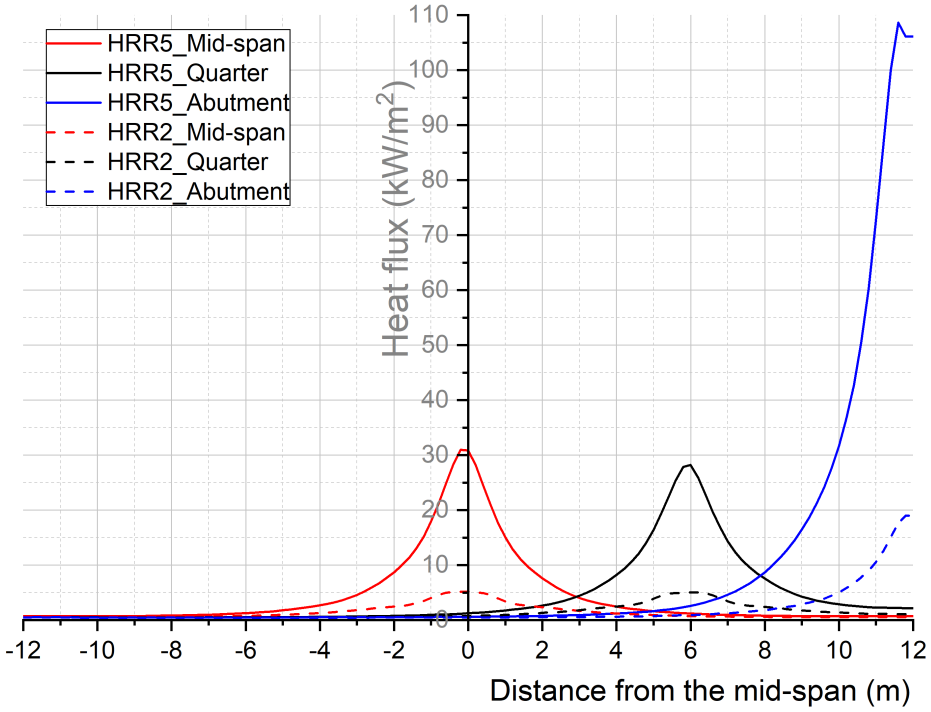

(b)

Figure 4.9: Heat flux variation with the distance from the mid-span for Low-Moderate fires with height (a) 1 m; (b) 1.6 m

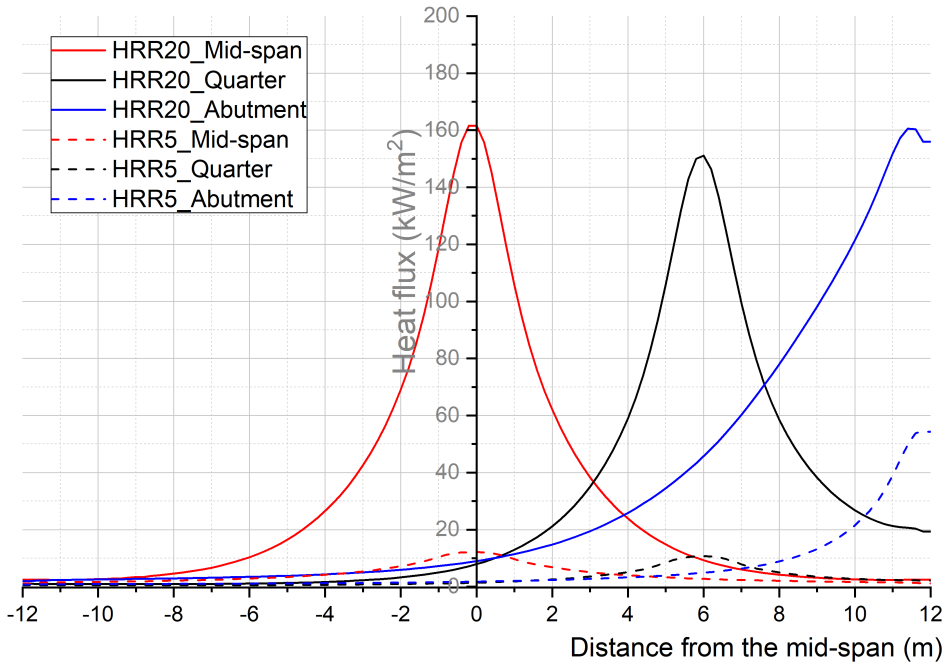

(a)

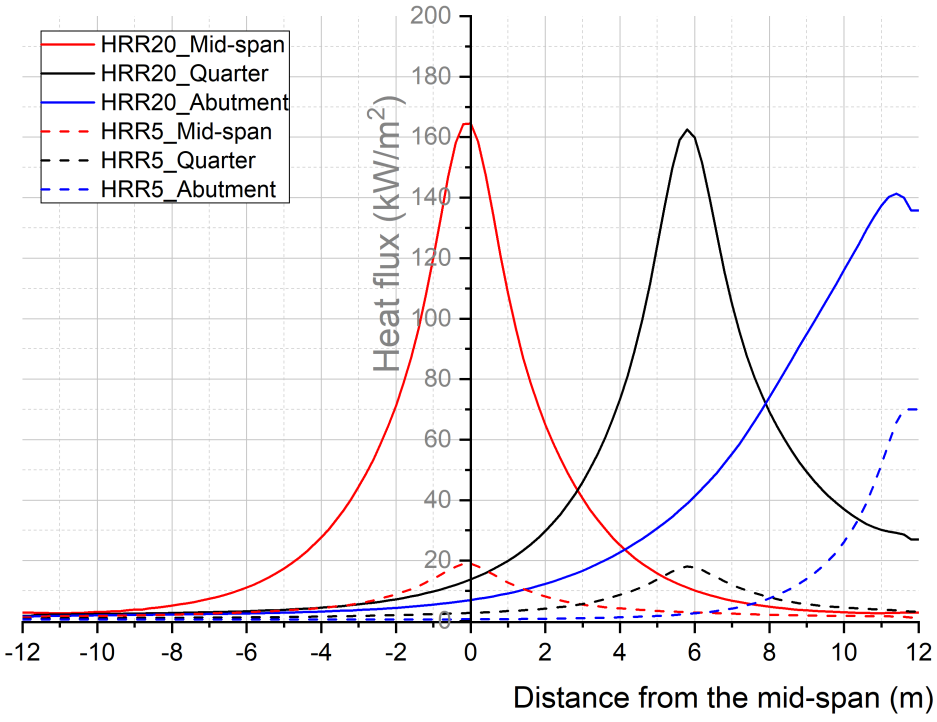

(b)

Figure 4.10: Heat flux variation with the distance from the mid-span for Moderate-High fires with height (a) 1.6 m; (b) 2.6 m

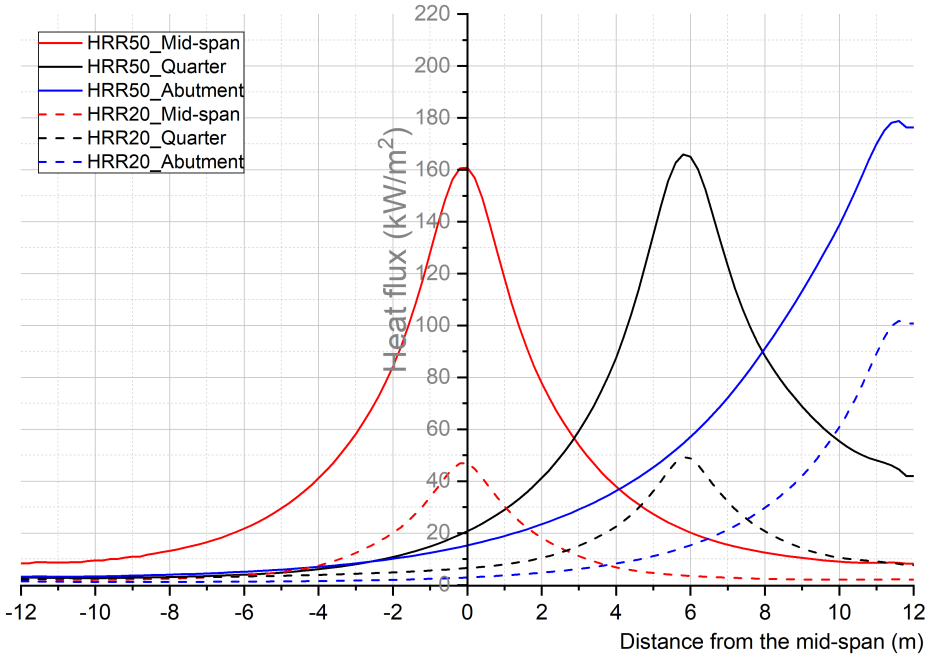

(a)

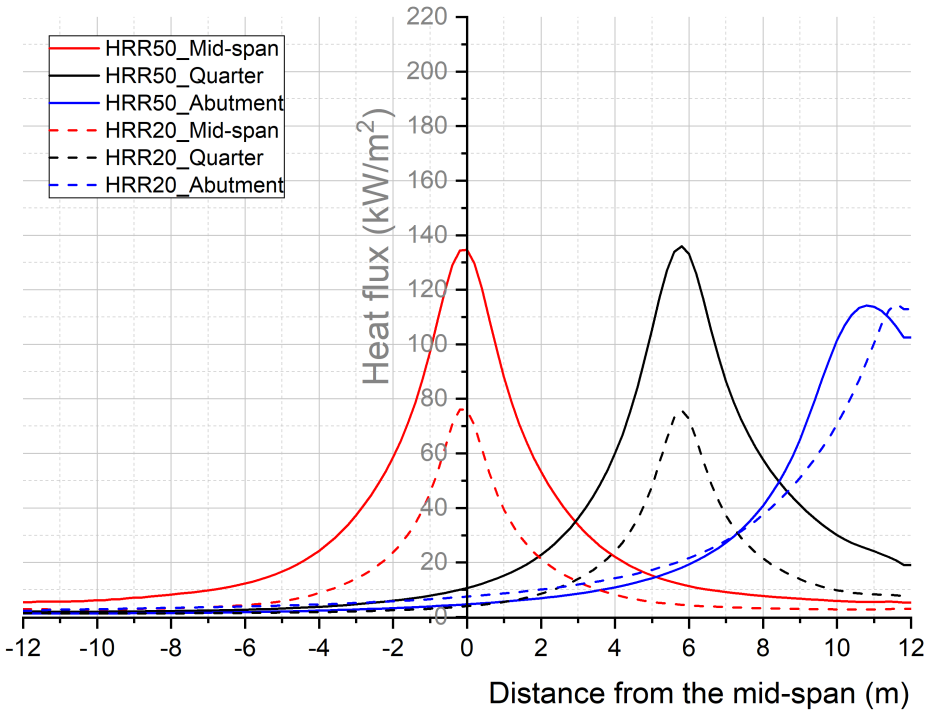

(b)

Figure 4.11: Heat flux variation with the distance from the mid-span for High-v. High fires with height (a) 2 m; (b) 4 m

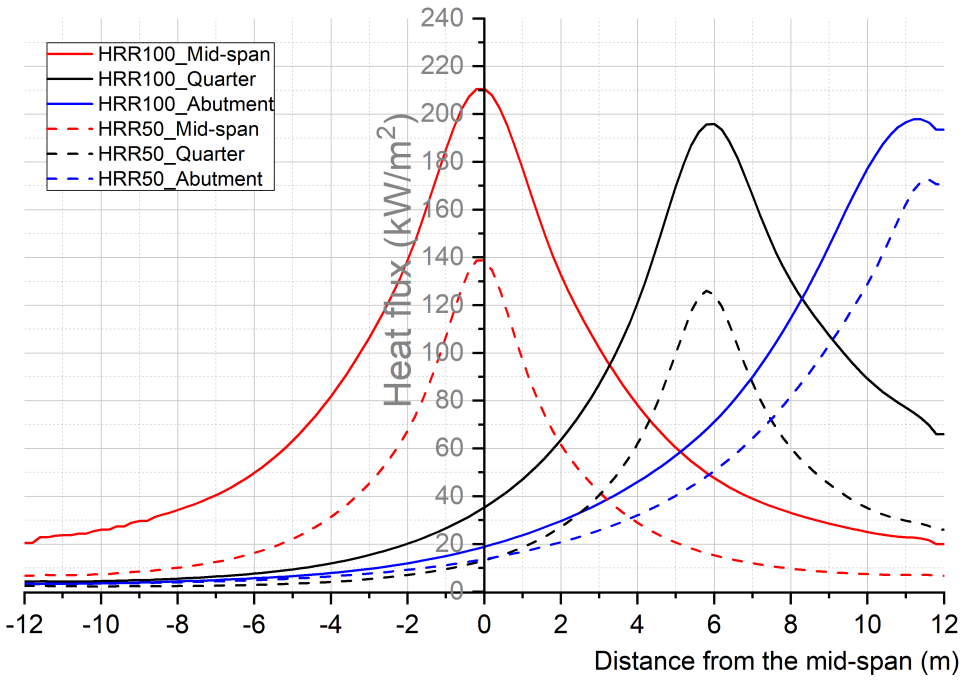

(a)

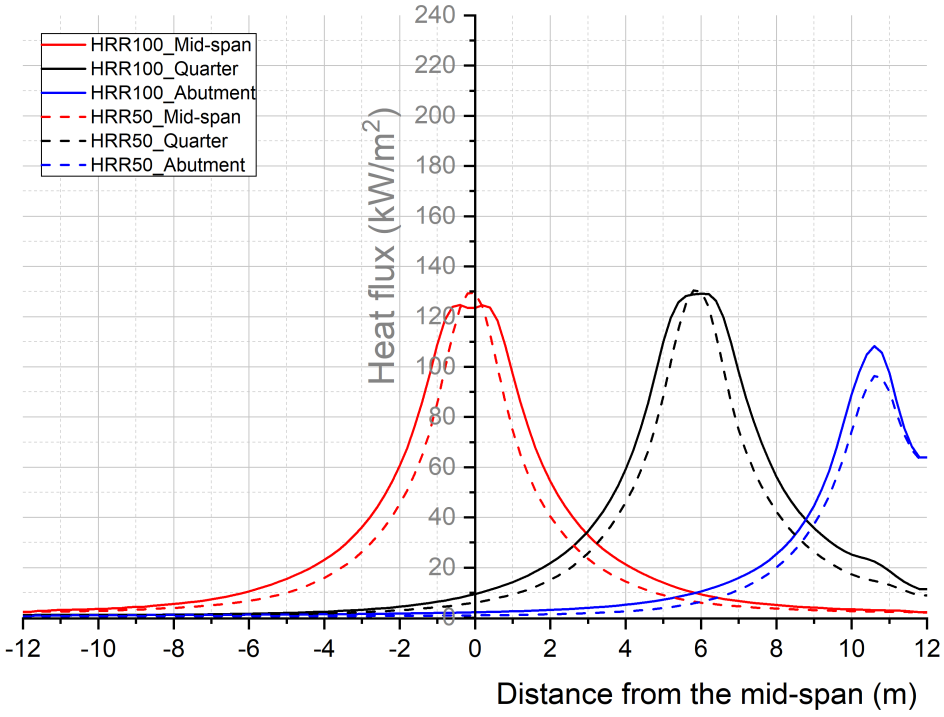

(b)

Figure 4.12: Heat flux variation with the distance from the mid-span for Exceptional fires with height (a) 2 m; (b) 4.6 m

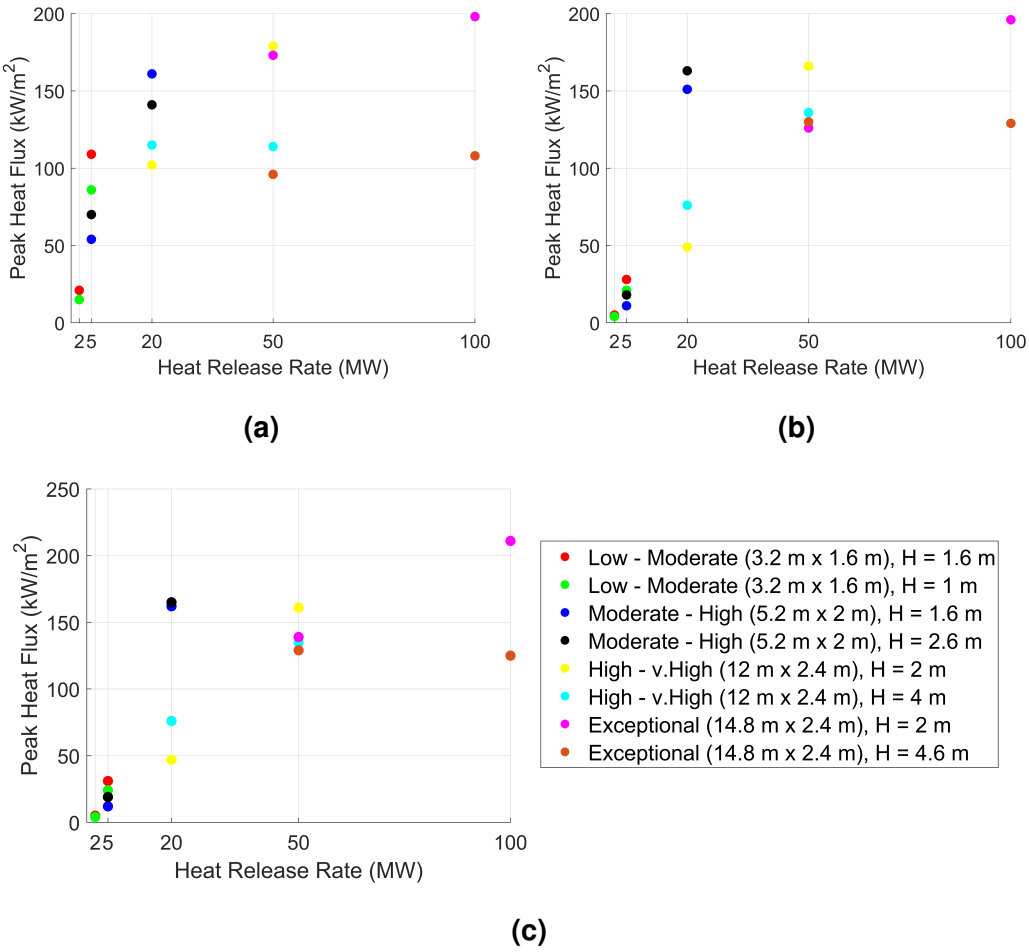

Figure 4.13: Heat flux variation with HRR when the fire (a) under the mid-span, (b) under quarter span and (c) near the abutment

Fig. 4.14 shows the example of the heat flux variation with various parameters for the exceptional fires. The gradient of incident heat flux along the longitudinal direction beam is much higher than across the section. This is contrary to the statement in Pchelintsev et al. (1997): "*the gradient of incident heat flux is larger in the vertical direction than in the axial direction within the beam.*" This is maybe due to the lower flange of beam section in their experiments which is not considered here.

For different locations across the beam section, the heat fluxes received at the bottom of the beam decay more quickly along the span than at the other positions, which is especially true for the near-field area above fuel bed. This is

caused by the high flame height which mainly heats the slab bottom and beam web. At the slab bottom, Point A' receives higher heat flux than Point A located at the corner of the section. This is caused by the geometric effect (concave or re-entrant corner), which is dead zones for flow so the convective heating is ineffective in these area.

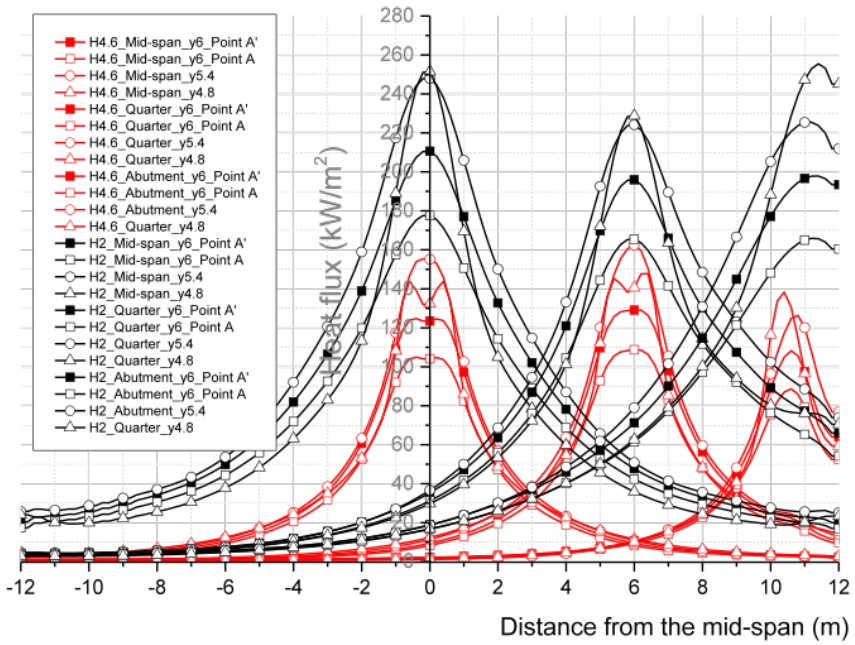

Figure 4.14: Exceptional fires with HRR 100 MW: Heat flux variation with fuel bed height (H), fire locations and received heat fluxes locations (y)

4.5 Conclusions

Only prescriptive code-based fire curves are currently available for assessing the performance of bridges in vehicle fires. This work proposes a powerful quantitative decision-making tool for bridge managers. This will allow a more realistic representation of vehicle fires for highway bridges, based on the CFD models that have been introduced in this chapter. The CFD models for vehicle fires with varying fire intensities will be consolidated and presented in

Appendix B to create generalised fire curves for use as design fires to assess the structural performance of bridges.

To develop a robust methodology for characterising the fire hazard to a bridge, a probabilistic approach should ideally be developed. However in this research discussion is restricted to a deterministic approach, albeit distinction was made between the vehicle types involved in order to be able to assign different levels of expected performance under fires of different magnitude.

The received maximum surface heat flux is significantly higher when the vehicle accident is near the abutment. This also happens when the fuel bed is located at an elevated location and is therefore closer to the bridge deck. However, for the very large fires with HRR larger than 50 MW, the models are counter-intuitive, showing that greater height or being close to the abutment does not always produce the greatest heat flux.

The effects of moving the fuel bed away from the abutment were investigated, however only the mid-point and quarter point of the span were considered. As expected the abutment does not have a significant effect on the scenario of a vehicle at quarter span, showing almost identical results as the vehicle at the mid-span. A closer position to the abutment may be studied in the future to determine the minimum distance from the abutment at which its effect can be neglected.

It is worth mentioning that the modelled vehicle fires do not represent the real fire scenarios due to the difficulty of simulation regarding the temporal variation and environmental conditions. According to Drysdale (2011), in natural fire, buoyancy is the predominant driving force and the behaviour of unbounded flames is influenced by the air around them. However, the wind effect is not considered in this preliminary study as neglecting it is to be a conservative assumption (Peris-Sayol et al., 2015a).

The vehicle fires proposed in this research are designed to represent the

fire hazard in highway bridges realistically, while also retaining sufficient simplicity so that they can be readily used by practising engineers. Real vehicle fires may have a large range of dimensions and orientations, however it is felt that the assumptions in this study capture the most important characteristics of vehicle fires and neglect details that are not significant from engineering design and performance assessment perspective.

The gas temperature of the Hydrocarbon fire was used in Chapter 3 for the heat transfer analysis. However instead of using adiabatic gas temperatures here, the received heat fluxes on bridge surfaces were obtained and will be used as an input data into HT analyses. This is because the work in this chapter is not purely for a comparison with the models using the Hydrocarbon fire. The normalised design vehicle fires use heat fluxes as the thermal boundary conditions to be consistent with code-based localised fires.

The beams for capturing outputs are modelled with rectangular sections with no lower flange width to that would create a shadow effect and reduce the radiant heat flux to the web. However this may not result in a significant difference of heat flux prediction for such large fires, a detailed study may be undertaken in the future work.

5

Fire Resistance of Highway Bridges Under Fuel Tanker Fires

5.1 Introduction

This chapter progresses the work in Chapter 3 by applying the new design vehicle fires (Chapter 4 & Appendix B) to analyse the fire resistance of a highway bridge. The design fires feature a decaying heat flux along the bridge span away from the vehicle which is likely to result in a different failure time compared to the uniformly applied standard fire such as the Hydrocarbon fire. It is assumed that the bridge is exposed to a fuel tanker fire under the span with

three locations: 1) near the middle support; 2) under the central span; and 3) near the abutment. The fire source near the middle support is investigated because failure has found occurred due to web buckling concentrated near the middle support for the skew bridge models (when modelled entirely using shell elements in Chapter 3). Although four types of vehicle fires have been studied in previous chapter, the high magnitude fuel tanker fires will be used in this work for a conservative comparison. The rectangular and skew bridge models without abutment will be discussed.

5.2 Thermal-stress FE Simulation

There are three ways to perform the thermal-stress analysis based on the interaction between multiple physics (Simulia, 2012):

1) Fully-coupled: temperature and displacement are simultaneously solved in a stress/deformation analysis;

2) Sequentially coupled: an uncoupled HT analysis yields results to be fed into a subsequent static structural analysis within the same software package;

3) Uncoupled: temperatures are calculated without considering stress/deformation state in structures and entering the temperature data directly.

In this chapter, the influence of heat on the structural response of the bridge can be considered as a weakly coupled problem, where the structural deformations are considered to have a negligible influence on the heat transfer. Therefore a sequentially coupled analysis should be sufficiently accurate for this kind of modelling.

Fully-coupled and sequentially coupled analyses were used at first to avoid the process of reading uncoupled HT results into the structural model. The

simulation of a single two-span composite beam was considered to represent the behaviour of the whole rectangular bridge. This assumption is reasonable to start with as all the beams behave almost identically in a rectangular shape (Chapter 3).

In order to accurately predict the HT and structural response in a *fully-coupled* thermomechanical analysis, 420 elements were used in the cross-section based on a sensitivity study (Chapter 3). The coupled displacement-temperature solid element C3D8T was used. Considering the requirements of a reasonable aspect ratio for the elements and adequate accuracy along the span direction, would result in hundreds of thousands of elements for just a single composite beam. The first second of simulation required 20 minutes of run time and there were convergence problems after the fire was applied. Therefore for the full bridge model with one whole span subject to fire, the fully-coupled analysis is considered prohibitively expensive.

In the *sequentially coupled* analysis, an uncoupled transient 3D HT model was at first analysed in which all nodal temperatures can be read into the subsequent mechanical model as a predefined field. Diffusive elements are available in the family of continuum and shell elements, therefore the heat transfer solid element DC3D8 was used for the HT model. Since the sequentially-coupled analysis also requires corresponding continuum or structural elements to be used in the structural model, the composite primary beam was modelled using C3D8R elements for structural analysis. The region of Span 2 in the structural model was heated by the temperatures generated from the HT analysis. In order to avoid the interpolation of the temperature results from the nodes in the HT model to the nodes of the structural model (Simulia, 2012), the mesh was designed to be identical between the thermal and stress analyses. Compared to the fully-coupled analysis, the sequentially coupled HT model is more economical, taking 5 hours for a 3600 second fire duration which is acceptable.

However, using continuum elements in the structural model of the same grid size as the HT model, a single two-span beam structural analysis took nearly 50 minutes for just 3.5 seconds of simulation, which is not acceptable.

Since the first two types of analyses require long simulation times, the third approach of *uncoupled* analysis is finally used although it requires a complicated temperature reading process using a MATLAB script. Since different element types can be used for HT and structural model in an uncoupled analysis, a one-span single composite beam and the whole bridge superstructure will be modelled for HT and structural analysis respectively. Only the fire-affected Span 2 was modelled in HT analysis to avoid unnecessary simulation. The modelling of the whole bridge will also simulate the thermal bowing and thermal expansion in the transverse direction to the span, which is likely to result in greater deflection in the middle compared to the edge beams.

For comparison purposes, the following assumptions are kept the same. For all the detailed definitions please refer to Chapter 3.

- Rectangular and skew shaped bridge with the same regularised dimensions
- Thermal and mechanical properties
- Fire located under the bridge span
- Only Span 2 is exposed to fire and Span 1 is assumed to unaffected by fire
- Fire has a 20 min duration
- No decay in time is considered (steady state assumption)

The difference between models for comparison:

- Hydrocarbon fire has a rapid growth period while design ‘Bridge Fires’ are steady-state (unvarying in time)

- Hydrocarbon fire is spatially uniform along the bridge span while design 'Bridge Fires' are spatially non-uniform along the bridge span (decaying with distance from the source)

- Heat transfer model is 2D (for saving computational cost when the HT along the bridge span is ignored) in Chapter 3 and 3D in this chapter

5.3 Thermal Analysis

In order to enable as conservative a comparison as possible with the thermo-mechanical behaviour of bridge under Hydrocarbon fire in Chapter 3, the most severe fuel tanker fires were selected to represent the design vehicle fires. In this section, two HT models with different fire locations were analysed, one with the fire source under the mid-span and another with the source near the abutment. Given the skew model is found to have local buckling near the middle support in Chapter 3, the results from the HT model with fire source near the abutment is also reversely applied on Span 2 in the structural model to represent the scenario of fire source near the middle support.

5.3.1 Heat Transfer Analysis for Rectangular Models

A transient 3D HT analysis of Span 2 (length 24 m) was performed. The model consists of 121,920 DC3D8 heat transfer elements. The adopted mesh size at cross-section was selected based on the sensitivity study in Chapter 3. In the direction along the span length, the element size was 0.1 m to capture the temperature variation over the span with a suitable element aspect ratio. Another mesh sensitivity study was performed for the 3D HT model by increasing the length of the element from 0.1 m to 0.2 m resulting in 60,960 elements in total.

Fig. 5.1 compares the temperature at the steel web centre at three locations along the span length when the fire source under the mid-span. The results are identical and show that halving the mesh resolution has no influence on the prediction of the temperature in the steel girder sections.

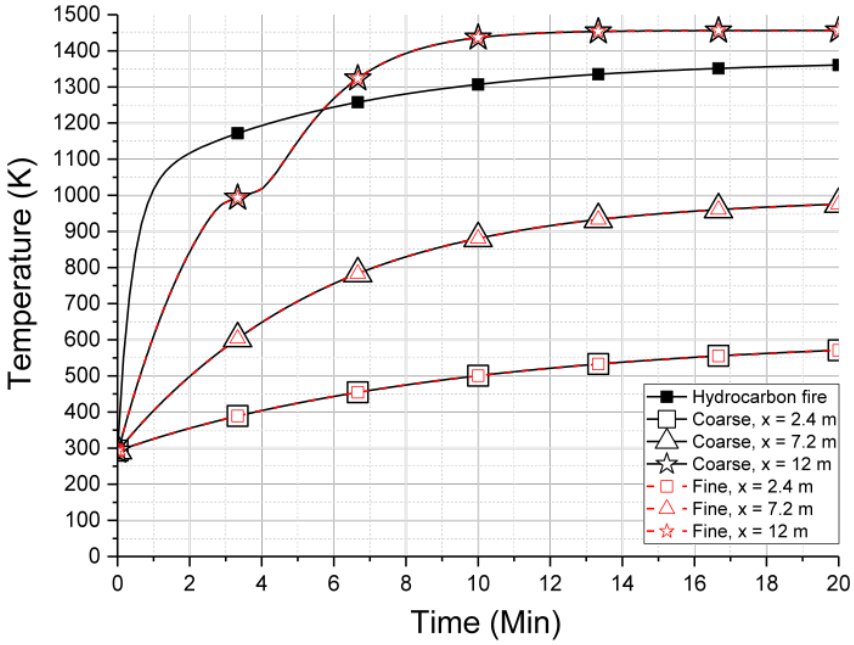

Figure 5.1: Heat transfer results of steel web centre using fine mesh (121,920 elements) and coarse mesh (60,960 elements) when the fire source is under the mid-span. x = 2.4, 7.2 and 12 m represents locations 2.4 m, 7.2 m and 12 m away from the middle support in Span 2

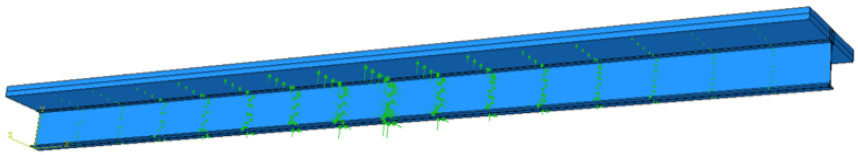

Figure 5.2: Heat flux curves applied on HT models for the fuel tanker fires under the mid-span

Surface heat fluxes from the design bridge fires were applied as boundary conditions to both HT models by specifying analytical fields on the selected

surfaces. This allows the user to define the spatially varying incident heat flux to the surfaces (non-uniformity can be seen in Fig. 5.2). Eq. 5.1 used for fuel tanker fires obtained from the results of Appendix B yields the curves shown in Fig. 5.3. In the expression, Q is 100 MW in order to represent a high magnitude fuel tanker fire. D_{x1} is 12 m and 24 m for the fire source under the mid-span and near the abutment respectively.

$$\begin{aligned}\dot{q}^{"} =& C_1(\frac{Q}{10^6})^{0.3} * (\frac{D_{x1}}{D_{x2}})^{0.01} exp(C_4(x - D_{x1})^2) + \\ & C_2(\frac{Q}{10^6})^{0.3} * (\frac{D_{x1}}{D_{x2}})^{0.02} exp(C_5(x - D_{x1})^2) + \\ & C_3\end{aligned} \tag{5.1}$$

Where C_1 = 28384, C_2 = 27984, C_3 = 7389.9, C_4 = -0.25515, C_5 = -0.023214

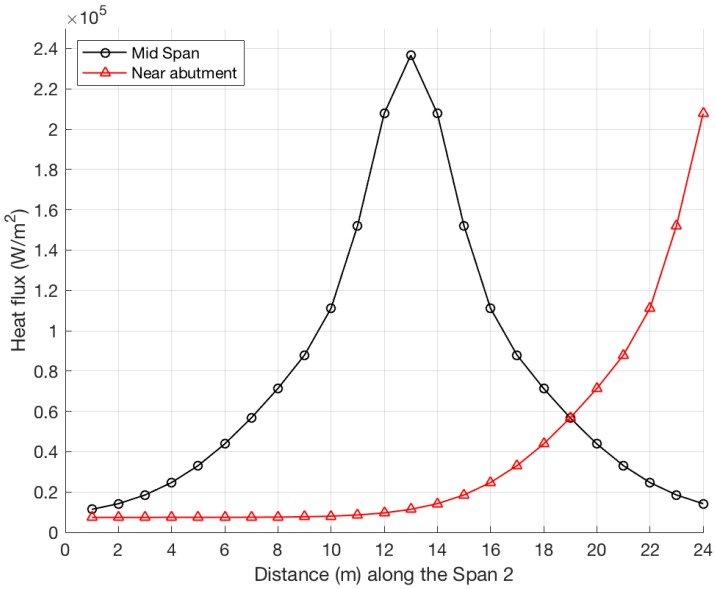

Figure 5.3: Heat flux applied on the selected surface of Span 2

Fig. 5.4 shows the HT models of Span 2 at 20 minutes for the two fire locations. HT results in Fig. 5.4b is reversely applied in Span 2 of structural model to represent the fire source near the middle support. Clearly seen in the contour plot, the highest temperature occurs at the centre of Span 2 or near the abutment at locations closest to the fire source as expected. It also clearly

shows the temperature decay along the span length which is likely to lead to different thermo-mechanical behaviour when compared to the spatially uniform Hydrocarbon fire. Since the two HT analyses have an identical maximum value of heat flux and temperature, only the HT contour at the cross-section of mid-span for the case of Fig. 5.4a is presented in Fig. 5.5 for illustration.

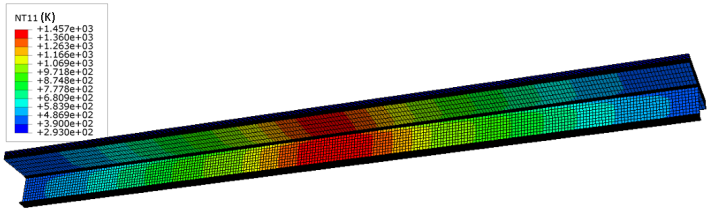

(a)

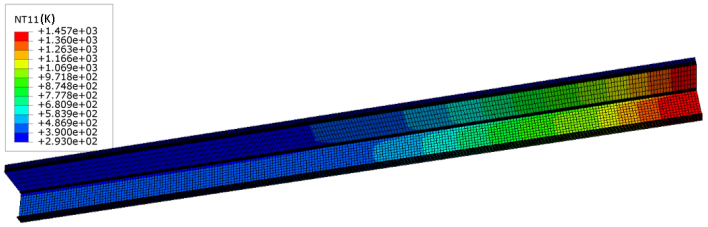

(b)

Figure 5.4: Heat transfer model results at 20 minutes when the fire source is: (a) under the mid-span, (b) near the abutment

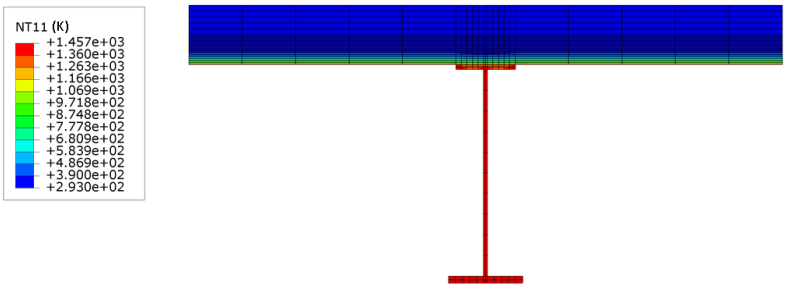

Figure 5.5: Heat transfer model results at 20 min for the composite section at the mid Span 2 (fire source under the mid-span)

The temperature evolution with time when the fuel tanker fire is under the mid-span can been seen in Fig. 5.6. Since the design 'Bridge Fire' is spa-

tially non-uniform, the highest temperatures occur at the cross-section near the mid-span and is therefore used to compare with the HT results from the Hydrocarbon fire. The temperatures in slab are recorded at 9.375 mm above the slab bottom for the model with the Hydrocarbon fire and 10 mm above the slab bottom for the model with the design fuel tanker fire. The slight difference is due to the minor difference of mesh dimensions used for modelling the slab in the two models.

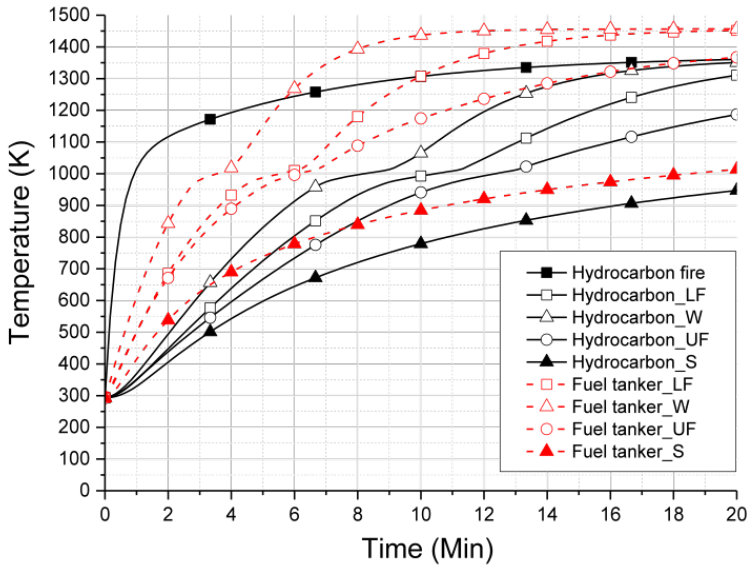

Figure 5.6: Temperature evolution with time at lower flange (LF), web (W) and upper flange (UF), comparison of HT models using Hydrocarbon fire and design fuel tanker fire

As shown in Fig. 5.6, the design fuel tanker fire generates much higher temperatures than the Hydrocarbon fire, especially in the steel web (around 400 K difference at 8 minutes). A more rapid rate of increase is also seen from the design fuel tanker fire for the first few minutes. Therefore it can be concluded that the HRR magnitude defined for the design fuel tanker fire should result in a conservative comparison against the Hydrocarbon fire. Further conservatism is ensured as follows:

1) There is a growth period in Hydrocarbon fire curve, while steady-state temperatures are considered in the fuel tanker fire (essentially a step function implying an infinite rate of increase).

2) Although identical convective coefficients and emissivity factors are used in the models of this chapter (as in the Hydrocarbon fire model of Chapter 3), the effect of these parameters is not equivalent between the two analyses. Temperature was used as the boundary condition for the Hydrocarbon fire, therefore convection and radiation are linked to the gas temperature at the boundary. In the design "Bridge Fire", instead of the net heat flux, the incident heat flux has been applied as the thermal load at the boundary. This method of applying thermal loading partially ignores the heat lost from the surface which will also lead to a higher prediction of the temperature within the composite structural cross-section.

The temperature profiles in the composite section at every 2.4 m (node spacings) from the HT models were applied to the structural model by using MATLAB scripts. The spatially non-uniform thermal loading along the span width was ignored due to the complex behaviour found in CFD modelling which was described in Chapter 4. Therefore the HT results of the single composite beam were repeatedly applied to the five beams of the rectangular bridge. The temperatures in the concrete transverse diaphragm were assumed to be the same as in the concrete slab.

5.3.2 Heat Transfer Analysis for Skew Models

The detailed description of the heat transfer models is not repeated in this section. The thermal model of a composite beam at Span 2 of the skew bridge is modelled which is modified based on the model in Section 5.3.1 with a longer span length (28.8 m). Fig. 5.7 shows the HT model of Span 2 at 20 minutes

for the two fire locations: fire under the mid-span and near the abutment. The HT results in Fig. 5.7b is used for the scenario of fire source near the middle support by reversely applying the temperature along Span 2. The applied heat flux curves on HT models are shown in Fig. 5.8.

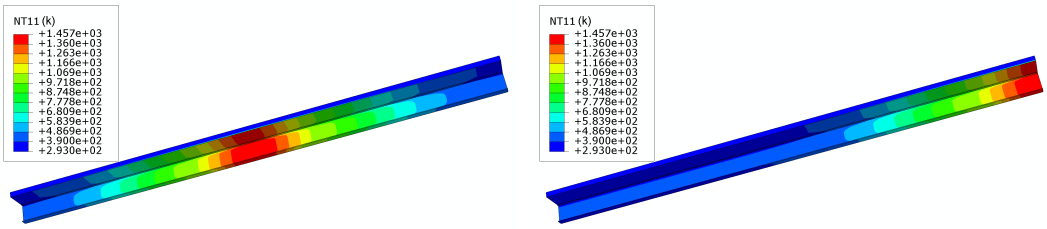

(a) **(b)**

Figure 5.7: Heat transfer model results at 20 minutes when the fire source is: (a) under the mid-span, (b) near the abutment

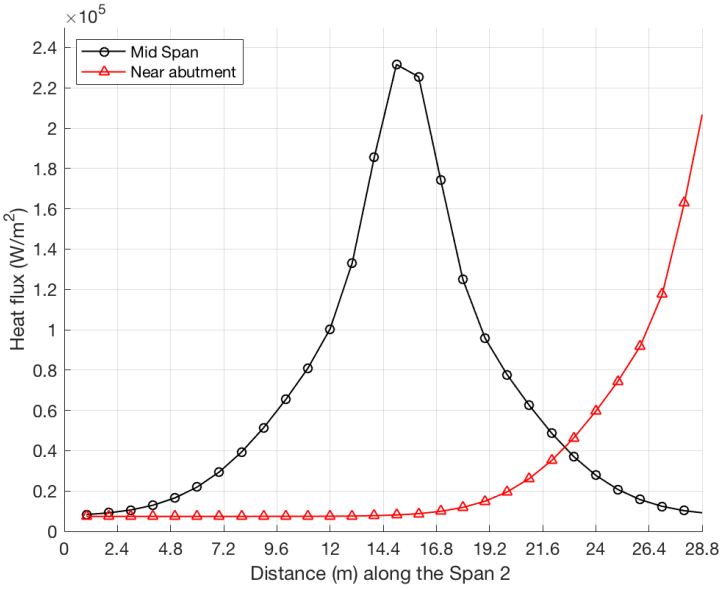

Figure 5.8: Heat flux curves applied on HT models for the fuel tanker fires

5.4 Thermo-mechanical Analysis

This section compares the structural responses of the rectangular and skew bridge to four different fires:

- Hydrocarbon fire
- A design fuel tanker fire under the middle support
- A design fuel tanker fire under the mid-span
- A design fuel tanker fire near the right abutment

For a comparison with Chapter 3, both beam and shell elements are used for modelling the primary beams.

5.4.1 Rectangular Models

The rectangular bridge shape without abutment model is used for analysing the structural response to the design fuel tanker fires. The deformed shape of the models (using beam and shell elements for the primary beams) exposed to fuel tanker fire are shown in Fig. 5.9. The five beams have symmetric deformed behaviour with BEAM No.3 as a symmetry axis. BEAM No.3 will be analysed as a representative beam in graphs due to its maximum deflection.

Unlike the striped pattern deflection contour plot observed at 20 min in the model with the Hydrocarbon fire, 'ponding' behaviour can be seen in Fig. 5.9. It is worth mentioning that the model with the Hydrocarbon fire exhibited 'ponding' behaviour (Fig. 5.10) when the maximum deflection in FAS was small ($0.27\,\mathrm{m}$). The model then tends to show a striped shape pattern with increasing deflection in FAS.

Fig. 5.11 compares the deflection history at mid-span point in NFAS and FAS between the models. Note the maximum deflection does not always occur at mid-span. The peak deflection sometimes moves toward the abutment.

For comparison purposes, the mid-span point is selected to plot the deflection history. The usage of either beam or shell elements does not have significant effect on the deflection history for the rectangular model (as presented in Chapter 3), the rectangular model with Hydrocarbon fire from Chapter 3 is plotted to compare with other models.

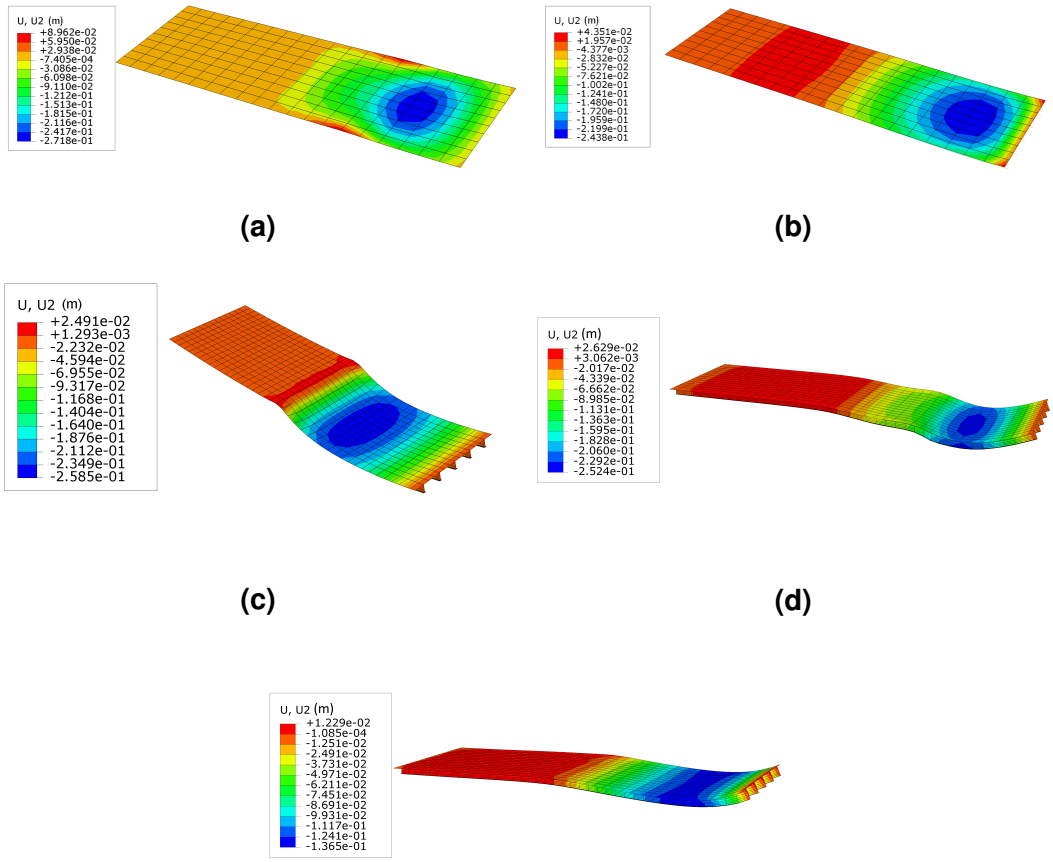

Figure 5.9: Deformed rectangular model (shell element for slab only) after 20 min of fuel tanker fire (a) under the mid-span and (b) near the abutment. Deformed rectangular model (shell element for all) after around 20 min of fuel tanker fire (c) near the middle support, (d) under the mid-span and (e) near the abutment after 5.4 min (due to convergence failure) of fuel tanker fire. Deformation scale factor 10

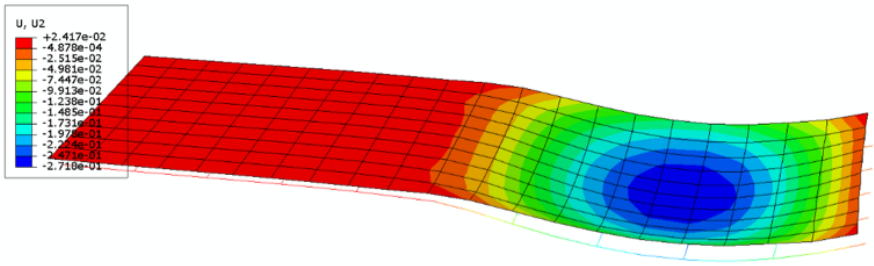

Figure 5.10: Deformed model after 5.55 min of the Hydrocarbon fire

In the models with design tanker fires as shown in Fig. 5.11, no runaway failure in FAS is observed because the fire is defined to be spatially non-uniform along the span. A much stiffer structural response in the design fuel tanker fire scenarios is seen than in the Hydrocarbon fire as seen by the steady deflection of around $0.2\,\mathrm{m}$. Initially the models with the design fuel tanker fire under mid-span deflects downwards faster than the model under the Hydrocarbon fire. This is caused by the intense steady-state heating from the fuel tanker fire. Then the temperature decay along the bridge span dominates the structural response with a much steadier behaviour. The fire source under the mid-span shows larger deflections than the scenario of fire under the middle support and near the abutment.

The horizontal displacement of free end is shown in Fig. 5.12. It shows that the right support of the models exposed to design fuel tanker fires keeps moving outwards and no reversal of horizontal displacement occurs as observed in the model with the Hydrocarbon fire.

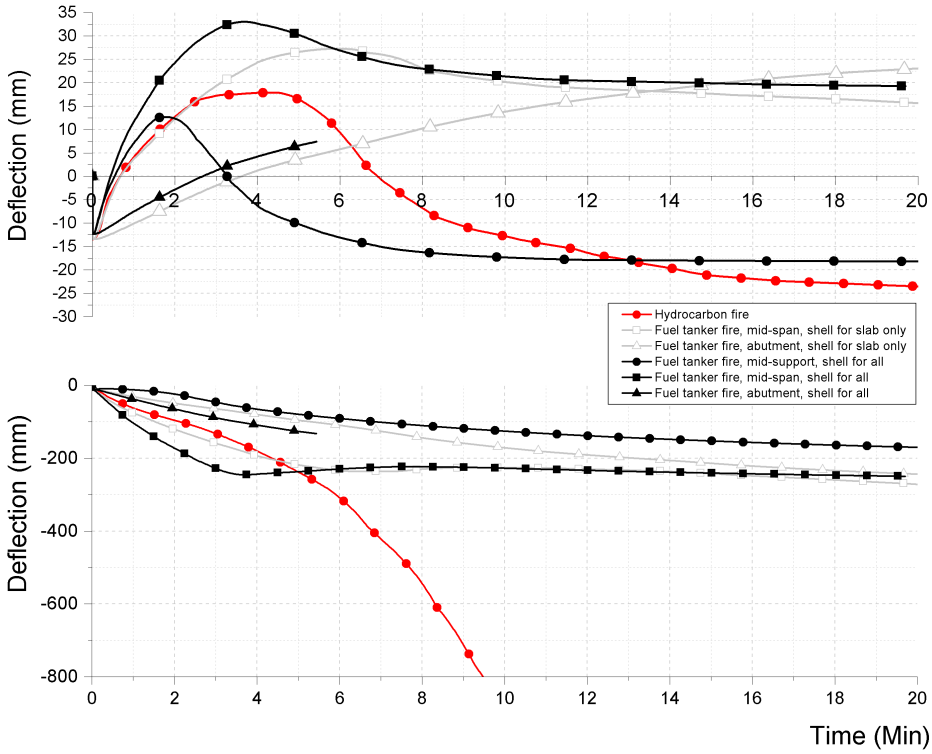

Figure 5.11: Comparison of the NFAS (top) and FAS (bottom) mid-span deflection variation with time

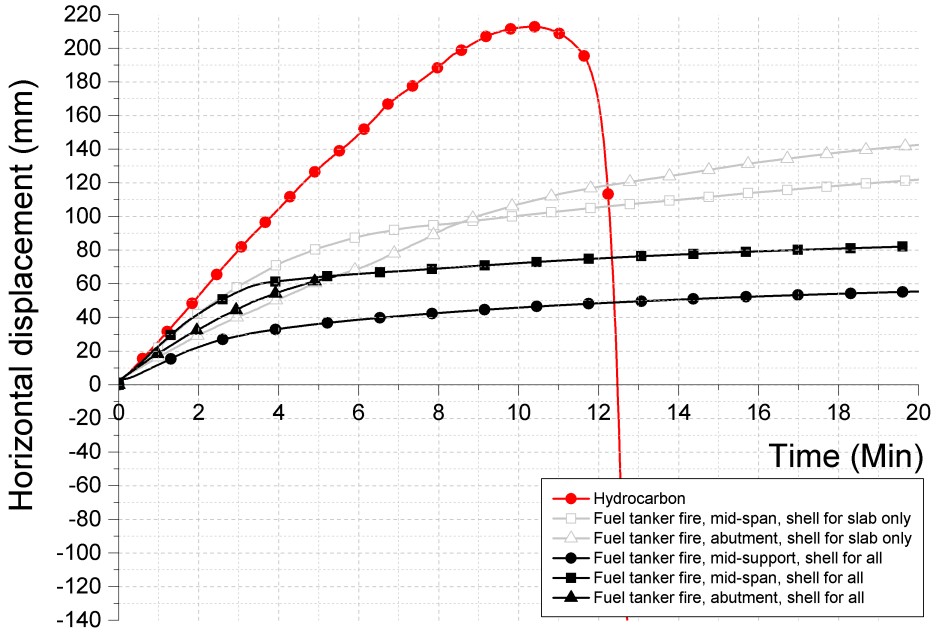

Figure 5.12: Comparison of the horizontal displacement at the right support

5.4.2 Skew Models

Same as the analysis above, this section compares the structural responses of the skew bridge to three different fires. The resulting deformed shapes at 20 minutes are shown in Fig. 5.13.

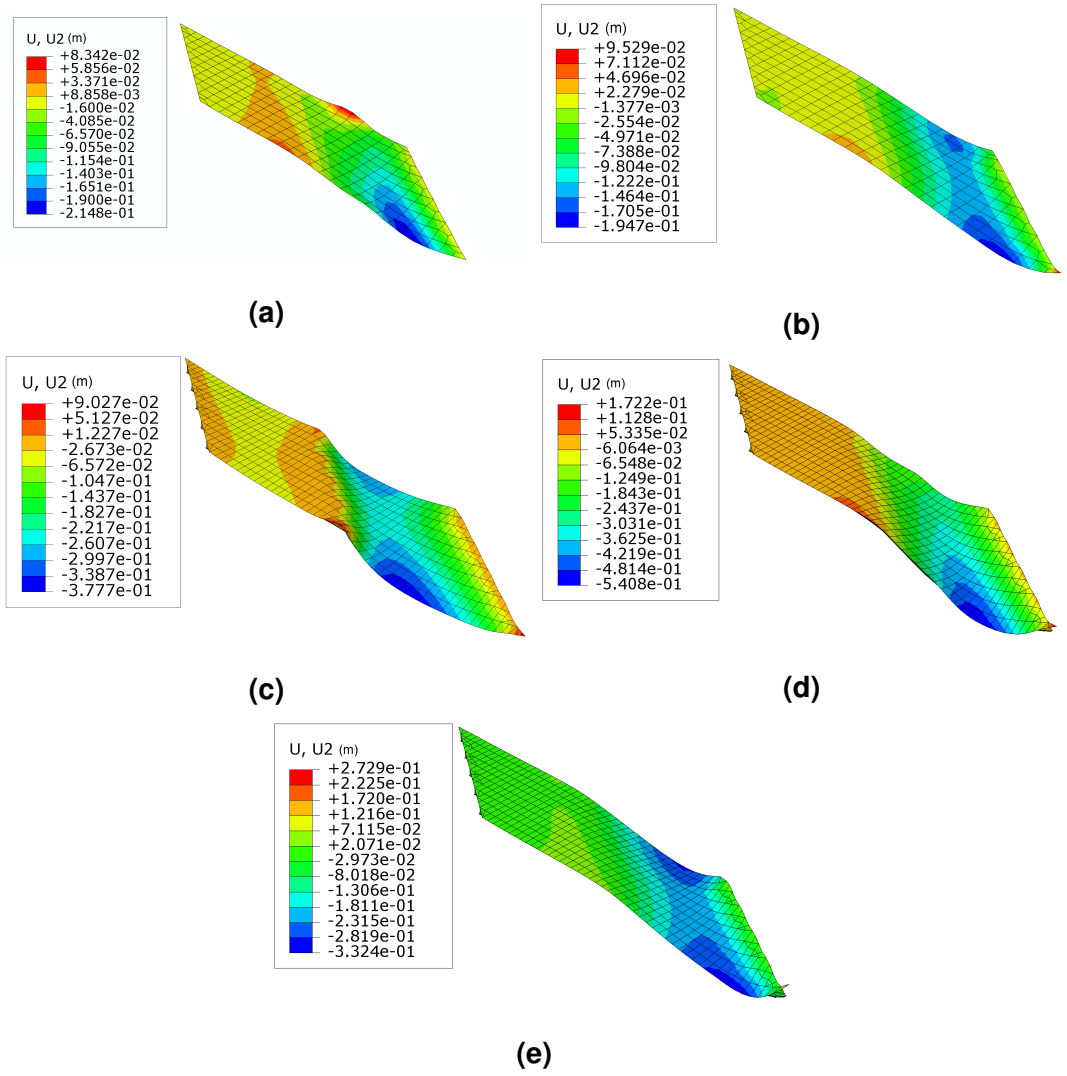

Figure 5.13: Deformed skew models (shell element for slab only) after 20 minutes of fuel tanker fire (a) under the mid-span and (b) near the abutment. Deformed skew model (shell element for all) after 20 min of fuel tanker fire (c) near the middle support, (d) under the mid-span and (e) near the abutment. Deformation scale factor 10

The deflection history at mid-span point of NFAS and FAS at Beam No. 5 between the skew models are compared in Fig. 5.14. The model with Hydro-

carbon fire using shell elements for primary beams is plotted for a conservative comparison. No runaway failure in FAS is observed from fuel tanker fire. Overall, a stiffer structural response is seen in the fuel tanker fire with lower deflection than the scenario of Hydrocarbon fire. The skew model with the design fuel tanker fire under the mid-span deflects downward faster than the model under Hydrocarbon fire. This behaviour has also been observed from the rectangular models. The horizontal displacement of the free end is compared in Fig. 5.15. It shows that no reversal of horizontal displacement occurs at the right support for all the models under fuel tanker fires.

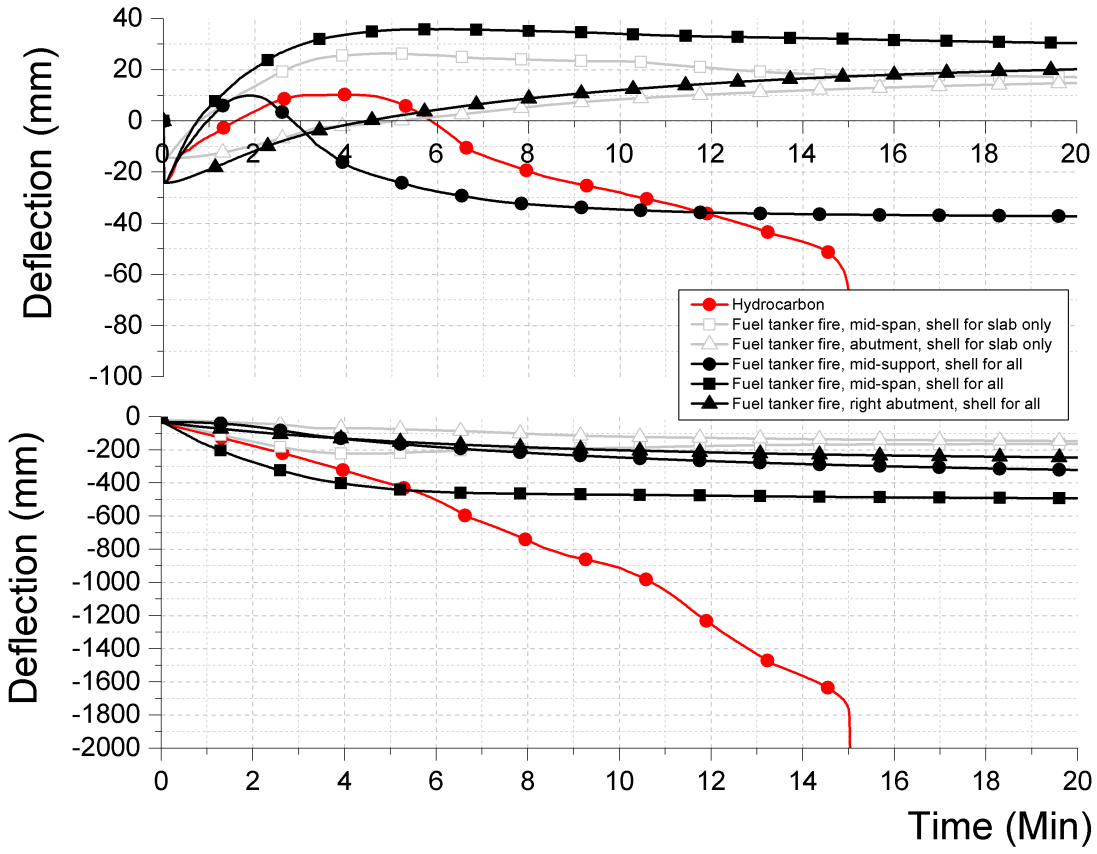

Figure 5.14: Comparison of NFAS (top) and FAS (bottom) mid-span deflection variation at Beam No. 5 with time

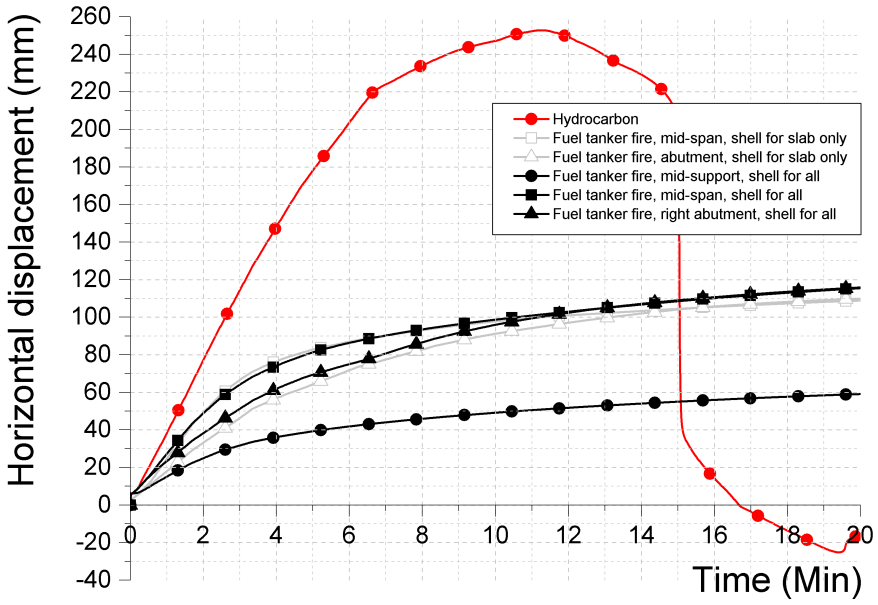

Figure 5.15: Comparison of the horizontal displacement at the right support

5.5 Conclusions

This chapter presents the structural response of the rectangular and skew shape bridge when exposed to the design fuel tanker fires. Three fire locations have been analysed including a location near the middle support, a location at the mid-point of span and a location near the abutment, to compare with the model under the Hydrocarbon fire analysed in Chapter 3. Both beam and shell elements are used to model the primary beams to investigate the possibility of local buckling of the steel web when the models are exposed to the fuel tanker fire. The following conclusions were drawn:

- No global failures are found based on the failure criteria of the reversal of horizontal displacement at the free end.
- No local buckling and corresponding runaway failure are found for all the models.
- The largest deflection observed in all the models is relatively small in comparison to the span length (1% and 1.8% of span length for rectan-

gular and skew models respectively). The bridge manifests a much stiffer response to the design fuel tanker fires than to the Hydrocarbon fire. Based on the results of this investigation it can be concluded that the Hydrocarbon fire is overly conservative for determining fire resistance of bridges.

- For both of the rectangular and skew models, initially the fuel tanker fire under mid-span causes larger deflection because there is no growth phase (steady-state) in the design fires. Then the temperature decay along the bridge span dominates the structural response during the later period, resulting in the final deflections are much lower in comparison to the Hydrocarbon fire.

- Although the design fuel tanker fires generate higher absolute temperatures in the composite section, the decay of thermal loading along the span dramatically reduces the influence of the design fire on the stability of the bridge superstructure.

Part III

‘Bridge Fires’ in OpenSees

6

Development of ‘Bridge Fires’ in OpenSees

6.1 Introduction

The fire resistance of bridges was analysed using prescriptive Hydrocarbon fire loading in Chapter 3 and using the new vehicle design fires in Appendix B. In the previous analysis, the commercial software ABAQUS 6.12 was used, which is a handy tool when the fire is uniformly applied along the bridge. However if spatially varying temperatures or heat fluxes from the heat transfer model need to be accurately applied to structural models, MATLAB scripts or Subrou-

tines are required to avoid tedious manual input. This process requires coding skills which would be usually difficult to implement in most practical engineering projects.

6.1.1 Objectives

This chapter presents a new module in an open-source software framework OpenSees which allows users to benefit from the embedded vehicle fire curves to automatically generate a HT and thermal response analysis. The 2D CFD localised fires which were developed in Chapter 4 and idealised as convenient mathematical functions in Appendix B are programmed into OpenSees for analysis of multiple vehicle fire scenarios under bridges.

In OpenSees, the temperature outputs from HT analyses can be automatically applied to the structural mesh. This simple tool can make it much easier for engineers to apply non-uniform thermal boundary conditions without any coding skills being required. This tool is especially convenient for assigning levels of expected performance under fires of different magnitudes. It is also an excellent tool for researchers to efficiently investigate a large range of realistic vehicle fire scenarios to obtain estimates of the uncertainty and bridge reliability within a probabilistic performance assessment framework.

6.2 OpenSees Development

OpenSees (Open System for Earthquake Engineering Simulation) is a free, object-oriented, finite element software, which was initially developed at UC Berkeley for earthquake engineering. In this software, Tcl is used as command language for finite element analysis.

Being open source, OpenSees allows new algorithms to be coded by other developers, thereby extending OpenSees' capability. OpenSees is implemented

primarily in C++ but uses considerable legacy Fortran code (McKenna, 2011). Commercial GUIs are now available (McKenna, 2011) from a few software companies, including nvStructural from Novel CAE Solutions, and CDS Win from Software Tecnico Scientifico. As described in Jiang and Usmani (2013), three phases are identified for an incremental-iterative nonlinear analysis:

1) Predictor: The resulting displacement increment can be calculated from an initial predicted out of balance force (due to thermal load and material degradation) and the stiffness matrix at the previous step. The thermal load is applied as an element load which is transformed into an equivalent nodal load.

2) Corrector: The total strain is updated for the new geometry of the structure and the stress state can be determined by subtracting the thermal strain from the total strain. The resisting force can be obtained by integrating the resisting stress along the section and is used to calculate the out of balance force for this iteration.

3) Convergence check: Equilibrium is checked at the end of each iteration to ensure that convergence is achieved in the new deformed configuration.

Until this project, only idealised building fires had been embedded in OpenSees, including the standard fire, parametric fire, EC1 localised fire, and a travelling fire (Dai et al., 2017). In this work idealised heat flux functions derived from the CFD fire models are implemented to provide more realistic scenarios for vehicle fires under bridges. The idealised design fire curves can be applied as boundary conditions for all the surfaces of the bridge superstructure exposed to fire, enabling OpenSees to predict the structural response of a bridge for the selected design fire scenario.

The new vehicle design fires are implemented through a C++ class in OpenSees which includes the heat flux functions for each vehicle category. This chapter

```
class BridgeFire : public FireModel
{
public:

    BridgeFire(int tag, double crd1, double crd2, double crd3, double Q, double loc_x1, double loc_x2, int vehicleTypeTag =
        1,
        int centerLineTag = 2, double startTime = 0.0);

    virtual ~BridgeFire();

    void applyFluxBC(HeatFluxBC* theFlux, double time);
    double getFlux(HeatTransferNode* the_node, double time);

protected:

private:

    double x1, x2, x3, q, Dx1, Dx2;    //q (unit in W)
    int centerLine;
    int VehicleTypeTag;        //indicates the type of the bridge fires
                               //1: car fire (default); 2: LGV fire, 3: HGV fires, 4: Exceptional fires
};
```

Figure 6.1: Interface of *BridgeFire* class.

describes the new implementation in the fire module where a new class *Bridgefire* (Fig. 6.1) is introduced, based on the existing *LocalisedFire*. Fig. 6.1 shows that OpenSees allows the users to select the vehicle types by assigning a tag number. The location of the fuel bed can be specified by defining the distance to the left and right boundaries of the bridge. The user needs to set the values of HRR and an error will show if the user-defined HRR is beyond the range of HRR for each vehicle type, such as the error: *'In car fires, fire size shouldn't be greater than 5 MW'*.

In order to perform HT analysis, various classes are required such as *HeatFluxBC*, *HeatTransferNode*, *HeatTransferElement*, etc. The details of the above classes in the heat transfer module and the interactions between the classes are described in Jiang (2012). The temperatures from the HT analysis can be applied to each fibre in the elements of structural models.

6.3 Application of The Exponential Functions

For the purposes of this chapter, the discussion will be restricted to steel frame, composite grillage type bridge structures, which is a very common motorway

bridge design in the UK. In order to analyse the post-fire behaviour of bridges, the HT from the flames to the surfaces needs to be determined first. This section presents a modelling study for a 2D composite section using OpenSees, where the embedded functions were used to define the thermal environment.

Before performing the OpenSees HT model with embedded 'Bridge Fires', a comparison with an ABAQUS model (Hu et al., 2015) was first carried out using the Hydrocarbon fire curve for verification. Fig. 6.2 shows the comparison of the temperature distribution along the cross section between ABAQUS and OpenSees. Fig. 6.3 illustrates the locations of the temperature outputs. Fig. 6.2 shows a good agreement of the predicted temperatures between the two software packages is found, especially for the centre of lower flange, the web, and the edge of the concrete slab. For the other three positions (centre of upper flange, $0.94\,\mathrm{cm}$, and $1.88\,\mathrm{cm}$ above the I-section centreline in slab), the temperature output of ABAQUS and OpenSees have a maximum difference of around 9% at 25-30 min, which is acceptable.

After the verification, two HT models were analysed in OpenSees, one with the fuel tanker fire, for a comparison with the ABAQUS model in Chapter 5, and another with the low to moderate car fire. Fig. 6.4 shows the HT results obtained using OpenSees using with new design 'Bridge fires' from a 100 MW fuel tanker fire and a $5\,\mathrm{MW}$ low to moderate fire. It also compares the temperature differences obtained with the Hydrocarbon fire. In the two FE models, the convection coefficient was set to $50\,\mathrm{W/(m^2K)}$ for the fire-exposed surfaces and $4\,\mathrm{W/(m^2K)}$ for the top surface of concrete (Franssen et al. (2009)). An effective emissivity factor of 0.7 was used for the fire-exposed surface and 0.8 for the unexposed surfaces.

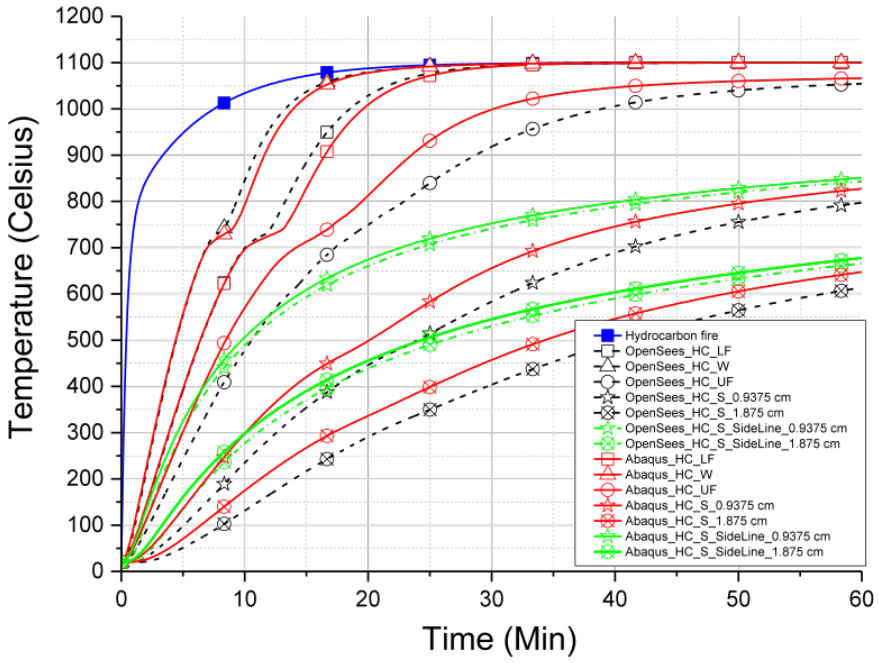

Figure 6.2: Comparison of heat transfer results for Hydrocarbon fire, between OpenSees and ABAQUS

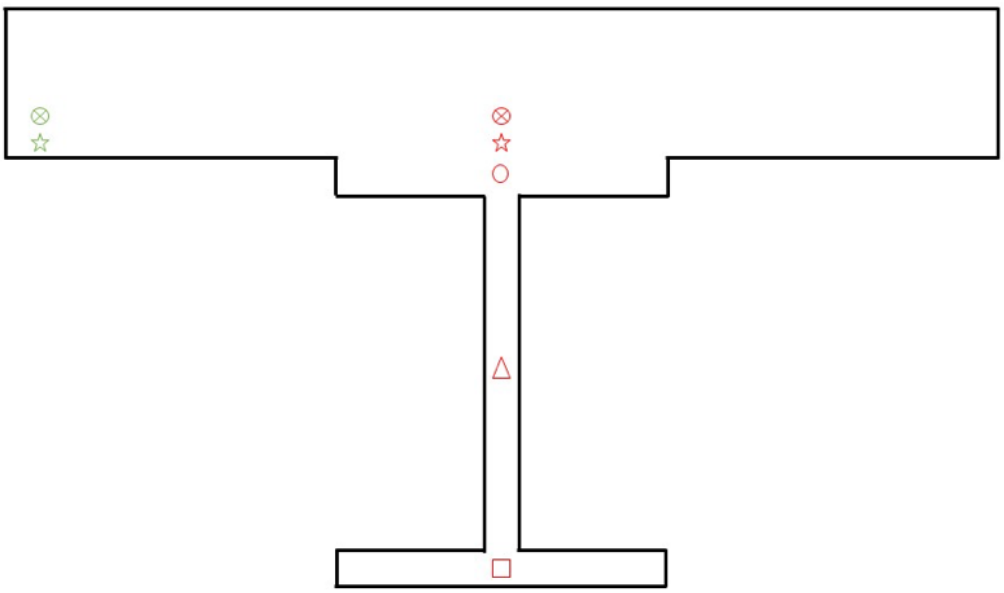

Figure 6.3: The output locations for the HT model under Hydrocarbon fire, corresponding to Fig. 6.2. Not to scale.

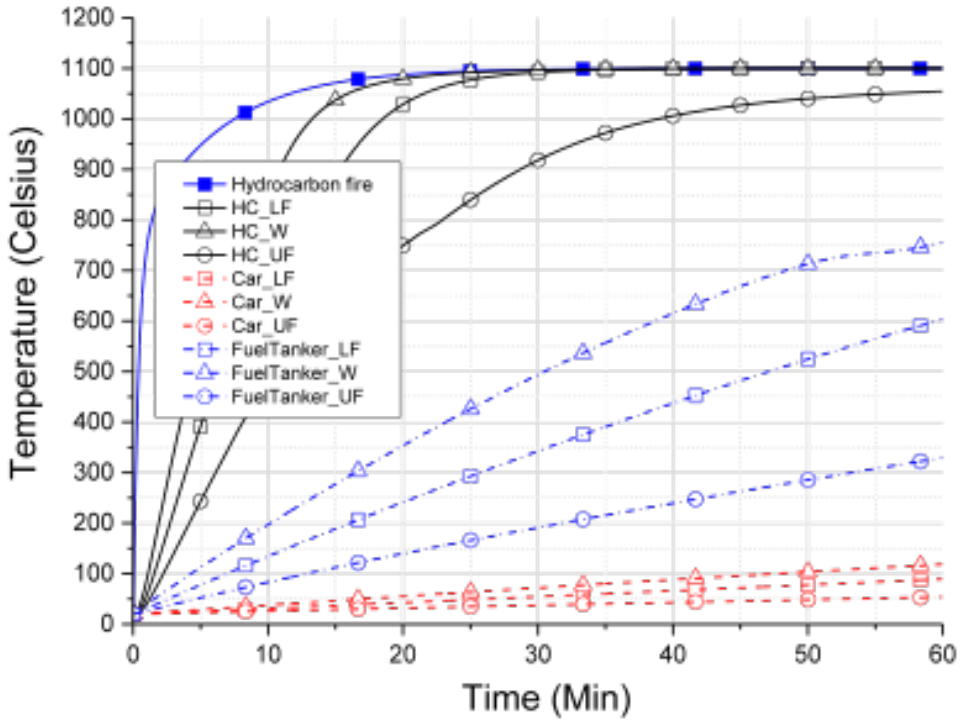

(a)

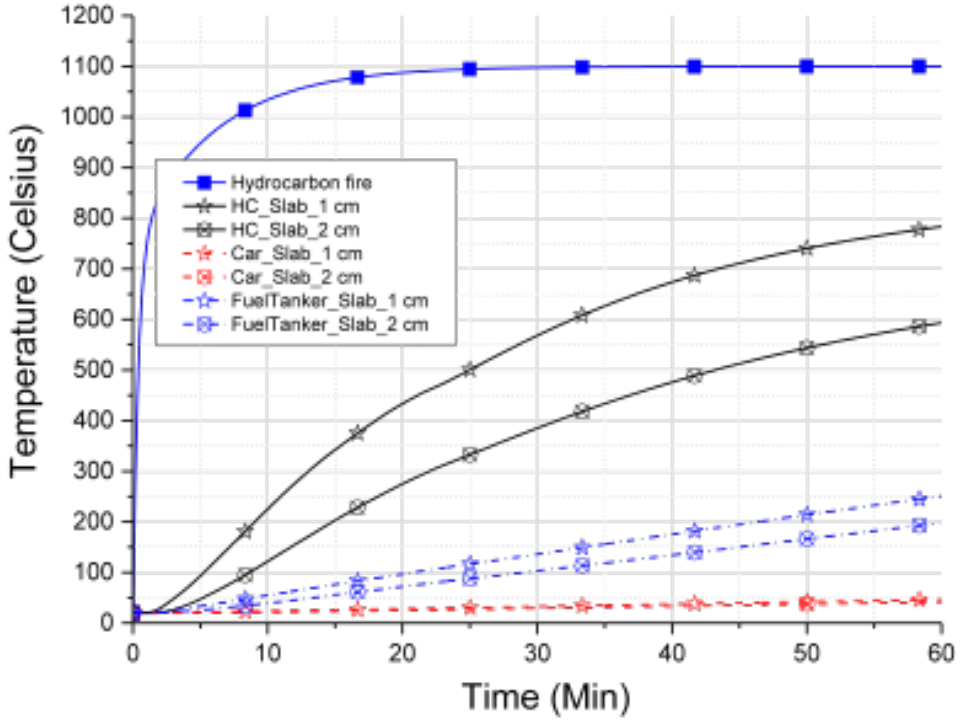

(b)

Figure 6.4: Temperature evolution with time within the (a) steel I-section and (b) concrete slab section, comparison of HT models using Hydrocarbon fire and 'Bridge fires' in OpenSees

Fig. 6.4 shows that the new design 'Bridge fires' provide a lower prediction of HT results even with the highest intensity fuel tanker fire. At the end of 60 min, 1100 °C is reached in the steel section under the Hydrocarbon fire, while maximum temperatures of 750 °C and 118 °C were achieved under the fuel tanker and the car fire, respectively. The Hydrocarbon fire results in a much quicker rate of temperature increase. When comparing the temperature at 20 min, where the failure of bridge is assumed to have happened under severe vehicle fires, there is 800 °C temperature difference (as shown in Fig. 6.4a) in the steel section between the HT models using the designed fuel tanker fire and the Hydrocarbon fire. The difference can be 1000 °C if a car fire is applied.

Fig. 6.4b shows that there are no large temperature differences in the concrete slab between the two HT models. The conservative assumptions in the models using the Hydrocarbon fire have been listed in Section 5.2. There is an additional conservative comparison in this chapter when the HT model was performed using OpenSees. The HT models in OpenSees were created in 2D and the analysis also neglects the longitudinal conduction along the bridge span. Furthermore, highest heat flux of each of the fire curves is used, all of which results in a higher prediction of temperature.

6.4 Conclusions

This chapter presents modifications to the current source code in OpenSees and the application of the new design fire models. With the newly added fire load module, OpenSees is able to perform HT analysis for bridge structures subject to vehicle fires. This framework is expected to overcome the complexity of using commercial FE software. It is suitable for a performance-based approach, in which the localised bridge fire and the bridge's resistance to fire can be determined. This framework can be used by authorities, who are re-

sponsible for managing a bridge network, to assess its vulnerability to vehicle fire incidents. The embedded new design fires in OpenSees are derived from the idealised curves in Appendix B, which envelop the fire curves of the CFD models.

7

Conclusions and Future Work

The detailed findings from each part of this work can be found in the previous chapters. This chapter lists the key conclusions of the work done based on the logical sequence of the thesis.

7.1 Conclusions

The literature review (Chapter 2) surveyed major bridge/fire accidents and showed that a vehicle fire under a bridge is likely to cause the most severe damage to that bridge. Therefore, this thesis started by numerically investigating the effects of a standard hydrocarbon fire load, applied to the underside of

a steel frame composite bridge superstructure (based on a real bridge structure existing on the Scottish highways network, which is of skew geometry in plan). The Hydrocarbon fire was applied to determine the structural response of bridge structures with rectangular and skew geometry in plan (Chapter 3). It was found that:

- The behaviour of the rectangular bridge models are almost identical when the bridge girders are modelled with either beam or shell elements. In the skew bridge models modelled entirely using shell elements, failure occurs due to web buckling concentrated near the middle support which does not manifest in the beam element model.

- The inclusion or otherwise of an abutment in the simulation does not significantly affect the failure time for the models (shell element for slab only) considered.

These conclusions are based on applying the Hydrocarbon fire uniformly along the bridge span, which may be too conservative and significantly over-predict the thermo-mechanical response. To provide more realistic representations of the bridge fire hazard, CFD fire models of localised vehicle fires were created (Chapter 4). Being localised fires, such representations naturally consider a heat flux decay along the bridge span, away from the vehicle. The results from these models show that:

- The maximum heat flux on the structure is generally higher when the fuel bed is closer to the bridge deck or to the abutment. However, for very large fires, this does not always hold.

- The heat flux on the structure has a significant decay along the bridge span, away from the fire location. This demonstrates that the structural response predicted using a uniformly applied fire along the full length of the bridge span is too conservative.

- The measured heat fluxes are not significantly affected by the abutment when the fuel bed is positioned at quarter span (6 m away from the abutment in this work).

The results from the CFD study were generalised into mathematical functions for vehicle fires (Appendix B). These may be used as inputs in structural analyses. It was found that:

- Simple exponential functions are able to capture the main characteristics of the heat flux results from the CFD study.

The functions developed for vehicle fires were used as "design fires" to assess the fire resistance of both rectangular and skew bridge model, using ABAQUS (Chapter 5). The extreme case of a fuel tanker fire was analysed, and compared with the Hydrocarbon fire results (from Chapter 3). The analysis shows that:

- In the initial stages of structural response, the realistic fuel tanker fire (when the fire source under the mid-span) produces larger deformations than the standard Hydrocarbon fire.

- However, after a few minutes of fire exposure, the flux decay dominates the structural behaviour, resulting in significantly lower deformations as a result of the fuel tanker fire, when compared to the Hydrocarbon fire.

- Overall, no global failure is predicted in the models using the fuel tanker fire, unlike the Hydrocarbon fire, which resulted in the collapse of bridge structure that was rectangular in plan. Thus it is shown that the Hydrocarbon fire loading is overly conservative for the bridge model investigated.

- No local buckling and corresponding runaway failure are found for all the models.

- As expected, the fuel tanker fire located under the bridge mid-span resulted in a largest deformation of the span, compared to a fire source positioned near the middle support and the abutment, but the difference is not significant.

As the task of implementing the heat flux functions into structural models requires coding skills, and would generally be too time consuming to do as part of a routine analysis. Therefore, the functions have been implemented into the OpenSees framework as the 'Bridge fires' module (Chapter 6). This has been validated by comparison with ABAQUS models.

- The new module in OpenSees allows the use of realistic vehicle design fires in a heat transfer analysis of bridges.

7.2 Future Work

Directions for future research were suggested in the literature review in Chapter 2. This section will recommend a further implementations which could be carried out to extend the work of this thesis:

- For a more equivalent comparison between using beam elements and shell elements for modelling bridge girders, stiffeners should be modelled to prevent local buckling which is not an uncommon strategy in bridge design.

- Due to time limitation, the '*Bridge fires*' module has only considered the key parameters which the author considers most critical to the structural response. Other factors, such as fire growth rate, could and should be considered in the future, resulting in time-dependent design fire curves, which may be more appropriate to use in certain cases, such as very wide or tunnel-like bridge.

- Phenomena observed from the CFD models are worthy of detailed future studies, especially investigation of the interactions between HRR and the height of the fuel bed surface.
- The structural response to *'Bridge fires'* in OpenSees needs to be validated.
- More full-scale experiments should be carried out for proper characterisation of the bridge fire hazard and structural response of different types of bridge construction (such as reinforced and prestressed concrete girder and box-girder bridges).

Bibliography

Aitken, L. WATCH: Car goes up in flames on Aberdeen bridge, 2017. URL https://www.eveningexpress.co.uk/fp/news/local/watch-car-goes-flames-aberdeen-bridge/.

Alos-Moya, J., Paya-Zaforteza, I., Garlock, M. E. M., Loma-Ossorio, E., Schiffner, D., and Hospitaler, A. Analysis of a bridge failure due to fire using computational fluid dynamics and finite element models. *Engineering structures*, 68:96–110, 2014.

Alos-moya, J., Paya-zaforteza, I., Hospitaler, A., and Loma-ossorio, E. Valencia bridge fire tests : Validation of simplified and advanced numerical approaches to model bridge fire scenarios. *Advances in Engineering Software*, 128(November 2018):55–68, 2019.

Alos-Moya, J., Paya-Zaforteza, I., Hospitaler, A., and Rinaudo, P. Valencia bridge fire tests: Experimental study of a composite bridge under fire. *Journal of Constructional Steel Research*, 138:538–554, 2017.

Apel, K. and Mason, H. Tanker truck driver killed in crash, explosion on I- 65 in Franklin, 2014. URL http://www.wsmv.com/story/26287745/interstate-65-closed-in-both-directions-after-tranker-truck-explosion.

Aziz, E. and Kodur, V. An approach for evaluating the residual strength of fire exposed bridge girders. *Journal of Constructional Steel Research*, 88: 34–42, 2013.

Aziz, E. M., Kodur, V. K., Glassman, J. D., and Moreyra Garlock, M. E. Behavior of steel bridge girders under fire conditions. *Journal of Constructional Steel Research*, 106:11–22, 2015.

Bajwa, C. S., Easton, E. P., Adkins, H., Cuta, J., Klymyshyn, N., and Suffield, S. The MacArthur Maze Fire and Roadway Collapse: A "Worst Case Scenario" for Spent Nuclear Fuel Transportation? In *Proceedings of the ASME 2012 Pressure Vessels & Piping Division Conference*, 2012. ISBN 9780791855065.

Barnes, J. Superhot supercar: £300k Lamborghini goes up in flames during London rush hour, 2016. URL http://www.express.co.uk/news/uk/678259/super-car-fire-london.

BBC NEWS. Burning Texas railway bridge collapses, 2013. URL http://www.bbc.co.uk/news/av/world-us-canada-22641179/burning-texas-railway-bridge-collapses.

British Standards. BS 476-20:1987, Fire tests on building materials and structures - Part 20: Method for determination of construction (general principles). URL http://anedidic.com/descargas/formacion-dermatologica/12/gingivitis-caracteristicas-y-prevencion.pdf.

Carvel, R. O., Beard, A. N., Jowitt, P. W., and Drysdale, D. D. The influence of tunnel geometry and ventilation on the heat release rate of a fire. *Fire Technology*, 40(1):5–26, 2004.

Carvel, R. Design fires for tunnel water mist suppression systems. In *3rd*

International Symposium on Tunnel Safety and Security, Stockholm, pages 163–171, 2008. ISBN 9789185829255.

Choi, J., Haj-Ali, R., and Kim, H. S. Integrated fire dynamic and thermomechanical modeling of a bridge under fire. *Structural Engineering and Mechanics*, 42(6):815–829, 2012.

Chuang, Y.-j., Tang, C.-h., Chen, P.-h., and Lin, C.-y. Experimental Investigation of Burning Scenario of Loaded 3.49-ton Pickup Trucks. *Journal of Applied Fire Science*, 14(1):27–46, 2006.

Dai, X., Welch, S., and Usmani, A. A critical review of "travelling fire" scenarios for performance-based structural engineering. *Fire Safety Journal*, 91(May): 568–578, 2017.

Department for Transport. Vehicle Licensing Statistics : 2011. 2012.

Department for Transport statistics. Vehicle Licensing Statistics, 2016. URL https://www.gov.uk/government/organisations/department-for-transport/about/statistics.

Directorate-General for Public Works and Water Management. Project 'Safety Test' Report on Fire Tests. Technical Report August, Directorate-General for Public Works and Water Management, 2002.

Dotreppe, J.-C., Majkut, S., and Franssen, J.-M. Failure of a tied-arch bridge submitted to a severe localized fire, structures and extreme events. pages 272–273. IABSE Symposium Lisbon, 2005.

Drysdale, D. *An introduction to fire dynamics*. John Wiley & Sons, 2011. ISBN 1119976103.

EN. Fire tests on building materials and structures - Part 20: Method for determination of the fire resistance of elements of construction (general principles) (BS 476-20:1987), 1987.

EN. Eurocode 1: Actions on Structures - Part 1-1: General Actions - Densities, Self-Weight, Imposed Loads for Buildings (BS EN 1991-1-1:2002), 2002a.

EN. Eurocode 3: Design of Steel Structures - Part 1.2: General Rules - Structural Fire Design (BS EN 1993-1-2:2005), 2005a.

EN. Eurocode 8: Design of structures for earthquake resistance – Part 2: Bridges (EN 1998-2:2005), 2005b.

EN. Eurocode 1: Actions on Structures - Part 1-2: General Actions - Actions on Structures Exposed to Fire (EN 1991-1-2), 2002b.

EN. Eurocode 2: Design of Concrete Structures: Part 1-1: General Rules and Rules for Buildings, 2004.

EN. Eurocode 3 : Design of steel structures — Part 1-1: General rules and rules for buildings (EN 1993-1-1:2005). 3, 2003a.

EN. Eurocode 1: Actions on Structures Part 1-3: General Actions - Snow loads (BS EN 1991-1-3:2003), 2003b.

EN. Eurocode 1: Actions on Structures–Part1-4: General actions-wind actions (EN 1991-1-4: 2005). *British Standard Institution, London*, 2005c.

Franko, K. Ohio to replace bridge after tanker fire, reroute traffic, 2015. URL http://newsok.com/article/feed/858383.

Franssen, J.-M., Kodur, V., and Zaharia, R. *Designing Steel Structures for Fire Safety*. CRC Press/Balkema, 2009. ISBN 978-0-203-87549-0.

Garlock, M., Paya-Zaforteza, I., Kodur, V., and Gu, L. Fire hazard in bridges: review, assessment and repair strategies. *Engineering Structures*, 35:89–98, 2012.

Godart, B. F., Berthellemy, J., and Lucas, J. P. Diagnosis, assessment and repair of the mathilde bridge close to collapse during a fire. Technical Report 3, 2015.

Gong, X. and Agrawal, A. Numerical Simulation of Fire Damage to a Long-Span Truss Bridge. *Journal of Bridge Engineering*, 20(Johnson):04014109, 2015.

Grove, J. Vehicle Licensing Statistics , Great Britain : Quarter 2 2012. Technical report, Department for Transport, 2012.

Grove, J. Vehicle Licensing Statistics , Great Britain : Quarter 2 (Apr-Jun) 2013. Technical report, Department for Transport, 2013.

Grove, J. Vehicle Licensing Statistics: Quarter 2 (Apr - Jun) 2014. Technical report, Department for Transport, 2014.

Grove, J. Vehicle Licensing Statistics: Quarter 1 (Jan - Mar) 2015. Technical Report 11 June 2015, Department for Transport, 2015a.

Grove, J. Vehicle Licensing Statistics: Quarter 4 (Oct - Dec) 2015. Technical report, Department for Transport, 2015b.

Grove, J. Vehicle Licensing Statistics : Quarter 2 (Apr - Jun) 2016. Technical report, Department for Transport, 2016.

Hanna, J. and Boyette, C. Atlanta I-85 collapse: Highway could be fixed by June 15, 2017. URL http://edition.cnn.com/2017/04/04/us/i-85-atlanta-fire-collapse/.

Hanna, J. and Rodgers, K. After I-85 fire, states are taking a closer look under their bridges, 2017. URL http://edition.cnn.com/2017/05/20/us/bridges-atlanta-collapse-states-policies/index.html.

Highways Agency. Highways Agency Initial Fire Risk Audit Report. Technical Report May, 2011.

Highways Magazine. 3D laser speeds-up Balfour's viaduct repair job, 2012. URL http://highwaysmagazine.co.uk/3d-laser-speeds-up-balfours-viaduct-repair-job/.

Hostikka, K. M. S., Floyd, R. M. J., and CraigWeinschenk Kristopher Overholt. Fire Dynamics Simulator Technical Reference Guide Volume 2: Verification, 2015.

Hu, J., Sanad, A., and Usmani, A. Structure response analysis of a highway bridge when subjected to accidental vehicle fires. In Usmani, A., Lu, Y., and Das, P., editors, *The First International Conference on Structural Safety under Fire & Blast*, pages 465–474, 2015.

Hu, J., Usmani, A., Sanad, A., and Carvel, R. Fire resistance of composite steel & concrete highway bridges. *Journal of Constructional Steel Research*, 148: 707–719, 2018.

Iles, D. Technical Report SCI Document ED008: Determining the Buckling Resistance of Steel and Composite Bridge Structures. Technical report, 2012.

Ingason, H. and Lönnermark, A. Heat release rates from heavy goods vehicle trailer fires in tunnels. *Fire Safety Journal*, 40(7):646–668, 2005.

Ingram, A. Ford Fiesta Dimensions – UK Exterior and Interior Stats, 2014. URL https://www.carwow.co.uk/blog/ford-fiesta-dimensions-919{%}0D{%}0D{%}0A.

Irons, K. and Turner, M. Principal Inspection Report. Technical report, BEAR SCOTLAND LTD, 2011.

Jiang, J. and Usmani, A. Modeling of steel frame structures in fire using OpenSees. *Computers & Structures*, 118:90–99, 2013.

Jiang, Y. *Development and application of a thermal analysis framework in OpenSees for structures in fire*. PhD thesis, The University of Edinburgh, 2012.

Joo, S., Kim, S., Kim, Y., and Park, C. Fire Risk Evaluation of Bridge underneath Conditions based on Field Investigation. *Procedia Engineering*, 210: 582–587, 2017.

Kodur, V., Aziz, E., and Dwaikat, M. Evaluating fire resistance of steel girders in bridges. *Journal of Bridge Engineering*, 18(7):633–643, 2013.

Lamont, S., Lane, B., Usmani, A., and Drysdale, D. Assessment of the fire resistance test with respect to beams in real structures. *Engineering Journal*, 40(2):63–75, 2003.

Lee, G. C., Mohan, S. B., Huang, C., and Fard, B. N. A Study of U.S. Bridge Failures (1980-2012). Technical report, the University at Buffalo, State University of New York, 2013.

Liu, X., Zhang, L., Guo, S., and Fu, M. A simplified method to evaluate the fire risk of liquid dangerous chemical transport vehicles passing a highway bridge. *Journal of Loss Prevention in the Process Industries*, 48:111–117, 2017.

Lönnermark, A. and Ingason, H. Gas temperatures in heavy goods vehicle fires in tunnels. *Fire Safety Journal*, 40(6):506–527, 2005.

McKenna, F. OpenSees: A framework for earthquake engineering simulation. *Computing in Science and Engineering*, 13(4):58–66, 2011.

Mercedes-Benz UK Ltd. ACTROS BLUETEC 5, 2011. URL http://tools.mercedes-benz.co.uk/current/trucks/specification-sheets/actros/actros-6x2-rigid.pdf.

Naser, M. Z. and Kodur, V. K. R. A probabilistic assessment for classification of bridges against fire hazard. *Fire Safety Journal*, 76:65–73, 2015.

Naser, M. and Kodur, V. Response of fire exposed composite girders under dominant flexural and shear loading. *Journal of Structural Fire Engineering*, 9(2):108–125, 2018.

National Fire Protection Association. NFPA 502: Standard for Road Tunnels, Bridges, and Other Limited Access Highways, 2011. URL http://www.nfpa.org/.

NBC 7 San Diego. Bridge to Be Demolished After Tanker Fire, 2011. URL http://www.nbcsandiego.com/news/local/Tanker-Fire-60-Freeway-Bridge-Demolition--135660998.html.

New York Post. Bridge to Las Vegas catches fire and collapses in CA, may 2014.

Nicoletta, B., Smith, M., and Gales, J. Toward fire resilience in Canadian bridge infrastructure. Technical Report July, Entuitive; York University, 2018.

Park, J., Cho, Y. K., and Shim, J. Resilient Fire Prevention and Management Strategies for Structures and Materials Stored under Urban Bridges. pages 584–593, 2018.

Payá-Zaforteza, I. and Garlock, M. E. M. A numerical investigation on the fire

response of a steel girder bridge. *Journal of Constructional Steel Research*, 75:93–103, 2012.

Pchelintsev, A., Hasemi, Y., Wakamatsu, T., and Yokobayashi, Y. Experimental and numerical study on the behaviour of a steel beam under ceiling exposed to a localized fire. In *Fire Safety Science*, volume 5, pages 1153–1164, 1997.

Peris-Sayol, G., Paya-Zaforteza, I., Alos-Moya, J., and Hospitaler, A. Analysis of the Influence of Structural Models in Fire Responses of Steel Girder Bridges. In *Asce*, number Pca 1936, pages 1530–1537, 2015a.

Peris-Sayol, G., Paya-Zaforteza, I., Alos-Moya, J., and Hospitaler, A. Analysis of the influence of geometric, modeling and environmental parameters on the fire response of steel bridges subjected to realistic fire scenarios. *Computers and Structures*, 158:333–345, 2015b.

Peris-Sayol, G., Paya-Zaforteza, I., Balasch-Parisi, S., and Alós-Moya, J. Detailed Analysis of the Causes of Bridge Fires and Their Associated Damage Levels. *ASCE Journal of Performance and Constructed Facilities*, 2016.

PIARC Committee on Road Tunnels. Fire and smoke control in road tunnels. Technical report, 1999.

Quiel, S. E., Yokoyama, T., Bregman, L. S., Mueller, K. A., and Marjanishvili, S. M. A streamlined framework for calculating the response of steel-supported bridges to open-air tanker truck fires. *Fire Safety Journal*, 73: 63–65, 2015.

Riebe, N. Former firefighter gets 24 months in jail for burning CN trestle bridge in Mayerthorpe, Alta., 2017. URL http://www.cbc.ca/news/canada/edmonton/mayerthorpe-arson-schalm-1.4192783.

SFPE. SFPE Handbook of Fire Protection Engineering Fifth Edition, 2016.

Simulia. Abaqus 6.12: Getting Started with Abaqus: Interactive Edition, 2012. URL http://www.maths.cam.ac.uk/computing/software/abaqus{_}docs/docs/v6.12/pdf{_}books/GET{_}STARTED.pdf.

Smart Contract Services Ltd. Vehicle Dimensions. URL http://www.smarthire.co.uk/vehicle-dimensions.htm.

Summers, C. How fire under M1 exposed vulnerability of motorways, 2012. URL http://www.bbc.co.uk/news/uk-16425491.

Tondini, N. and Franssen, J. M. Analysis of experimental hydrocarbon localised fires with and without engulfed steel members. *Fire Safety Journal*, 92(May): 9–22, 2017.

Tonicello, E. and Desanghere, S. Fire analysis of a new steel bridge. In *... on Structures in Fire*, 2012.

Torero, J. L., Law, A., and Maluk, C. Defining the thermal boundary condition for protective structures in fire. *Engineering Structures*, 149:104–112, 2017.

USA TODAY NETWORK. One day later, we still don't know what caused Atlanta's I-85 bridge fire, 2017. URL https://www.usatoday.com/story/news/nation-now/2017/03/31/what-we-know--85-collapse-atlanta-and-how-detour-around-damages/99862628/.

Usmani, A., Rotter, J., Lamont, S., Sanad, A., and Gillie, M. Fundamental principles of structural behaviour under thermal effects. *Fire Safety Journal*, 36:721–744, 2001.

Volvo. Volvo 9700 Specifications. URL https://www.volvobuses.co.uk/en-gb/our-offering/coaches/volvo-9700/specifications.html.

Vulliamy, E. Blackfriars Bridge fire: Road closed to traffic as black cab goes up in flames, 2017. URL http://www.independent.co.uk/news/uk/home-news/blackfriars-bridge-closed-delays-fire-taxi-cab-a7142506.html.

Wright, W., Lattimer, B., Woodworth, M., Nahid, M., and Sotelino, E. Highway Bridge Fire Hazard Assessment. Technical report, Virginia Polytechnic Institute and State University, 2013.

Zahirasri, M., Tohir, M. & Spearpoint, M. Distribution analysis of the fire severity characteristics of single passenger road vehicles using heat release rate data. *Fire Science Reviews*, 2:5, 2013.

A

Heat Release Rate Data

Table A.1: Heat release rates experimental data of liquid pool/spill fires (Carvel et al., 2004; Ingason and Lönnermark, 2005; Wright et al., 2013)

Liquid	Test facility	Diameter (m)	Heat release rate (MW)
Pool Fires			
JP-5		0.75 - 2.0	0.72-7.0
Gasoline		0.7-1.5	0.71-4.07
Methanol	Tunnel	0.10	1.2 kW
		0.15	3.2 kW
		0.20	7.5 kW

Table A.1: Heat release rates experimental data of liquid pool/spill fires (Carvel et al., 2004; Ingason and Lönnermark, 2005; Wright et al., 2013)

Liquid	Test facility	Diameter (m)	Heat release rate (MW)
	Open	0.25	23 kW
		0.10	1.2 kW
		0.15	3.0 kW
		0.20	5.5 kW
		0.25	8.5 kW
Methanol	Tunnel	0.4 x 0.4;	40 kW
Heptane	Tunnel	0.15	58 kW
Heptane	Open	0.15	14 kW
Methanol	Tunnel	2.0 x 1.0;	0.9
Diesel	Tunnel (Mont Blanc Tunnel)		6
60% (mass) n-heptane, 40% toluene	Tunnel (2nd Benelux)	1.8 x 1 x 0.1 m 4 steel fire basins	5 MW per fire basin (not fully attained).
Spill Fires			
JP-8, 1-3L spills		1.4-2.6	0.46-2.3
JP-8, 0.4-1.7 L/min spills		0.75	0.14
JP-8, 0.4-1.7 L/min spills		1.0-1.75	0.34-1.04
JP-5, 0.4-1.7 L/min		0.75	0.14
JP-5, 0.4-1.7 L/min		1.5-2.0	0.76-1.35
Gasoline, 0.25-1 L		0.7-1.5	0.19-0.87
Gasoline, 100 gal (378.5L)		15.5	82

Table A.2: Heat release rates experimental data for cars (Directorate-General for Public Works and Water Management, 2002; Wright et al., 2013; Zahirasri, M., Tohir, M. & Spearpoint, 2013)

Make/Model	Test Facility	Peak HRR (MW)
Peugeot 406 Berline (1994)		8.283
Peugeot 406 Break (1994)	Corner calorimeter	9.854
Renault 5 (1980s)		3.439
Renault 18, 80's	Unknown	2.1
Unknown mini car, 1995		4.063
Unknown compact Car, 1995		8.188
Ford Taurus Late 1970s		1.521
Datsun 160 J Sedan (Late 1970s)		1.859
Datsun 180 B Sedan (Late 1970s)		1.972
Unknown, compact car (1970-late 1990s)		3.801
Unknown, medium car (1970-late 1990s)		4.073
Unknown, medium car (1970-late 1990s)		3.650
Unknown, heavy car (1970-late 1990s)		3.332
Honda Accord (1998)		0.780
Honda Accord (1998)	Open calorimeter	1.189
Chevrolet Camaro (1997)		1.181
Chevrolet Camaro (modified) (1999)		2.973
Chevrolet Camaro (1999)		3.173
Ford Explorer (1998)		0.484
Plymouth Voyager (1996)		4.797
Chevrolet Camaro (1997)		1.161
Ford Explorer (1998)		1.337
Dodge Caravan Sport (1996)		1.545
Unknown (minivan) (1995)		2.405

Table A.2: Heat release rates experimental data for cars (Directorate-General for Public Works and Water Management, 2002; Wright et al., 2013; Zahirasri, M., Tohir, M. & Spearpoint, 2013)

Make/Model	Test Facility	Peak HRR (MW)
Unknown (1998)		3.618
Trabant Limousine (1963-1990)		3.630
Rover-Austin Metro LS (1990s)		1.710
Citroen BX 16 RE (1970s or 1980s)		4.470
Unknown (1990s)		3.560
Unknown (1990s)	Room calorimeter	3.633
Unknown (1990s)		1.990
Unknown (1990s)		3.039
Renault Espace (2001)		3.800
Ford Focus (2002)		4.800
Opel Kadett (1962-1991)		4.549
Peugeot 309 (1985-1993)	Parking garage	8.872
Renault Espace (1984-late 1990s)		4.270
Fiat 127, late 70's Renault		3.6
Renault Espace J11-II, 1988	Tunnel	6.206
Fiat 127 (1971-1983)	Road tunnel	3.560
Renault Laguna (1993-1999)	Unknown	8.354
Opel Kadett, 1990, u=1.5m/s		4.9
Opel Kadett, 1990, u=6m/s	Unknown	4.8
Citroen BX 14 RE (1986)		4.390
Austin Maestro (1982)	Rail shuttle car	8.482
Opel Kadett (later than 1990) Ventilation: No Test5		Unknown
Opel Kadett (later than 1990) Ventilation: No T6	Tunnel (2nd Benelux)	4
Opel Kadett (later than 1990) Ventilation: 6 m/s T7		2

Table A.3: Heat release rates experimental data for LGVs (Carvel et al., 2004; Chuang et al., 2006; Directorate-General for Public Works and Water Management, 2002)

Make/Model/ Commodity	Test Facility	Peak HRR (MW)
Pick-up truck with 890kg wood pallets	Unknown	23.38
Pick-up truck 890kg wood pallets	Unknown	20.92
Pick-up truck 452kg plastic barrels	Unknown	47.47
Van	Des Monts tunnel	2.0
Citroen Jumper, 18 wooden Euro-pallets T11	Tunnel (2nd Benelux)	7

Table A.4: Heat release rates experimental data for HGVs (Directorate-General for Public Works and Water Management, 2002; Ingason and Lönnermark, 2005; Wright et al., 2013)

Make/Model/Commodity	Test Facility	Peak HRR (MW)
HGV-Trailer with 11010 kg 82% wood pallets (1.2m x 1m or 0.8m x 0.15m) and 18% plastic pallets (1.2m x 0.8m x0.15m)	Runehamar Road Tunnel height of the platform floor from the road surface: 1.1 m	201.9
HGV-Trailer with 6930 kg, 82% wood pallets and 18% foam mattresses		156.6
HGV-Trailer with furniture, fixtures, and 10 large rubber tires, polyester tarpaulin		118.6
HGV-Trailer with corrugated paper cartons with plastic cups		66.4
Trailer with 2 tons furniture	Tunnel	128
Trailer with 72 wood pallets		26
Trailer with 36 wood pallets		13-19
Simulated truck load		17
(in conformity with that of a small HGV); Canvas HGV hood: 4.5 x 2.4 x 2.5 (L x W x H); 36 wood pallets (4 stacks) Ventilation: No (natural) T8	Tunnel (2nd Benelux)	13
(in conformity with that of a small HGV); Canvas HGV hood: 4.5 x 2.4 x 2.5 (L x W x H); 36 wood pallets (4 stacks), Ventilation: 6m/s T9		19
(in conformity with that of a small HGV); Canvas HGV hood: 4.5 x 2.4 x 2.5 (L x W x H); 36 wood pallets (4 stacks), Ventilation: 6 m/s		16
T10 72 wood pallets (8 stacks), Ventilation: 1–2 m/s T14		25
Aluminium HGV hood: 4.5 x 2.4 x 2.5 (L x W x H); 36 wood Eruo-pallets (4 stacks); Ventilation: 3m/s T12		6
Aluminium HGV hood: 4.5 x 2.4 x 2.5 (L x W x H); 36 wood Eruo-pallets (4 stacks)		13

Table A.4: Heat release rates experimental data for HGVs (Directorate-General for Public Works and Water Management, 2002; Ingason and Lönnermark, 2005; Wright et al., 2013)

Make/Model/Commodity	Test Facility	Peak HRR (MW)
Ventilation: 0-3m/s T13		
HGV, 1994 kg of mixed furniture, 75% cellulose material and 25% plastic; The HGV consisted of a diesel powered tractor unit (Leyland DAF 310 A) and a 12.2 m long double axel trailer with twin axles at the rear.	Tunnel (Repparfjord Tunnel, Norway. EUREKA 499 programme)	128
Weighting platform using densely packed wood cribs supplemented with rubber tyres and plastic material		16
HGV trailer	Tunnel (Mont Blanc Tunnel)	23

Table A.5: Heat release rates experimental data for Buses & Coaches (Wright et al., 2013)

Make/Model/ Commodity	Test Facility	Peak HRR (MW)
Volvo bus, 12m long, 40 seat (25-35 years old)	Tunnel	29
Bus		34

B

Functions for ‘Bridge fires’

B.1 Introduction

Chapter 4 simulated a series of CFD models for vehicle fires under a bridge. This appendix develops exponential functions using MATLAB R2016a for the CFD results, to reduce the reliance on prescriptive fires or CFD modelling in conventional analyses of thermo-mechanical behaviour of bridges. These functions are able to predict incident heat flux distributions for different parts of a composite beam under a bridge superstructure for four types of vehicles fires. This will provide more realistic fire curves and will lead to efficient modelling for engineers. Later, the developed flux functions will be used in a FE

analysis (Abaqus models in Chapter 5) and programmed into the OpenSees software framework (Chapter 6).

B.2 Data Cleaning and Preparation

There are multiple parameters used in the CFD model as shown in Fig. B.1a, including Q, l, w, y, D_y and the position of the fuel bed. y is the height of the point receiving the heat flux. D_y is used to represent the distance between the fuel bed surface and the slab bottom, which corresponding to the fuel bed height (parameter h in Chapter 4). As shown in Fig. B.1b, in the fitted functions, the location of the fuel bed will be represented through the values of D_{x1} and D_{x2} which are defined as the distance from the fuel bed to the left and right piers/abutment respectively. The summation of D_{x1} and D_{x2} represents the bridge span length.

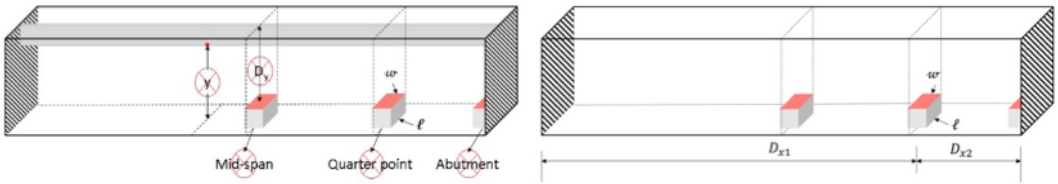

(a) **(b)**

Figure B.1: Parameters used in (a) the original CFD models and (b) the fitted heat flux curves

There are 4 levels of fire intensity considered. Each category includes 2 values of HRR, 2 levels of D_y, 4 levels of y and 3 fire positions. This produces 48 curves for each category, resulting in 192 curves in total for all four categories. To make such a complicated dataset suitable for practical use, several challenges exist for curve fitting and function development:

1) To develop the target design curves, only one function associated with

one set of coefficients is expected to represent all the curves for each category; a different set of coefficients for each curve is not recommended.

2) The coefficients should have similar magnitude.

After several preliminary studies, the author opted to ignore some of the less significant parameters to reduce the size of the dataset in order to simplify the fitting process. Heat flux results in Chapter 4 show that the location of received heat flux across beam depth has less significant influence compared to the other parameters such as HRR and the locations of the fuel bed. Consequently, the parameter y was eliminated from the functions by enveloping the curves. This is a conservative way to reduce the number of curves. It was also found that the curves with different D_y have relatively similar forms and therefore being enveloped and there will be only 2 curves at each fire position resulting in 6 curves in total for one category of vehicle. Fig. B.2 shows the finalised fire curves for the four types of vehicles (cars, LGVs, HGVs, and fuel tankers). The 24 curves include the most influential parameters, HRR and fire location.

To further simplify the fitting process and obtain a conservative prediction, the 24 curves have been grouped and considered in two ways:

1) Based on the *fire locations*, resulting in 3 functions in total where each function covers 8 curves for all four fire intensities at the same location;

2) Based on the *fire intensity*, resulting in 4 functions in total where each function covers 6 curves at all three fire locations within the same category.

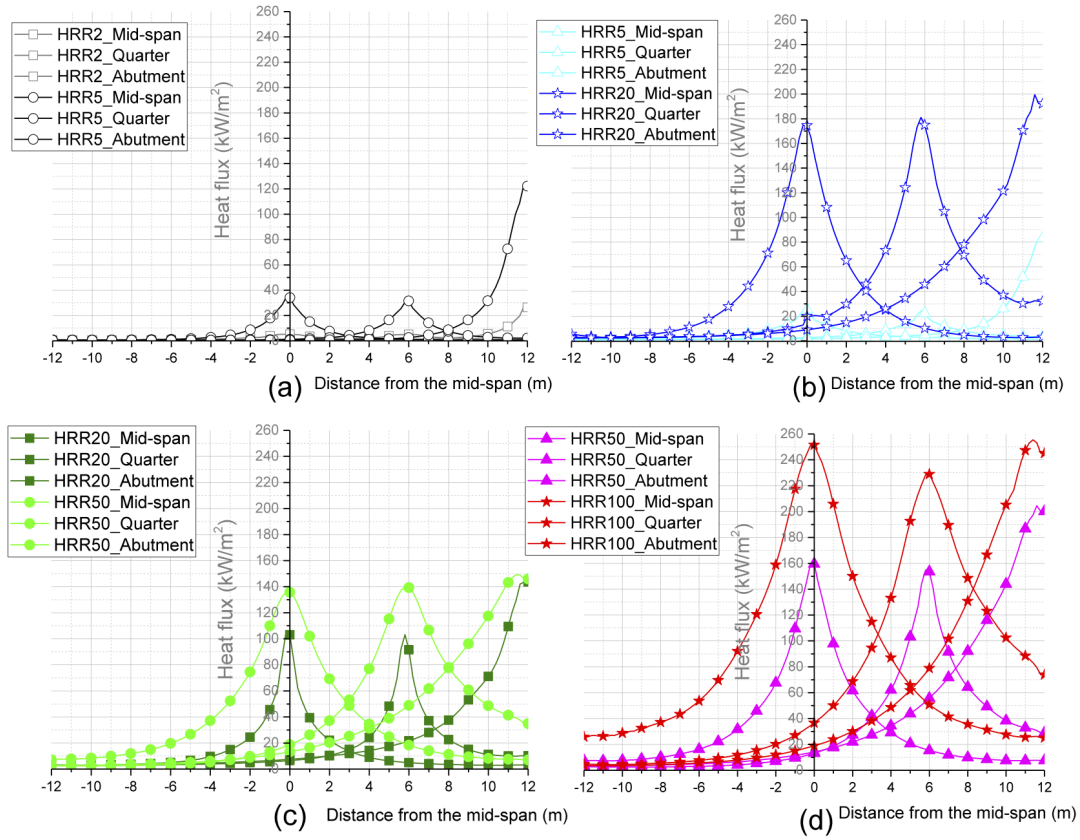

Figure B.2: Lateral distribution in the heat flux along the span with distance from the fuel bed for (a) Low-Moderate; (b) Moderate-High; (c) High-v.High; (d) Exceptional models.

The first method is considered because the decay rate of the curves are similar within all categories. This can possibly allow the set of curves to be fitted using the same coefficients. However, the first method eventually proved to be difficult to implement because the peak values of the 8 curves do not follow any apparent trends.

The second grouping method was therefore used. In this method, the parameters l and w are eliminated from the functions because the fuel bed dimensions are identical within each category. The drawback of this elimination is that the users are not allowed to specify the fuel bed dimensions for the design fire curves, however the author believes that the four fire intensities provided in the thesis should be adequate to describe the majority of bridge

fires. The fuel bed is assumed to be of a small size for each fire intensity, and if the users specifies a larger size of pool fire, the predicted heat flux would be lower. The elimination of l and w is therefore acceptable and provides a conservative prediction of heat fluxes.

B.3 Curve Fitting

The heat flux $\dot{q}^{"}$ (w/m^2) onto structural surfaces exposed to a vehicle fire is a function of distance x (m) which is the location along the bridge measured from the left wall, as shown in Eq. B.1.

$$\dot{q}^{"} = fn(Q, D_{x1}, D_{x2}, x) \tag{B.1}$$

Where Q is the heat release rate (W)
D_{x1} is the distance (m) between the fuel bed and left wall
D_{x1} is the distance (m) between the fuel bed and right wall

The curves in Fig. B.2 appear to be of a Gaussian shape, consisting of an exponential function with a concave quadratic function. An exponential model $y = c * e^{a(x-b)^2}$ was used, where x is the position receiving the heat flux along the bridge span; y is the heat flux; the value of *c* affects the maximum value of heat flux and slightly affects the slope; the value of a affects the decay rate and should be a negative value to plot an exponential decay; the slope is greater if the absolute value of *a* is greater. The value of b determines the location of central axis or peak value of the curves.

A one-term function does not fit all 6 curves in the same category, using only one set of coefficients. The curves are well described by multi-term exponential functions, in the form $y = ae^{bx} + ce^{dx}$ which will be used in this chapter to

appendix allow for two decay modes. The final fitted functions for each level of fire intensity are listed as follows.

1) Low-Moderate Car fires:

$$\begin{aligned}\dot{q}^{"} =& C_1(\frac{Q}{10^6})^2 * (\frac{D_{x1}}{D_{x2}})^{0.5} e^{C_4(x-D_{x1})^2} + \\ & C_2(\frac{Q}{10^6})^2 * (\frac{D_{x1}}{D_{x2}})^{0.5} e^{C_5(x-D_{x1})^2} + \\ & C_3\end{aligned} \tag{B.2}$$

2) Moderate-High LGV fires:

$$\begin{aligned}\dot{q}^{"} =& C_1\frac{Q}{10^6} * (\frac{D_{x1}}{D_{x2}})^{0.1} e^{C_4(x-D_{x1})^2} + \\ & C_2\frac{Q}{10^6} * (\frac{D_{x1}}{D_{x2}})^{0.1} e^{C_5(x-D_{x1})^2} + \\ & C_3\end{aligned} \tag{B.3}$$

3) High-v. High HGV fires:

$$\begin{aligned}\dot{q}^{"} =& C_1(\frac{Q}{10^6})^{0.3} * (\frac{D_{x1}}{D_{x2}})^{0.1} e^{C_4(x-D_{x1})^2} + \\ & C_2(\frac{Q}{10^6})^{0.3} * (\frac{D_{x1}}{D_{x2}})^{0.1} e^{(C_5(x-D_{x1})^2} + \\ & C_3\end{aligned} \tag{B.4}$$

4) Exceptional Fuel Tanker fires:

$$\begin{aligned}\dot{q}^{"} =& C_1(\frac{Q}{10^6})^{0.3} * (\frac{D_{x1}}{D_{x2}})^{0.01} e^{(C_4(x-D_{x1})^2} + \\ & C_2(\frac{Q}{10^6})^{0.3} * (\frac{D_{x1}}{D_{x2}})^{0.02} e^{(C_5(x-D_{x1})^2} + \\ & C_3\end{aligned} \tag{B.5}$$

Fig. B.3 - B.6 show the data from the CFD model predictions. Since the curve fitting result is highly dependent on the defined function and is sensitive

Table B.1: The coefficients for each function

	C_1	C_2	C_3	C_4	C_5
Low-Moderate	298.98	571.26	132.52	-0.10123	-0.89754
Moderate-High	3988.2	3079.1	362.5	-0.52988	-0.040459
High-v. High	17885	17084	4403.3	-0.30683	-0.028384
Exceptional	28384	27984	7389.9	-0.25515	-0.023214

to the initial estimate, in each category, the author first determined the suitable function and coefficients for the 3 curves with the highest HRR for each category (top 3 graphs in Fig. B.3 - B.6). Once the coefficients were obtained for a reasonable fit, the resultant function was used to determine the other 3 curves (bottom 3 graphs in Fig. B.3 - B.6). Some errors which can be observed between the predicted curve and the data from the CFD models, especially at the peak heat flux. These errors are considered acceptable in this work as:

1) For a realistic design vehicle fire scenario, the spatial decay is more important than the exact value of the maximum heat flux.

2) Overfitting would lead to information lost and hence reduce the power of prediction.

3) The fitting errors are on the conservative side.

As seen from the above correlations, the basic components are the same for all categories. A small magnitude coefficients was used to reduce the influence caused by certain parameters such as D_{x1}/D_{x2}.

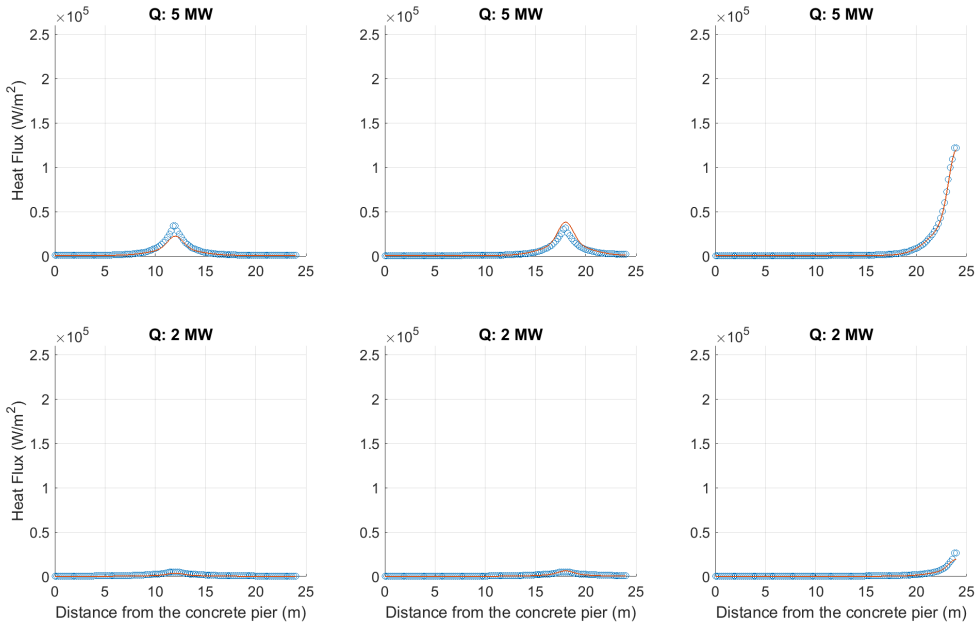

Figure B.3: Results of the exponential fit for Low to Moderate fires

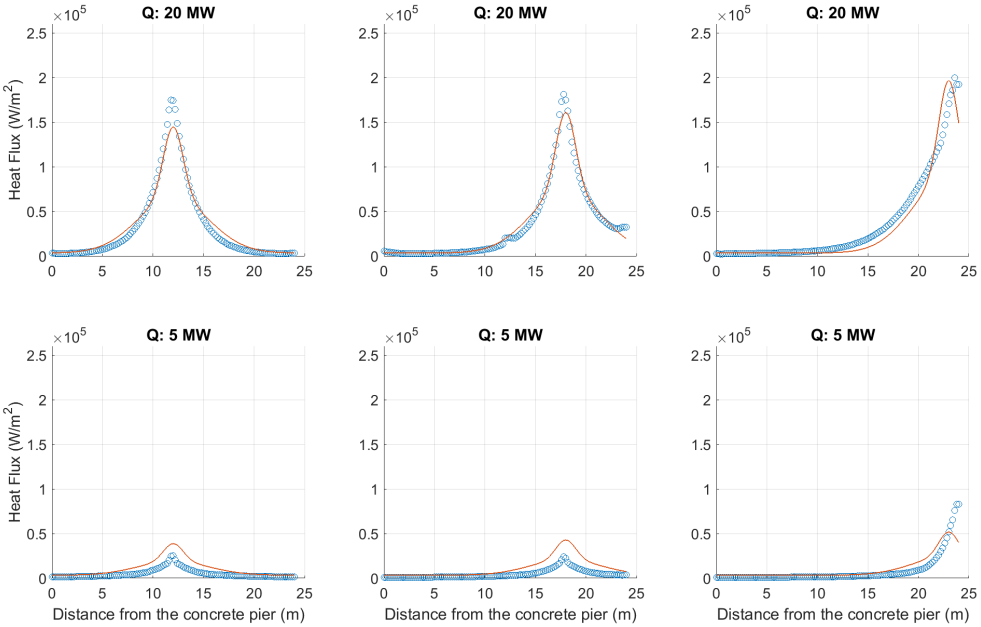

Figure B.4: Results of the exponential fit for Moderate to High fires

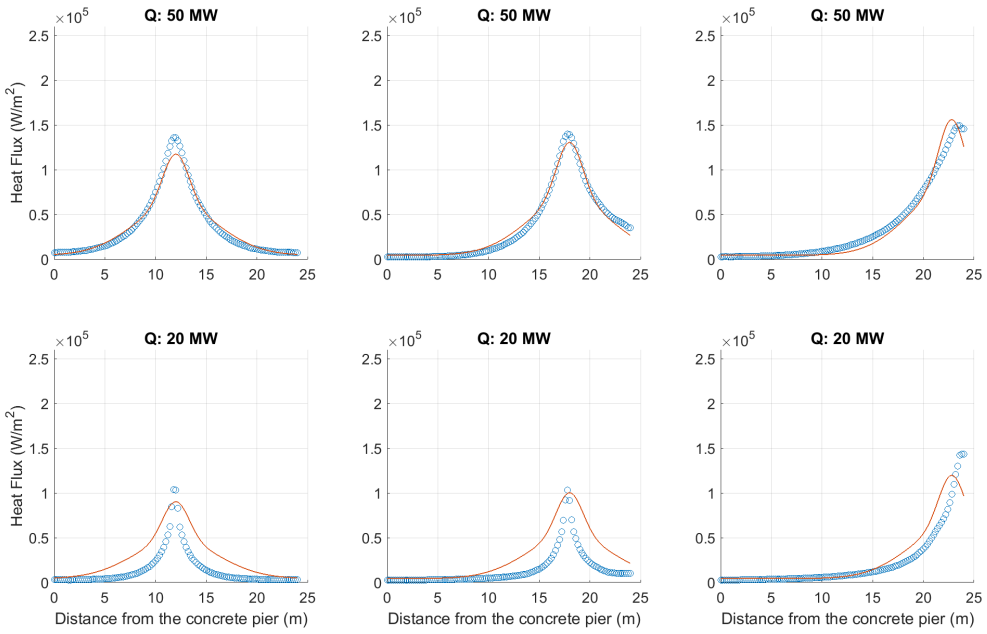

Figure B.5: Results of the exponential fit for High to v. High fires

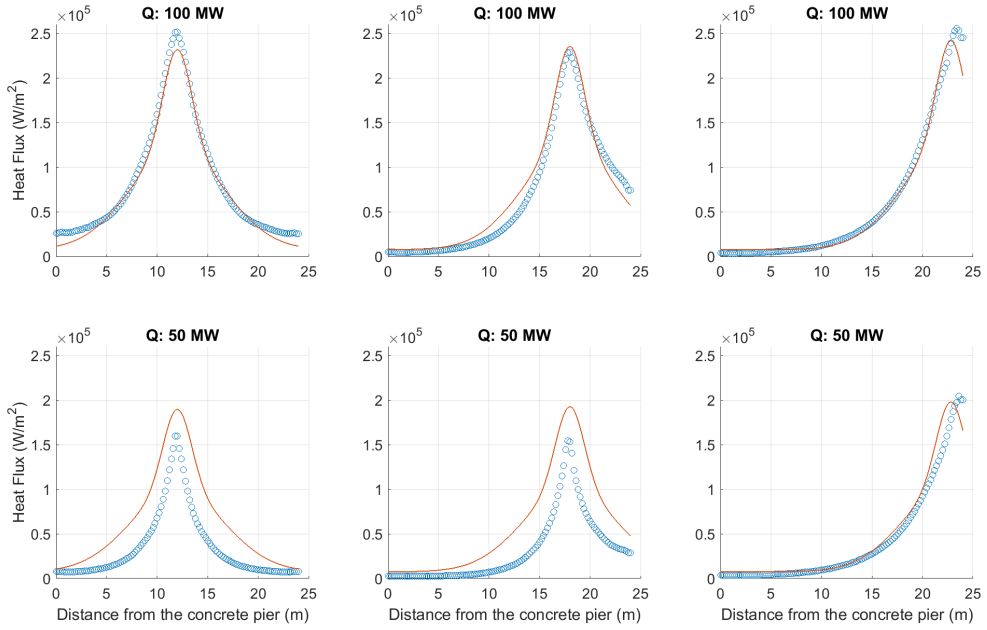

Figure B.6: Results of the exponential fit for Exceptional fires

B.4 Conclusions

Spatially non-uniform flux correlations have been developed in this appendix to quantify the incident heat flux on a bridge superstructure as a result of a vehicle design fire. Some of the parameters considered in the CFD modelling have been neglected in developing the design fire curves. Including all the parameters may produce better fitting results, but it is not necessary from a practical engineering design point of view. To ensure the generalisation of the fitting results and avoid too many features, the raw data was conservatively processed by enveloping a range of curves through a MATLAB script.

The correlations are sufficiently accurate to capture the heat flux variation from the CFD models and should provide reasonable estimates of incident heat flux to the slab and beams in a bridge superstructure.

The functions are more realistic compared to prescriptive fire curves, however these functions are currently limited to fires with the HRR and fuel bed dimensions defined in this work. It has not been established whether the correlations would hold for fire sources larger than 100 MW.

Along with the spatial decay modelled in the functions, a range of values of the peak heat flux for different fire categories can be suggested in future work. Other parameters could be considered, such as the beam depth to span length ratio.